INL/EXT-21-61607
Revision 2

Management of the Three Mile Island Unit 2 Accident Corium and Severely Damaged Fuel Debris

November 2022

Contribution to
International Atomic Energy Agency
Coordinated Research Proposal T13015

Philip L. Winston
Engineer

Changing the World's Energy Future

Idaho National Laboratory

INL is a U.S. Department of Energy National Laboratory operated by Battelle Energy Alliance, LLC

INL/EXT-21-61607
Revision 2

Management of the Three Mile Island Unit 2 Accident Corium and Severely Damaged Fuel Debris

Contribution to International Atomic Energy Agency Coordinated Research Proposal T13015

Philip L. Winston
Engineer

November 2022

Idaho National Laboratory
Idaho Falls, Idaho 83415

Page intentionally left blank

EXECUTIVE SUMMARY

The Three Mile Island, Unit Two (TMI-2) pressurized water reactor core underwent a significant meltdown in 1979 due to an untimely combination of maintenance problems that led to a loss of feedwater, followed by a series of operational misunderstandings and errors. Primary coolant discharging through a malfunctioning valve represented what was analyzed as a "small-break" loss-of-coolant accident (LOCA) and ultimately became a full core meltdown. The melted core recovery process required the development of a wide array of tools. After approximately three years of water management and other cleanup actions, the first views of the core revealed a much higher degree of damage than previously expected. Approximately 62 metric tons of the core had melted, leaving only 42 of the 177 fuel assemblies standing with fuel rods intact. The core to be recovered was composed of loose, gravel-like and granular particulate material and a central solidified mass of formerly molten fuel. Molten fuel had also penetrated some of the pressure vessel internals and resolidified below the main core support structure. Robotic tools that had been designed for the task were of limited effectiveness due to the range of material types and phases.

Over a period of several years, the central melt was broken up, primarily by use of a drill originally designed to acquire samples through the depth of the debris field. The broken pieces were loaded into specially-designed debris canisters by the use of long-handled pick-and-place tools and suctioned into baffled knockout canisters using an airlift vacuum system. A remotely operated underwater plasma-arc torch was developed for removal of the lower core support structure to be able to retrieve the fuel pieces and secondary melt that had solidified on the bottom reactor vessel head. Canister design played a central role in defining the initial retrieval process and later affected transportation, interim wet and its current interim dry storage.

Due to concerns about the potential for radiolysis of residual water in the debris and other canister material during transportation, the canisters were fitted with hydrogen-recombiner catalyst units to prevent a buildup of flammable gas and potential pressurization. To confirm the effectiveness of the recombiners, eight dewatered canisters were kept sealed for up to 205 days with periodic sampling of the headspace gas. The highest hydrogen value (9 vol%) was observed in a canister held for 147 days while the longest stored canister resulted in a 5% hydrogen concentration. The oxygen concentration never exceeded 0.5 %, and the primary backfill was >80% argon, meaning there was no flammability risk. Radiolytic hydrogen was also observed in wet pool storage, where the vented canisters discharged a portion of the water backfill as a result of gas production. The 344 canisters (268 fuel debris, 62 filter, and 12 knockout type) were dewatered, loaded in groups of seven into a double-barrier shipping cask, and transported to the U.S. Department of Energy site in Idaho for 10 years of pool storage.

Decisions were made to move the debris to dry storage, and the canisters were dried by heated vacuum drying. Heated drying was required due to the low decay heat of the debris (maximum 60 W per canister, average 29 W/canister) and the presence of low-density concrete filler in the void space of the debris canisters. Drying was necessary to minimize radiolytic hydrogen production and to assure the elimination of water moderator for prevention of recriticality. Groups of 12 dried canisters were loaded into welded, vented, selectively shielded carbon steel dry-storage canisters that were moved from the pool area and placed into horizontally oriented concrete shield modules at a location approximately 18 miles from their wet-storage facility. Monitoring of the canisters for radiolytic hydrogen buildup has shown no significant hydrogen production and no release of radioactive material through the high-efficiency particulate sintered-metal filter vents. Various issues remain that need to be resolved prior to transfer of the material to what is assumed to be ultimate repository disposal.

A portion of this report discusses the process of debris recovery, which was, as part of the management action, approximately a decade of eventful investigation and development of solutions to problems that became progressively clearer as obstructions were cleared. Implicit within the design response were solutions that created later challenges. Although long-term interim storage has been uneventful, the debris were not treated to eliminate potential for production of radiolytic hydrogen, or to minimize the potential for water intrusion, which could have an effect during long-term disposal.

The current proposed approach for final disposal is to remove the individual debris canisters from the dry-storage system canister and repackage them into standardized canister overpacks that would be incorporated into a final-storage system canister. The standard overpacks would probably be transported to the disposal site for insertion into the final-disposal canister assembly.

Some management challenges exist due to institutional uncertainty regarding the ultimate disposition of the material. If the fissionable material had been recovered from the debris immediately following retrieval, a substantial amount of void and container volume necessary to store the debris would have been eliminated. Alternately, the loose debris could have been processed into a monolithic waste form suitable for disposal, eliminating voids and concerns of water intrusion and the attendant issues of radiolytic hydrogen generation and recriticality. Recovery by conventional dissolution and reprocessing would have been problematic due to inconsistent solubility of the ceramic phases of the melt. Reprocessing of commercial fuel in the United States has been prohibited by executive order since 1976. Treatment of the debris by conversion to a glass or glass-ceramic form could be achieved by the use of cold-crucible melt technology.

The entire operation of recovery was performed with the oversight and approval of the U.S. Nuclear Regulatory Commission (NRC), whose representatives were called upon early in the recovery process to engage quite directly in the design and decision-making process because of the uncertainty of the conditions and the immediacy of the need for clear direction. Due to the engagement of federal regulations, the process also included the development and approval of a Programmatic Environmental Impact Statement. At present, the debris-storage system is monitored according to an aging-management plan as part of its NRC license. This plan addresses structural concrete monitoring and inspection of the external surfaces of steel components such as the dry-shielded canister (DSC).

Prior to the year 2035, the debris is mandated to be repackaged for incorporation into a final waste-disposal package for removal from Idaho according to a 1995 agreement between the State of Idaho and the U.S. Department of Energy. This is expected to require the design and construction of a facility capable of opening the DSC and transferring the TMI-2 canisters into an alternate overpack.

CONTENTS

FIGURES

TABLES

ACRONYMS

ACES	automatic cutting equipment system
ALARA	as low as reasonably achievable
ASME	American Society of Mechanical Engineers
B&W	Babcock and Wilcox
BS	borosilicate
CEA	Comissariat A L'Energie Atomique Et Aux Energies alternatives (French Atomic Energy Commission)
CRDM	Control Rod Drive Mechanism
DOE	Department of Energy
DSC	dry shielded canister
EG&G	Edgerton, Germeshausen & Grier, Inc.
EPRI	Electric Power Research Institute
GEND	General Public Utilities, Electric Power Research Institute, Nuclear Regulatory Commission, U.S. Department of Energy
GPU	General Public Utilities
HEPA	high-efficiency particulate air
HEU	Highly enriched uranium
HSM	horizontal storage modules
HVDS	heated vacuum drying system
INEL	Idaho National Engineering Laboratory
INL	Idaho National Laboratory
INPO	Institute of Nuclear Power Operations
INTEC	Idaho Nuclear Technology and Engineering Center
ISFSI	independent spent fuel storage installation
JRC	Joint Research Centre, Karlsruhe
LCSA	lower core support assembly
LICON	light-weight concrete
LOCA	loss-of-coolant accident
MELCOR	Sandia Laboratory-developed integrated coremelt software
NRC	Nuclear Regulatory Commission
NUHOMS	NUTECH horizontal modular storage system
NUTECH	Nuclear Technology, Inc.
OD	outer diameter
PORV	pilot-operated relief valve
PWR	Pressurized water reactor

ROSA	remotely operated service arm
RPV	reactor pressure vessel
SAR	safety analysis report
SDS	submerged demineralizer system
SEM	Scanning Electron Microscopy
SSTR	Solid-state track recorders
TAN	Test Area North
TLD	thermoluminescent dosimeter
TMI	Three Mile Island
US	United States
USDOE	United States Department of Energy
VECTRA	Formerly Pacific Nuclear Technologies, bankrupt in 1997, previously NUTECH. Assets acquired by Chem Nuclear, storage designs acquired by Transnuclear/Framatome, later AREVA, now ORANO

Management of the Three Mile Island Unit 2 Accident Corium and Severely Damaged Fuel Debris

1. Management of Severely Damaged Fuel and Corium

The best-documented and longest-managed example of severely damaged nuclear fuel and corium is the debris from the meltdown accident at Three Mile Island Nuclear Generating Station, Unit 2, (TMI-2) located in Dauphin County, Pennsylvania, USA, near Harrisburg. An aerial view of the facility is shown in Figure 1. The process of system recovery and core removal was done forensically, to understand the effects of loss-of-coolant, the dynamics of the melt and the release of fission products. As the recovery progressed, international laboratories participated in the characterization and analysis of the debris to understand the sequence of events that occurred in the core.

The accident recovery and debris management process following initial post-meltdown stabilization included core status, melted core characterization, and design phases for core removal, packaging, and transportation. Following interim wet storage, a dry storage system design was identified and adapted for use with the debris and its unique canister designs.

1.1 Background

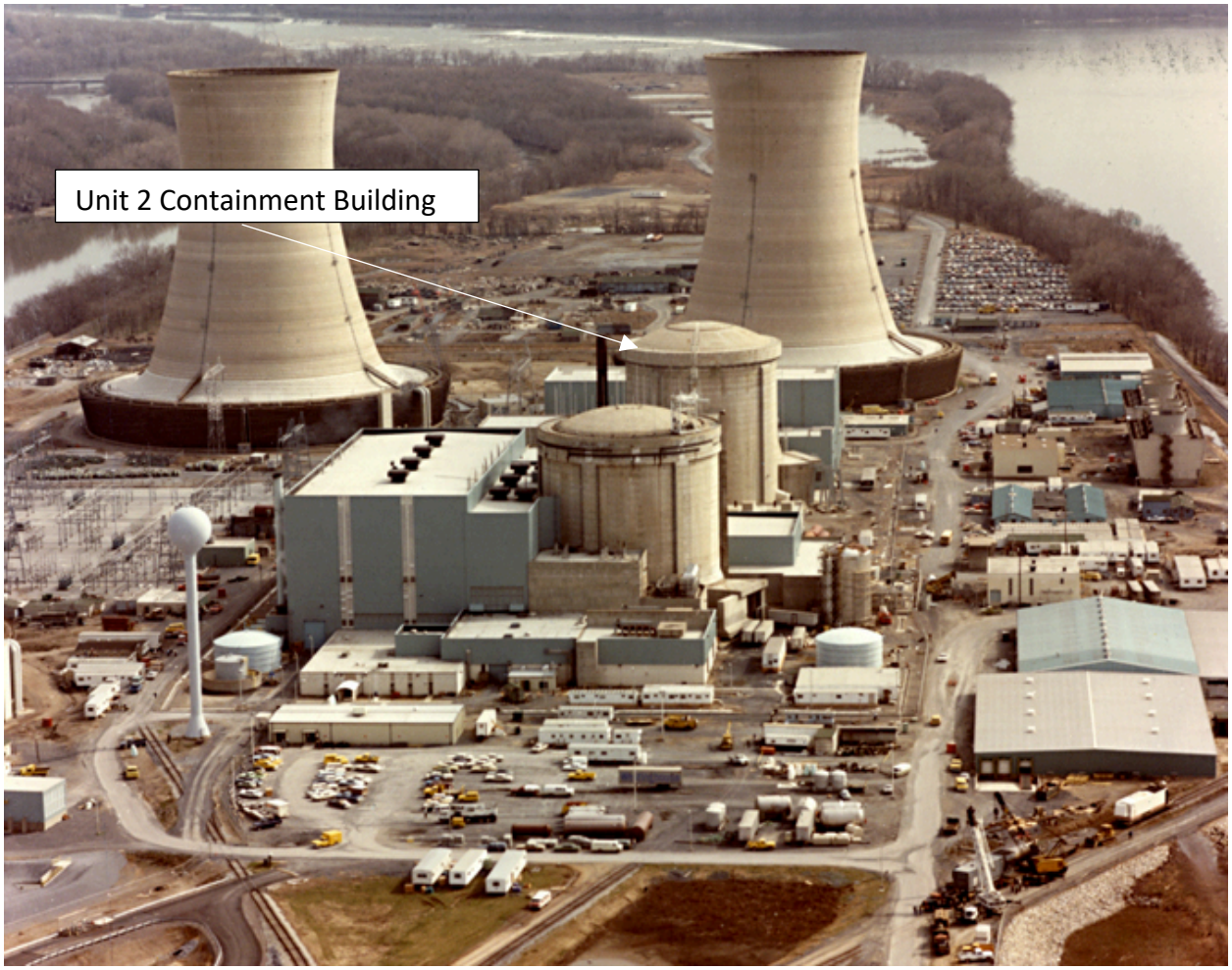

Figure 1. Aerial View of Three Mile Island Nuclear Generating Station. (Courtesy INL)

TMI-2 was a Babcock and Wilcox (B&W) 177FA pressurized water reactor (PWR) rated at 890 MW electric (2770 MW thermal) output with two primary cooling loops, each having a once-through steam generator and a core composed of 177 fuel assemblies. The assembly design used a 15 × 15 rod array containing 208 3.9 m-long fuel rods with an active fuel length of 3.7 m, 16 Zircaloy control rod guide tubes, and one Zircaloy center-position instrument tube with eight Inconel-814 spacer grids to maintain rod positioning and upper and lower end fittings of Type 304L stainless steel. A graphic depiction of the 15 × 15 rod fuel assemblies is shown in Figure 2. The fuel was composed of 9.36 mm OD uranium dioxide (UO_2) pellets with enrichment ranging up to 2.98 wt%. Seventy-two of the assemblies contained Zircaloy rods with 1% boron carbide (B_4C) burnable poison, interspersed within 94% alumina (Al_2O_3) pellets amounting to a total of 626 kg. The total UO_2 fuel mass was 94,029 kg, with an average ^{235}U enrichment of 2.265 wt%. The Zircaloy-4 cladding mass was 23,177 kg, with zirconium being 97.9 wt% of the alloy. (GEND-INF-082)

Sixty-one control rod assemblies, using 304L stainless steel-clad rods that contained 3403 mm of silver-indium-cadmium alloy provided reactivity control in the core. At the time of the meltdown, the control rods were fully inserted. The fuel burnup at that point was 3175 MWD/MTU. In a PWR design, the control rods are positioned in the core through the reactor pressure vessel upper head.

Eight stainless steel-clad axial power-shaping rods, containing 914 mm sections of silver-indium-cadmium, were included in the core.

The general reactor pressure vessel configuration, taken from a B&W training aid is shown in Figure 3.

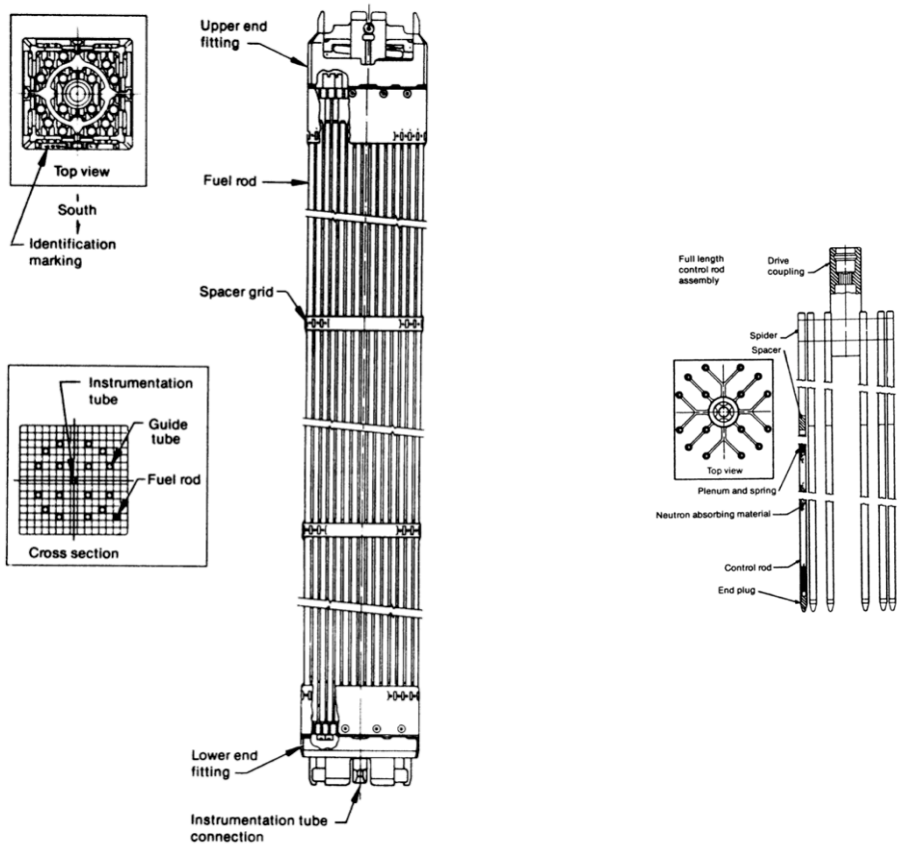

Figure 2. General Configuration of 15 × 15 Fuel Mark B Assembly, left; Control rod Assembly right. (GEND-INF-082)

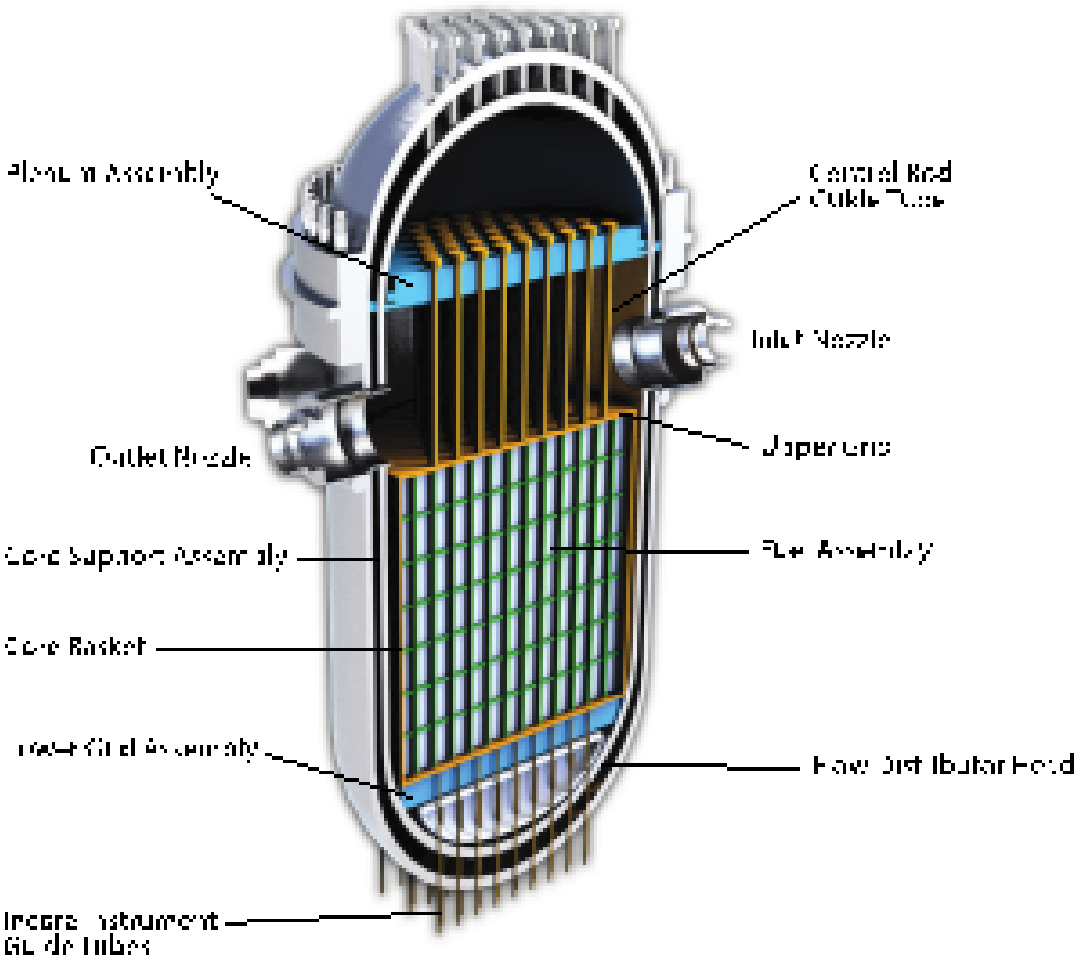

Figure 3. General PWR Reactor Pressure vessel Configuration. (Courtesy of INL).

The pressure vessel was constructed of ASTM A533 Grade B low alloy steel made as a forged cylindrical shell with a welded hemispherical bottom head. The inner surfaces were lined with austenitic 300 series stainless steel to prevent corrosion due to contact with primary coolant. The vessel inner diameter was 434 cm with a wall thickness of 21.44 to 21.74 cm, with an inner liner thickness of 0.48 cm. (Strosnider, 1994) Nominal height of the complete vessel is 13.4 m. Instrument penetrations welded into the bottom head of the vessel were made of Inconel 600. (Stickler, 1994)

PWR designs have a pressurized primary cooling loop that circulates water through the core to absorb fission energy, which is transferred via heat exchanger to water in the secondary loop(s) from which steam is generated, flowing to drive turbine-generator sets to produce electrical power. The B&W 177 design has two loops, each comprised of an independent steam generator and pumping systems. High temperature coolant goes from the core via one hot leg and enters the top of the steam generator. Reduced temperature coolant exits the steam generator and is returned to the core via two cold legs which each

have a coolant pump. Primary cooling water contains boron to provide supplemental reactivity control. Steam is produced in the secondary side of the steam generator, isolated from the primary coolant. Feedwater in the secondary is demineralized with ion exchange resins to minimize any dissolved chemical constituents that could cause problems in the steam system. The B&W once-through steam generator design has a smaller secondary coolant volume than that used in comparable Westinghouse or Combustion Engineering PWRs that use U-tube steam generator designs. In the event of a loss of feedwater, the once-through design may will boil dry more rapidly than the larger systems. (NUREG/CR-5640, 1989) Steam condensed following passage through the turbines was returned to the system by condensate pumps. The primary cooling loop was operated at 15.5 MPa at 288C as controlled in a pressurizer vessel to maintain the primary core cooling water in the liquid phase. The pressurizer vessel is maintained partially full of steam and partially of water to allow for expansion of the primary coolant due to core temperature heatup. If the system exceeds design pressure, the pressurizer has a relief valve that discharges to an overflow tank. System operability depends on having water in the secondary steam generator loops to remove the heat generated by fission. A schematic version of the plant is shown as Figure 4.

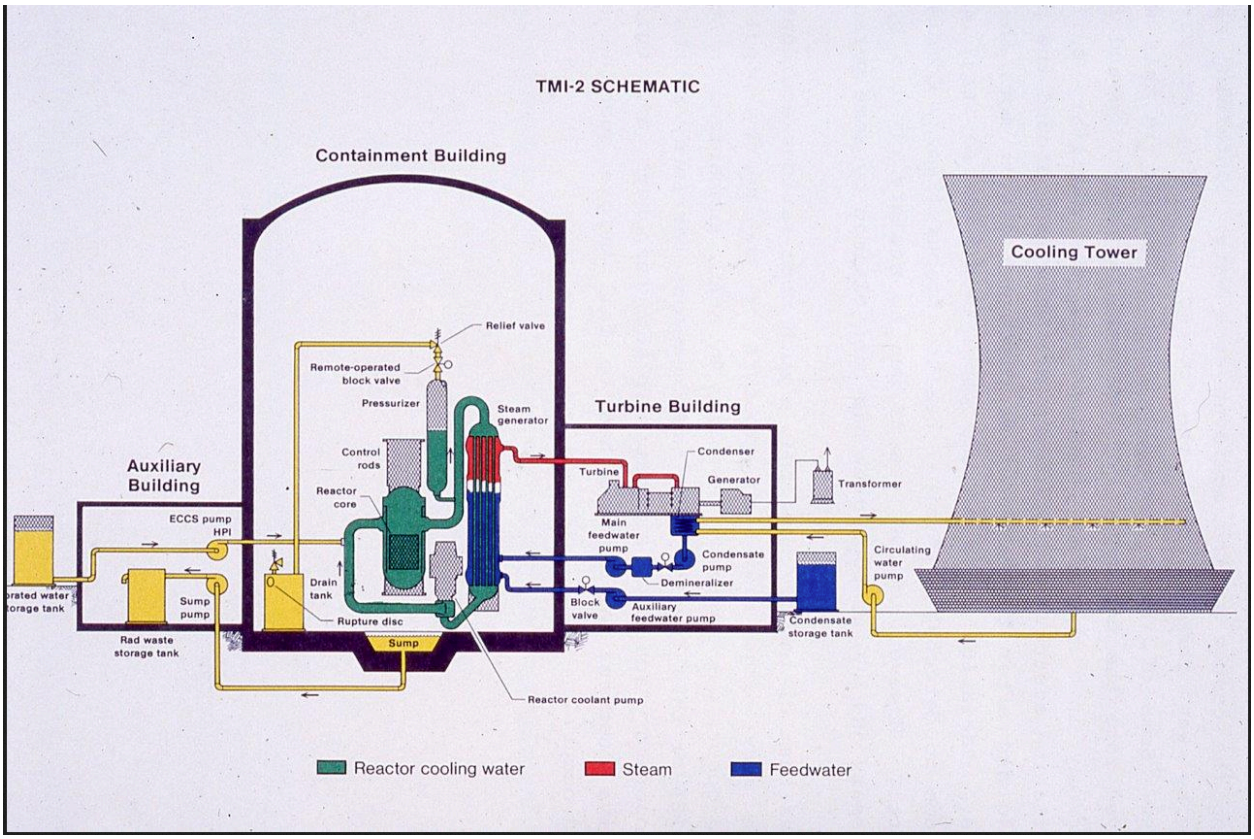

Figure 4. Simplified TMI-2 Reactor Process. (Courtesy NRC/INL tmi2kml)

Accident Description

At 4 am on March 28, 1979, Three Mile Island Unit 2 condensate pumps supplying feedwater to the secondary loop shut down while the reactor was operating at 97% power with four reactor primary cooling pumps running. The reactor had operated since March 7 without interruption. The loss of feedwater would normally have been compensated for by the auxiliary feedwater system, however the supply to the auxiliary feedwater pumps was valved out following a maintenance test on the feedwater ion exchange system. Lacking secondary loop circulation to remove fission and decay heat, the primary coolant increased in temperature and volume, increasing the system pressure to the extent that the electrically-actuated Pilot-Operated Relief Valve (PORV) on the pressurizer vessel opened within four seconds of the loss of feedwater. After nine seconds, the reactor shutdown system inserted control rods to terminate criticality. System pressure decreased as a result of the valve opening and the core shutdown. The PORV should have closed as a result of the reduced pressure. A design flaw in the valve caused it to remain open, and a control system flaw gave operators the indication that the valve had closed. The high-pressure water injection system automatically started to maintain the water level in the primary loop. Because the PORV was open, the pressurizer was not able to maintain the coolant in the core in the liquid phase, allowing steam to form, causing an increase in water level in the pressurizer. The indication of increased water level in the pressurizer caused the operators to shut off the high-pressure water injection system, on the assumption that operational vapor space in the pressurizer was needed to allow system control. The pressure in the system decreased and the water level increased. Due to the increase of steam in the primary loop, the primary cooling pumps began to cavitate due to the vapor-liquid composition. The operating pumps were shut down approximately 100 minutes after the initial feedwater shutdown. Lacking the circulation of the primary pumps, the coolant boiled off to the point that the fuel in the core became uncovered, allowing the temperature to rise further. A significant increase in containment building radiation instruments occurred at 142 minutes. Thermocouple data indicated that by 150 minutes, the core temperature rose to the point at which the zircaloy cladding began to fail, with zirconium metal reacting with the steam, releasing fission products into the primary coolant water. The steam-zirconium reaction is highly exothermic, generating hydrogen and raising the net core temperature further. Molten fuel sank to lower levels in the core, solidifying at the vapor-liquid interface. Despite the high temperatures and high hydrogen content of the system, oxygen was being consumed in the zirconium metal to zirconium oxide reaction, resulting in a condition with low potential for explosion or deflagration. During this time, water and steam were being discharged to the drain tank to the extent that the tank rupture disk failed, allowing release of the contaminated coolant to the reactor-building sump.

Approximately two and one-half hours after the incident started, after consultation with the vendor, operators were able to determine that the pressurizer relief valve was stuck open and closed the block valve downstream of the relief valve (PORV). Once the relief block valve was closed, a primary coolant pump was started briefly to try to cool the core and stabilize the system. The influx of water is believed to have caused the upper sections of the relatively intact remaining fuel to shatter and fall onto the top of the melted material in the center of the vessel. Introduction of water from the cooling pump and the emergency injection system resulted in raising the core water level to the point that the core was again covered by 210 minutes. In another fifteen minutes, the core temperature had risen to the melt temperature of the uranium-zirconium oxide mixture that formed the bulk of the melt, causing a portion of the melt flow through a hole in the side baffle plates, draining through the Upper and Lower Core Support Assemblies, solidifying on the bottom head of the reactor vessel. The presence of cooling water kept the reactor pressure vessel wall from reaching the melting temperature of the steel, although some attack was later noted on the in-core instrumentation nozzles.

At this point, it was no longer possible to circulate water using the primary cooling pumps, so the core was cooled using once-through operation through the relief system to remove the heat load. The system was stabilized after about 16 hours and core steam generation ceased. Hydrogen from the zirconium-steam reaction had been released into the air-filled reactor containment building via the tank overflow to the sump, ultimately reaching a concentration in excess of 4 vol/%, which it is assumed was ignited by some electrical switchgear, resulting in a deflagration that produced a pressure surge of 0.19

MPa, significantly less than the containment building design pressure.

The water that had been discharged from the drain tank into the containment building sump was highly contaminated from the fission products being released from the melting core, meaning that manned entry into the building was not performed until July of 1980. Cleanup of the water progressed for several years. Boric acid was added to the water as a criticality prevention measure.

The first video inspection of the core was not accomplished until 1982, followed by ultrasonic mapping of the core void in 1983. Probing of the melt determined that loose material was present on the upper surface. Samples of the loose material acquired in 1984 gave the first indications of the character of the melt. Ultrasonic mapping of the upper debris surface and a ten-location core bore through the depth of the melt to the lower core support structure was performed in 1986.

As a result of the accident, approximately 62 tons of the core assemblies melted, and an estimated 20 tons of core material flowed from the central core region and solidified on the lower vessel head. The upper plenum was largely intact, and analysis of the control rod lead screws indicated that the temperature above the central core region reached 1250 K while the perimeter only reached 700 K, with the damage zones approximately 1.2 m in diameter and confined to the areas below the upper spacer grid. (Osetek 1990)

Core damage was defined in terms of four zones, 1) a 9.3 m^3 void 1.5 to 2 m deep in the center of the upper core, 2) a 0.6 to 1 m deep layer of loose fragmented debris that reached 2200 K, 3) 32.7 metric tons of solidified metal and ceramic mixture, formerly molten core, primarily composed of uranium and zirconium oxide with metallic silver and iron inclusions, and 4) partial and full-length fuel assemblies around the periphery of the melt. The central melt was surrounded by a crust, with the 10 cm layer below the melt composed of zirconium, iron and silver metal, and the 1 to 3 cm upper crust containing iron and silver with indium and nickel.

The core support assembly was damaged in the east quadrant, where baffle plates partially melted, allowing molten material to flow into the lower core support assembly and contact the wall of the reactor pressure vessel.

Low-volatility fission products, ^{144}Ce, ^{154}Eu, and ^{155}Eu, and medium-volatile fission products, ^{90}Sr, ^{125}Sb, and ^{106}Ru, were detected in melt samples while ^{85}Kr, ^{137}Cs and ^{129}I were largely released from the fuel. Approximately 3.5% of the medium-volatility species were transported beyond the reactor- vessel, with only 0.1% reaching the reactor coolant-bleed tanks in the auxiliary building. Isotopes ^{125}Sb and ^{106}Ru were found to have been selectively deposited in the metallic region below the core at concentrations six to 20 times that found in the fuel. Isotopes ^{85}Kr, ^{137}Cs and ^{129}I were transported by the cooling-system and distributed throughout the reactor-building basement. Approximately 20% of the ^{137}Cs and ^{129}I was retained in the fuel debris, while 85% of the ^{85}Kr was released to the containment building atmosphere.

A consortium including General Public Utilities (GPU), Electric Power Research Institute (EPRI), the U.S. Nuclear Regulatory Commission (NRC), and the U.S. Department of Energy (DOE), collectively known as GEND, was responsible for determining the recovery process and directing the research into the cause and effects of the accident. A series of GEND reports containing predictions and documenting design choices was produced; they are available for review.

Over a period of seven years, the reactor building was decontaminated, the water treated, the reactor vessel head was removed, the core was recovered with the reactor vessel full of water, the recovered core debris was placed in canisters and shipped from Pennsylvania to Idaho National Laboratory for wet storage. In 1995 a decision was taken to move the debris from wet-to-dry storage. This decision was based on the economics of actively maintaining controlled conditions and assuring that no contaminated water could leak into the environment in a wet pool system versus the passive operation of an above-grade dry-storage system. The transfer of the debris to dry storage began in 1999 and was completed by 2001. The stored debris has been maintained in vented dry storage canisters at INL's Idaho Nuclear Technology and Engineering Center (INTEC) CPP-2774 facility under license from the U.S. NRC since its transfer.

Management of the debris was done according to primary concerns that included prevention of criticality during material recovery and packaging, avoiding potential chemical reactions including pyrophoricity and hydrogen ignition, preventing personnel radiological exposure beyond regulatory limits and prevention of environmental radiological release.

Recent review of the accident root cause targets the lack of analysis of loss-of-coolant accident (LOCA) scenarios with a small discharge cross-section (such as that resulting from the stuck PORV) and the fact that the PORV was not identified as a safety-significant component. Because the Safety Analysis Report did not include a small-break LOCA scenario, operators had no training on the correct response to this type of incident. Given that PORVs had failed to close at other facilities on at least 8 other occasions, having that information available to the operators might have allowed them to identify the problem in time to prevent further core overheating. It is also noted that the type of PORV used in this design was prone to having closure problems after discharging a two-phase steam-water flow. (Rosztoczy, 2019) The valve is shown in Figure 5.

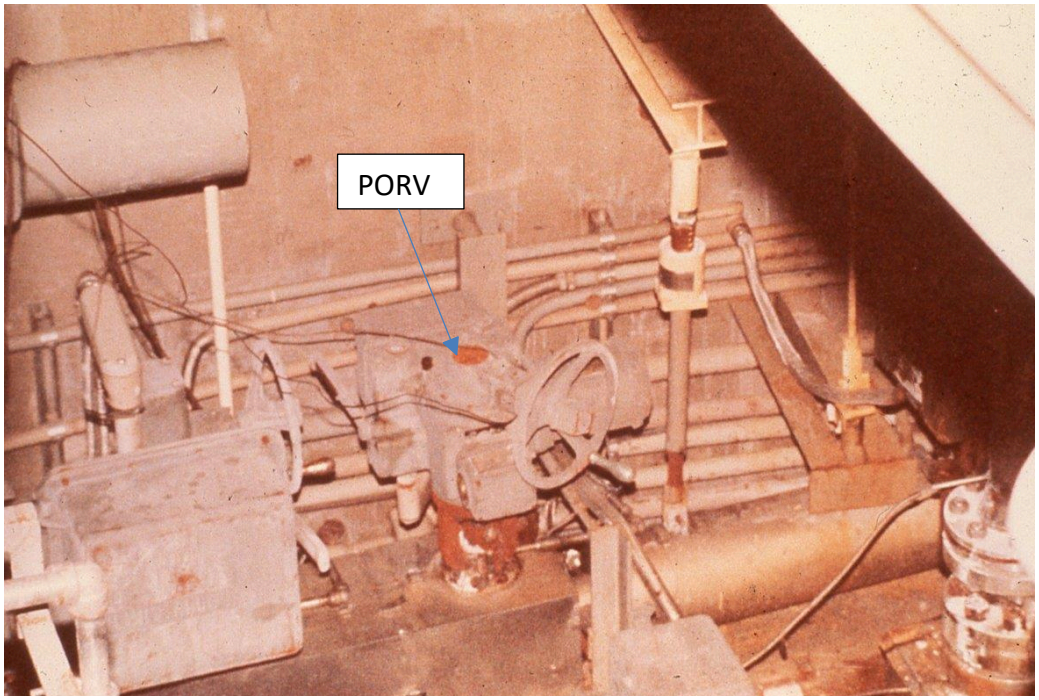

Figure 5 Pilot Operated Relief Valve. (Courtesy of INL)

It should be noted that a multitude of documents have been generated regarding virtually all aspects of the TMI-2 recovery. The GEND reports discuss recovery design and progress and are available through several on-line libraries, and various scientific papers have been published in Volume 87 of the journal Nuclear Technology 1989, Parts 1 and 2. This document is a digest of parts of this substantial history. Idaho National Laboratory maintains a knowledge management library on behalf of the Nuclear Regulatory Commission (NRC) at the website https://tmi2kml.inl.gov/, as well as at the INL Digital Library website https://inldigitallibrary.inl.gov/TMI. Many of the documents and figures used in this report originate from these two sources. Pennsylvania State University and the University of Tennessee also maintain document archives on TMI-2.

1.2 Timeline of Three Mile Island Unit Two Cleanup

- March 1979: TMI-2 loss-of-coolant accident; EPICOR-I water treatment system begins operating
- April 1979 Installation of 4-57,000 L and 2-95,000 L contaminated water storage tanks

- July 1980: 43,000 Ci ^{85}Kr vented from reactor building; First manned entry into reactor building
- March 1981: NRC directs core debris removal from the site; SDS system begins water decontamination
- May 1982: Quick Look video inspection
- 1983: Ultrasonic mapping using core topography system
- September–October 1983/March 1984: Loose debris grab sampling and analysis; Leadscrew analysis
- 1981–1984: Defueling equipment design
- 1984: Shipping cask design
- February 1984 Polar crane load-tested, authorized for use; July 1984: Reactor vessel head removed
- December 1984: Upper plenum jacked up; May 1985: Plenum removed to defueling pool
- October 1985: Defueling begun
- July 1986: Shipment of 125 tons of core debris to INL begun
- April 1990: Complete 22 rail shipments to INL; debris in wet storage
- May 1995: DOE/State of Idaho Settlement (Batt) Agreement mandates wet-to-dry conversion
- June 1997: Initiation of NRC license process for dry-storage facility
- March 1999: TMI-2 independent spent fuel storage installation (ISFSI) NRC licensed for core material
- March 1999: First shipment of core debris from Test Area North (TAN) to Idaho Nuclear Technology and Engineering Center (INTEC) at INL using OS-197 cask transfer to NUTECH horizontal modular storage system (NUHOMS) storage modules
- April 2001: Last shipment (29 truck shipments) from TAN to dry storage
- Present: Core debris in vented dry storage at INL; Aging-Management Program monitoring hydrogen and structural conditions
- Future: Repackaging for final disposal to be completed prior to 2035. (per Settlement Agreement)

2. Water Treatment and Reactor and Auxiliary Building Cleanup

The initial response included cleanup of approximately 2.12 million liters of water from the flooded reactor containment and auxiliary building. The temporary, portable EPICOR-I unit was returned to the facility the day after the accident and began processing lower activity (<1 μCi/ml) water immediately.

The EPICOR-II system was developed to process higher-activity water (1-100 μCi/ml) to supplement the EPICOR-I system. It began operation in October 1979, and used a three-stage system of prefilters and organic resins to remove particulate and dissolved fission products. The submerged demineralizer system (SDS), was developed to process water with activity greater than 100 μCi/ml and was installed in the TMI-2 fuel pools, beginning operation in September 1981. The SDS used a series of filters and zeolite inorganic ion exchange media to remove dissolved fission products. A schematic of the filtration and treatment systems is shown in Figure 6.

2.1 Decontamination

Although it is common to focus on the mechanical and logistical heroics involved in removing the melted core material from the reactor vessel that occurred years after the accident, a major part of the initial post-accident recovery was decontamination of various parts of the reactor, auxiliary, and fuel-handling buildings. Contaminated water was released to the reactor-building sump in the early minutes of the accident when the primary coolant being dumped to the reactor-coolant drain tank caused the overflow valve to open and then the rupture disc to burst. This sump water was transferred to the auxiliary building sump tank. Other systems, including the makeup and purification system, also received highly radioactive core material. A relatively small quantity of core debris, estimated to be less than 10 kg, was spread through these systems following the opening of the PORV.

Reactor-building dose reduction started with processed-water flushes of all surfaces of the accessible areas between the 305 and the 347-foot levels. This was followed by mechanical scabbling (surface removal) of painted and concrete surfaces to remove embedded activity. Cleaned areas were sealed with epoxy paint and other coatings to minimize recontamination potential.

Due to the material's porosity, surface material needed to be removed from some concrete-block wall surfaces using a remotely operated water lance. The internal voids of the block were flushed to remove sediment that had settled inside.

The water generated by the flushing, scabbling and scarification was processed through the submerged demineralizer and Epicor-II filtration and ion exchange systems. The surface-cleaning operations generated an estimated 4900 kg of sludge. A remotely operated sludge-suction system was able to remove sludge from approximately 40% of the accessible reactor-building basement-floor area. An estimated 4 kg of fuel was contained in the sludge.

Fuel material and contamination in the reactor cooling-system were removed using spray nozzles and submersible pumps during the first phase, followed by a remotely operated submersible that was used to pick up large discrete pieces that were present in the pressurizer vessel.

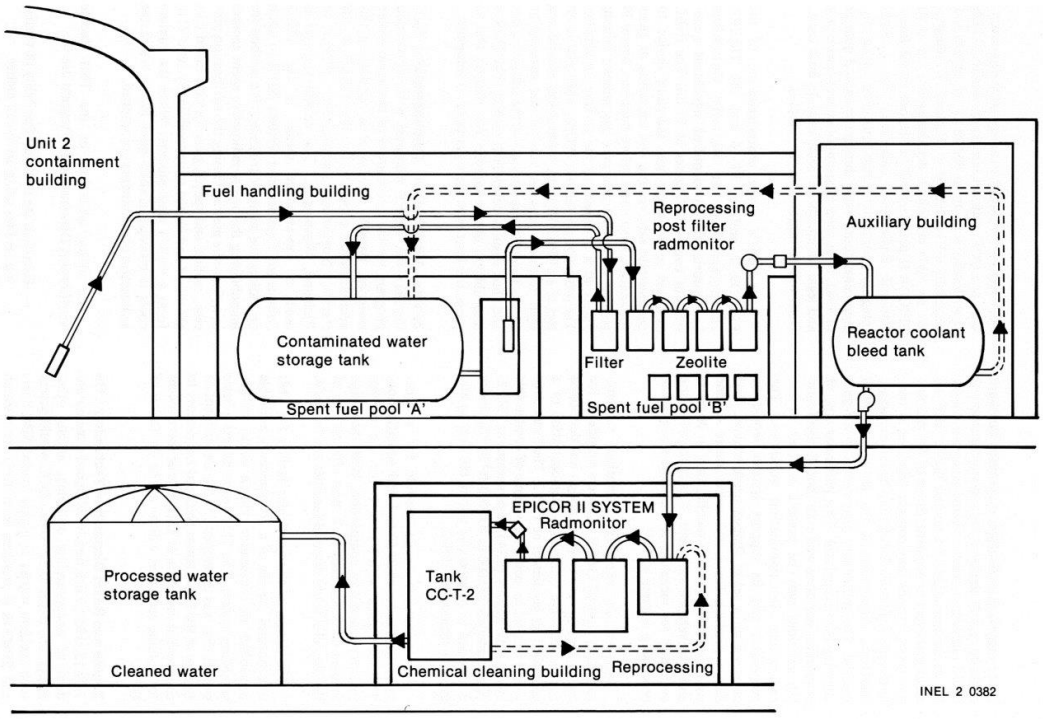

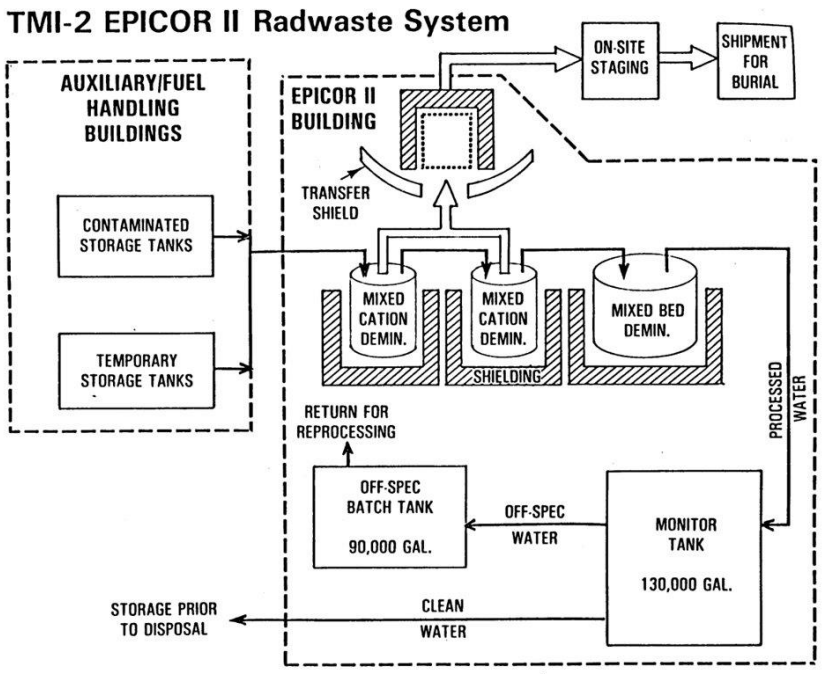

Figure 6. SDS and EPICOR Water-cleanup schematics. (Courtesy of INL)

Following treatment, the water was contained onsite in two 1.9 million-liter epoxy-coated welded carbon steel tanks. In some instances, the water was recycled to be used for decontamination purposes.

In accordance with the supplement to the Environmental Impact Statement, 8.7 million liters of treated water was disposed by evaporation through the processed-water disposal system. This unit was a closed-cycle evaporator that discharged the vapor through the facility's 30.5 m tall exhaust stack. Included in the vapor released to the environment was an estimated 1020 curies of tritium and 2.3 curies of other nuclides including ^{90}Sr, ^{14}C and ^{137}Cs. An estimated 136 tonnes of boric acid was included in the effluent. (GPU, 1993)

3. Core Condition Assessment

The response to the TMI-2 meltdown followed a progression of investigation of the problem and design of tools and processes in the absence of clear information. During the cleanup of the buildings and management of the large quantity of water, analytical efforts were made to reconstruct the accident and project the degree of damage that the core had undergone. Several scenarios were considered and integrated into a report identified as GEND-007. This document served as a design basis for the various proposals for core recovery. A primary assumption in this document was that the majority of the fuel assemblies were intact. Some of the predictions were developed using a computer model called MELCOR, which was developed for the U.S. NRC by Sandia National Laboratory. MELCOR is an integral model which simultaneously solves for values of material melting temperature, fission-product release and associated chemical reactions to predict the extent of core damage. MELCOR is still available as predictive tool, having been revised extensively as various aspects of actual and experimental work have been done to validate it. Other aspects of loss-of-coolant behavior were analyzed using RELAP/SCDAP to evaluate the thermal-hydraulic performance of core cooling systems.

To proceed with core recovery, it was necessary to validate the predictions by means of visual examination. Video inspection was performed by inserting a camera into the reactor vessel through a control rod penetration. After the confirmation that a significant amount of the fuel had been destroyed, the DOE-funded investigation of the characteristics of the damaged fuel for the purpose of understanding the nature of the meltdown from the standpoint of material interactions.

Due to boiling and selective condensing, the primary coolant's boron concentration was found to be well below the operating condition of 1000 ppm, and due to uncertainty about the condition of the core, the boron concentration of the water filling the reactor vessel was raised to 3000 ppm and, ultimately≤ to 4350 ppm during defueling to assure that the debris remained subcritical even when the material geometry was not being controlled.

Characterization of the melted core had aspects regarding technical issues regarding the extent and progression of the accident. The technical issues addressed were:

- What part did reactor-system thermal hydraulics play in the meltdown?
- What was the core damage progression?
- In what modes could the reactor pressure vessel have failed?
- What were the mechanisms of fission-product release and transport?

Characterization also was needed as the basis for safe handling and interim storage of the debris, especially regarding chemical and physical material stability, potential for contamination spread, pyrophoricity and criticality. Ultimately, characteristics important to long-term storage and potential disposal like leachability were identified when the debris was transferred to dry storage by measuring the constituents in the canister water in which the debris was immersed for ten years. This data is provided in Table 10.

To answer these questions, data on the core and system conditions were needed. A characterization campaign was undertaken as part of the overall cleanup activities.

Characterization

Characterization included:

1. In situ examination of the core and vessel by video camera and acquisition of samples of loose material accessible within the axis of the leadscrew nozzle (grab samples) was performed prior to reactor vessel head removal.
2. Following removal of the upper head, surface-contour mapping using ultrasonic sensors was performed, individual discrete components were recovered, and core bore samples were extracted and analyzed.
3. Examination of cooling-system artifacts, including debris from the plenum cover and filters from the makeup and letdown system and control rod components such as leadscrews and support tubes.
4. Chemical analysis (gamma and mass spectrometry to establish radiological retention and elemental composition) of rubble-bed grab samples, fuel-rod segments and other identifiable control rod cluster and fuel assembly components, as well as control rod leadscrews and the coremelt samples.
5. Optical and electron microscopy as well as microprobe analysis to identify chemical constituent distribution and localized inclusion composition within samples
6. X-ray and neutron diffraction to identify sample crystal form
7. Microprobe analysis to identify chemical composition of a sample.

3.1 Vessel Internal Inspection

Several options were considered for doing a visual inspection of the reactor vessel, but logistics of crane availability and equipment movement limited the alternatives, which ultimately would have led to multi-year delays. Core characterization began in earnest in 1982 with the Quick Look program, which involved insertion of a Westinghouse Model ETV-1250 black and white analog video camera into the reactor vessel through the 35 mm ID control rod drive mechanism penetrations following the removal of the leadscrew (EPRI-7156). The camera was 31.75 mm OD × 355.6 mm long. Figure 7 illustrates the video camera insertion approach, and Figure 8 shows video images of the debris from that camera. Figure 8 shows a view of fuel components still attached to the lower side of the upper grid plate.

The initial plan was to insert the camera at center, mid-radius and outer diameter positions in the core, but removal of the B-8 control rod proved impossible, so no outer diameter location was available. The camera was suspended by its cable and used a second wire that could be used to change the camera angle for a lateral view. The camera could also be fitted with a right-angle lens for lateral viewing. In-vessel views showed a 1.2 m deep void in the center of the core. A steel probe could be inserted into the debris 30 cm before encountering a rigid layer hard stop. Pivoting the camera to look at the lower side of the core upper grid plate showed the remains of partial rods as seen in Figure 9. Suspended particulate in the water limited visibility, resulting in an incomplete understanding of core conditions.

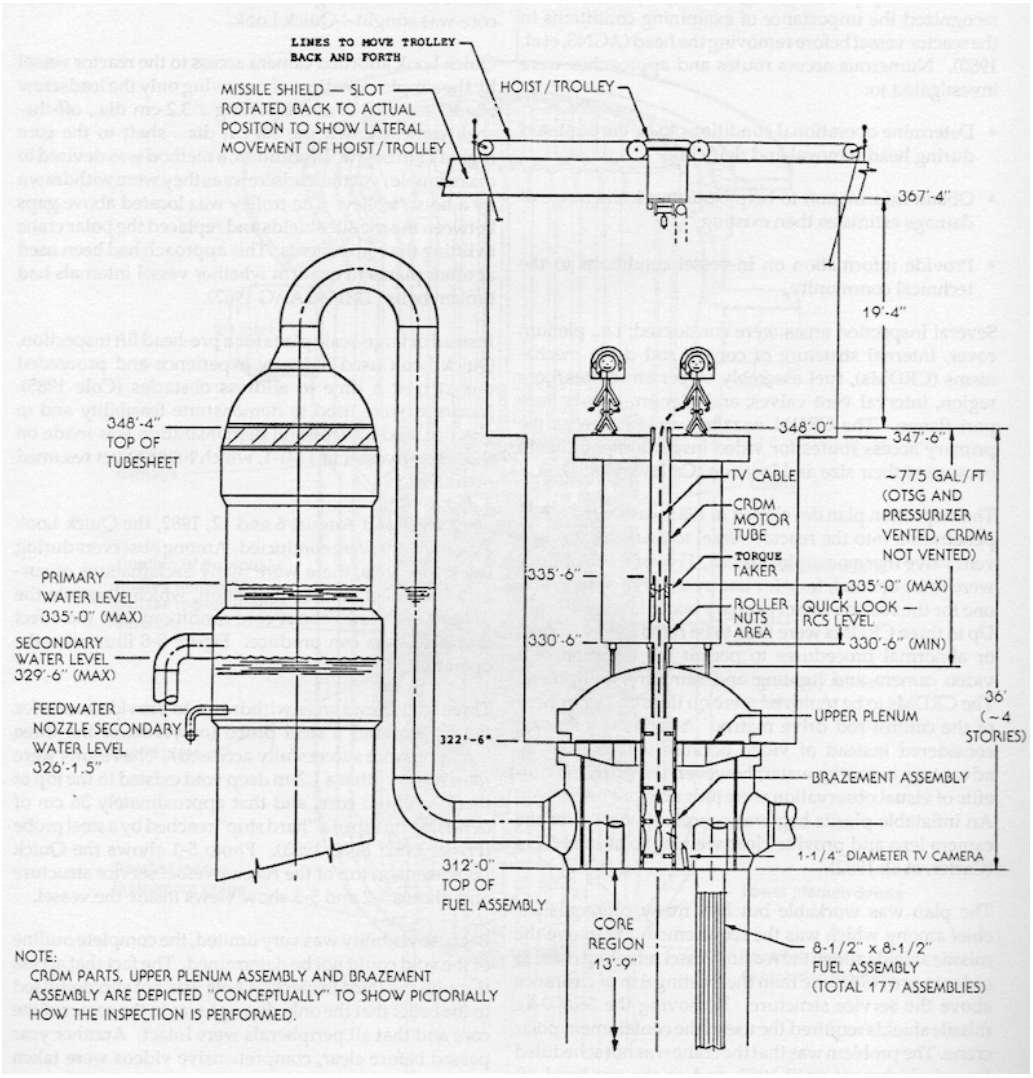

Figure 7. Quick Look video schematic cartoon. (Holton, EPRI-6931, 1990)

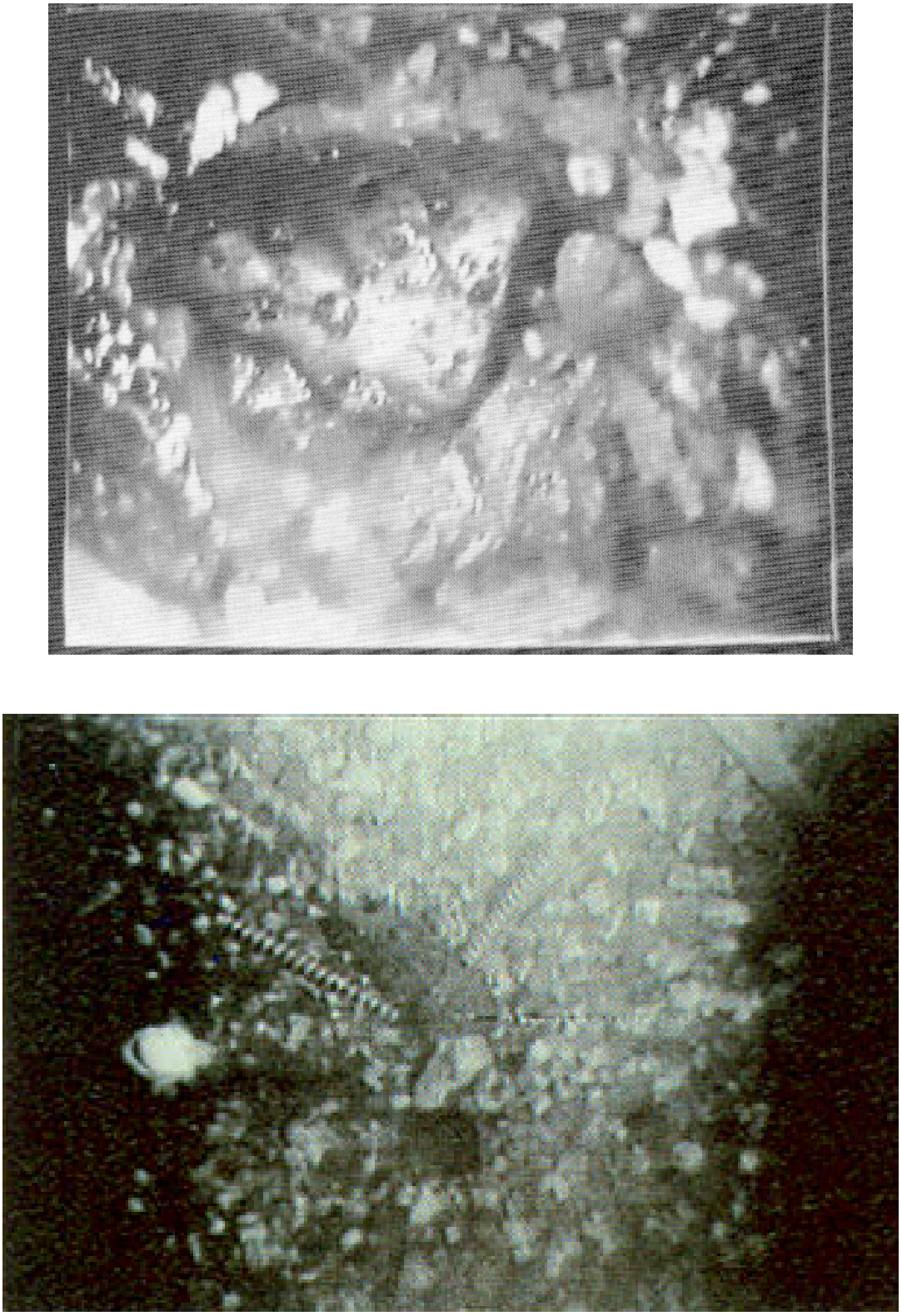

Figure 8. Quick Look video images of debris bed. (Holton, EPRI-NP-6931, 1990)

Figure 9. Fuel Assembly Remnants Hanging from Upper Grid Plate. (Courtesy of INL)

Following the Quick Look video work, debris samples were removed from the vessel using a rotating point cup sampler and a narrow clamshell tool, also inserted through control rod drive penetrations, as illustrated in Figure 10. Figure 11 shows elevation and plan views of the sampling locations.

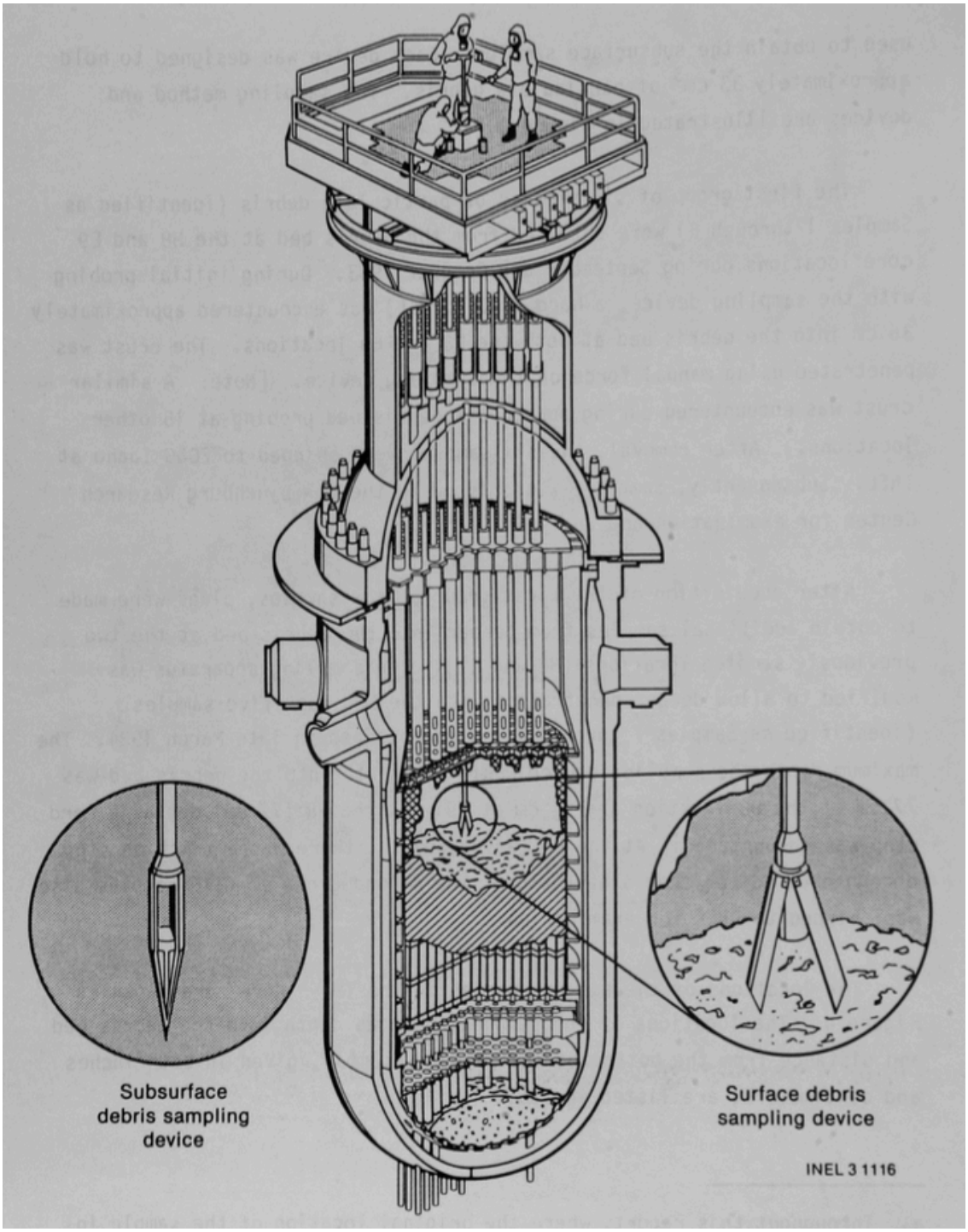

Figure 10. Loose debris grab sampling (Akers, GEND-INF-075 Part 1, 1986) October 1983 and March 1984.

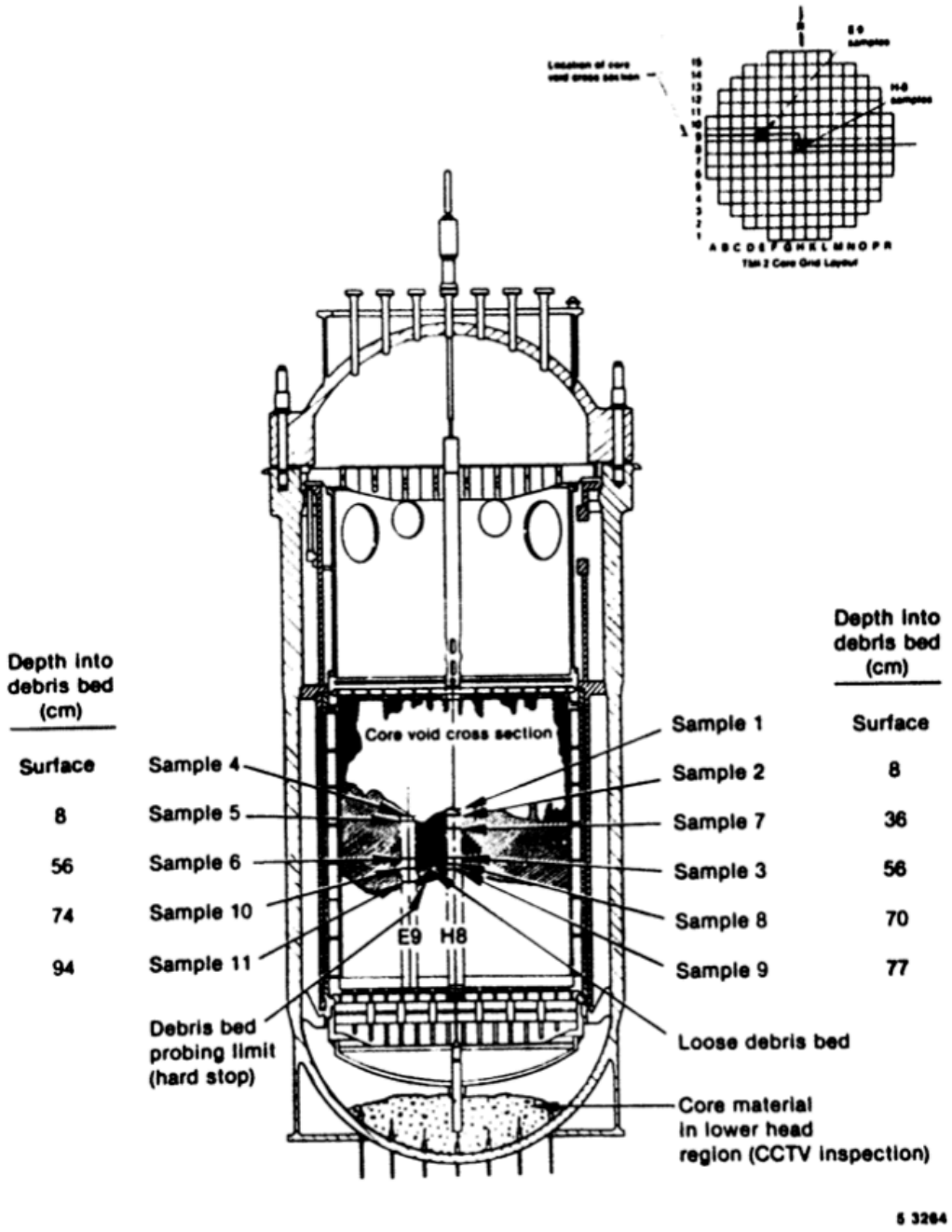

Figure 11. Loose debris sampling locations. (Akers GEND-INF-075 Part 1, 1986).

Additional video work was done after the vessel head was removed and the plenum was jacked up. A Rees model R-93 black and white analog video camera 40 mm in diameter was lowered through the downcomer area between the vessel wall and the core former barrel to inspect the area below the core support structure. This inspection required additional lighting to be able to clearly see the debris that had relocated to the bottom head. After the plenum was removed a more controlled video survey of the lower head was done, again with a Rees Model R-93 camera. Improved control was achieved by using an aluminum pole with an articulating joint to position the camera rather than just allowing it to hang from

its cable. A significant amount of the main debris recovery work in the vessel was done using the R-93 camera that had been fitted with a zoom lens and remote light and focus controls as well as a pan and tilt function. Variations of the Rees R-93 are still available through Mirion Corporation.

The underside of the plenum and the upper grid plate were imaged both with the camera submerged, and after the water level was lowered, in air so that damage and fuel debris presence could be assessed.

As the standing fuel assembly fragments were removed from the periphery of the core, damage to the baffle plates was visible, and a Welch-Allyn video probe as well as a Diaguide fiber optic camera were used. These cameras had higher resolution than the Westinghouse and Rees cameras and could operate in lower light. These views helped recovery engineers develop estimates of the amount of fuel present behind the baffle plates and design retrieval methods.

A Rees R-93 camera was inserted into the holes created during the core boring in the stratification investigation to get images at various depths inside the melt.

Eventually, color video technology was provided in the form of a fixed focal-length lens Bore Tech BT2020 camera that produced high-resolution analog images. Despite the lack of a zoom lens, this unit was a significant improvement in that being able to visualize color allowed the team to distinguish different aspects of the components being disassembled in 1988 and 1989.

To estimate the amount of fuel debris remaining in the vessel for final accountability, inspection was primarily done with the Bore Tech model BT2020 color camera. A Rees model R-93 camera was used to inspect the inaccessible areas under the Lower Core Support Assembly (LCSA). The camera was dropped through holes in the LCSA with a right-angle lens mounted to look laterally around the perimeter of the assembly. Thirty hours of video were recorded to provide evidence of the thoroughness of the recovery effort.

Radiation Detection for Fuel Location Determination

Quartz crystal solid-state track recorders were inserted into the space between the biological shield and the reactor vessel for approximately three weeks in 1983 to do neutron dosimetry to map the flux profile of the vessel. Seventeen dosimeters mounted at specific elevations on a cable indicated that the equivalent of four fuel assemblies was present in the lower head of the reactor vessel. The parameter being measured was fission rates of fissile ^{235}U, ^{239}Pu and ^{237}Np. (Gold, 1985.)

Other efforts to measure the mass of fuel in the lower head included insertion of a Westinghouse miniature ionization detector into the core through one of the accessible in-core detector tubes on the bottom of the reactor pressure vessel.

Thermoluminescent Dosimetry combined with a shielded, collimated Geiger Muller detector were used to establish a gross radiation profile of the material behind the core baffle plates by lowering a unit containing the detector and several Thermoluminescent dosimeters (TLDs) into the lower head region.

3.2 Initial Grab Sampling

Eleven samples of loose material lying on the top of the melt were recovered before the reactor vessel head was removed. These grab samples provided indications of the highly varied nature of the loose debris. Material was acquired from the center and mid-radius positions normally occupied by fuel assemblies H8 and E9. In the center location, the sample tool was pushed into the loose debris to a depth of 77 cm from the top of the debris bed and to 94 cm at the mid-radius position. The sample tools included a clamshell device and a pointed penetrator with a cup into which loose material flowed. The samples were taken from the debris surface as well as at depths of 8 cm and 56 cm from the surface. (Akers, GEND-INF-075 Pt. 1, 1986.) Figure 12 shows one type of sampler with granular material recovered.

Figure 12. Clamshell Grab Sampler with Recovered Material. (Courtesy INL)

Analysis of Grab Samples

The grab samples recovered 1.37 kg of material. Ten of the samples were analyzed at Idaho National Engineering Laboratory (INEL). Sample density and particle-size distribution measurement allowed initial classification of the sample material and gave the recovery design teams information on the material to be recovered. The bulk samples were also tested for the presence of pyrophoric and magnetic material. Gamma-ray spectrometry was used to establish fission-product retention while neutron activation analysis was used to determine fissile material content. The solid samples were dissolved to the extent possible and inductively-coupled optical emission spectroscopy (ICP-OES) was employed to determine the elemental composition of the samples, specifically for silver, aluminum, boron, cadmium, chromium, copper iron gadolinium, indium, manganese, molybdenum, nickel, niobium, silicon, tin, tellurium, uranium and zirconium. X-ray diffraction was performed to identify crystal structure. Metallographic mounting, polishing and etching revealed grain structure, and electron microscopy was able to identify elemental distribution in the exposed prepared sample surfaces.

Sample Preparation

Dissolution of the samples for wet chemical analysis was initially tried using nitric and hydrofluoric acids, which left a significant fraction of undissolved solids. The remaining solids were made soluble following high-temperature treatment using a potassium bisulfate fusion. The pyrosulfate technique included use of a caustic vapor trap to collect volatile iodine to establish the retention fraction for ^{129}I.

Strontium was separated from the solutions as a carbonate precipitate, which was counted for beta emissions to evaluate ^{90}Sr content of the samples.

Select particles greater than 1 mm in diameter were mounted and polished for optical metallographic imaging at between 15 and 500x. These samples were also examined at up to 2000x using scanning electron microscopy with energy dispersive spectroscopy for elemental analysis. Boron and oxygen content was quantified using Scanning Auger Spectroscopy. One sample was sent to the Babcock & Wilcox Research Center for investigation by the reactor vendor. Fractions of seven particles were analyzed with differential thermal analysis at the Rockwell Hanford Operations (DOE operation at

Hanford Washington) laboratories. Twenty-two particles were selected and sent to Argonne National Laboratory. The bulk material was quite radioactive, having dose rates reported as 1 Sv/hr (100 R/hr). (Akers, GEND-INF-075, 1986)

The results of the various analyses determined that most of the loose particles had inclusions that were previously molten uranium-zirconium oxide. This composition provided definitive indication that the core temperature exceeded 2800 K at various points. Some particles containing exclusively UO_2 had crystal phases consistent with having been melted, resulting in the hypothesis that temperatures may have exceeded 3100 K. Aluminum, chromium, iron and nickel were present at levels ranging from minimum detection to majority constituent in most samples in voids and at grain boundaries. An estimated 10% of the silver component of the control rods was projected to have been retained in the core based on the grab samples.

Sample Particle Size

In physical size distribution, the grab samples ranged from 30 to 6000 microns with a size bias toward large particles on top of the debris field and smaller particles at the depth of the impenetrable (hard-stop) layer. Loose debris included discrete fuel pellets, pieces of cladding, porous material, metallic surfaces, and particles that included fuel, clad and structural material. An example of a typical debris piece is shown in Figure 13. Particles with dimensions between one and five thousand microns accounted for approximately ninety percent of the samples.

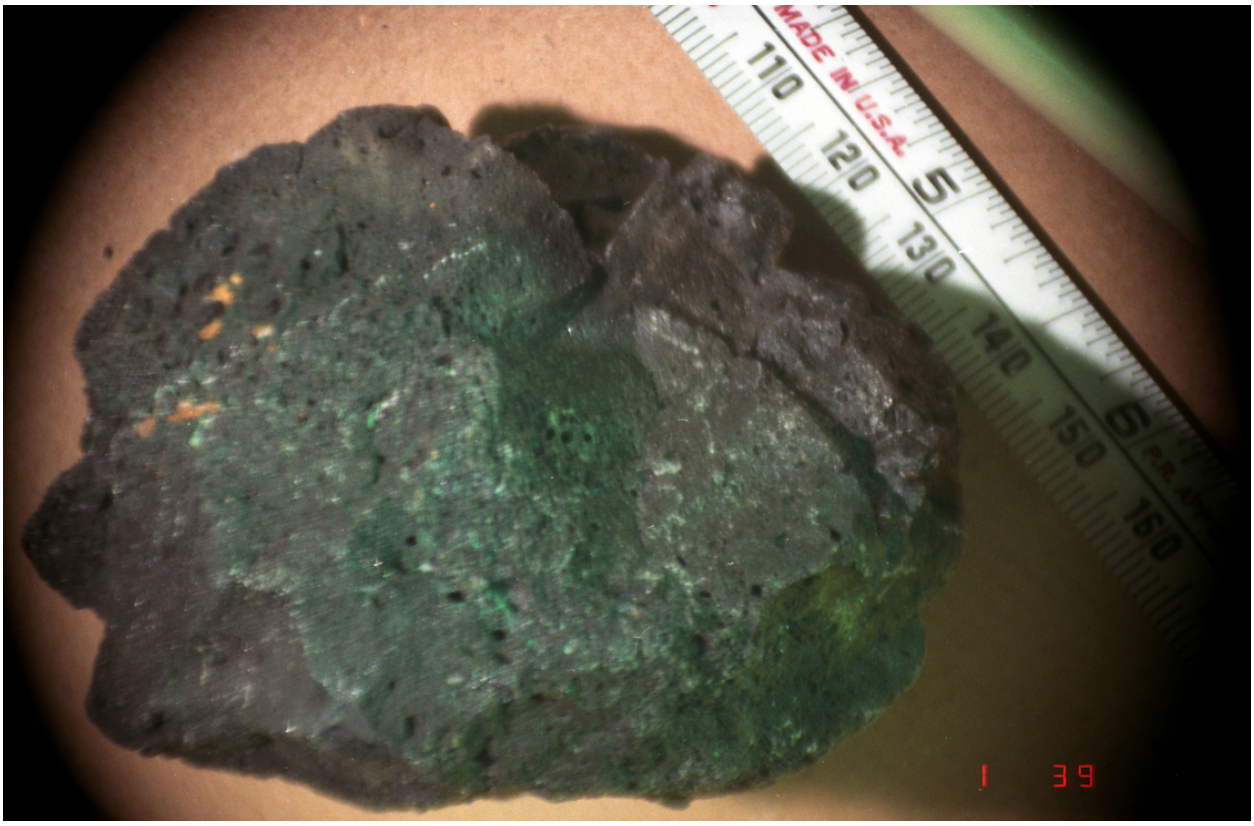

Figure 13. Debris piece retrieved from surface of the debris field in the center of the core void. (Courtesy of INL, 1984).

Examples of the general size distribution, discrete character and shape recovered from samples of loose debris material are shown in Figure 14 and Figure 15.

Figure 14. Loose material retained on sieve for size analysis. (Courtesy of INL, 1984)

Figure 15. Typical Debris Pieces. (Courtesy of INL, 1984)

Grab Sample Optical Evaluation

The grab sample material was generally categorized according to the constituents that could be identified and the apparent phases that were present. Samples were frequently described as “foamy”,

presumably resulting from gas production during the reaction from metal to oxide. The combination of composition and physical properties was used to evaluate the range of possible temperatures that had been reached for various materials. The dominant constituents were uranium and zirconium, which were present in almost all samples, either exclusively or in combination with metals from control rods or structural material. This determination involves more than single-component melt temperatures such as zircaloy, which melts at 2030K and uranium dioxide, which melts at 3120K. The various expected melt temperatures can be found in temperature-composition phase diagrams. Because diverse materials are present in the core, each combination may represent a eutectic alloy, in which the reaction between two materials lowers the melt temperature appreciably. Uranium dioxide and zirconium may form single-phase liquids that solidify into zirconium and zirconium-uranium metallic components in the absence of oxygen. Steam oxidation of solidified formerly molten material can convert zirconium metal to zirconium dioxide and uranium-zirconium oxide as discrete phases. Oxidation while molten material is at temperatures below 2800K generally results in a single-phase uranium-zirconium oxide solid solution with little porosity. Melting and formation temperatures of the core materials involved in the melt are shown in Table 1. Qualitative temperature projections were made based on the grab samples as shown in Table 2. Note that these samples were taken from the top of the debris field and are the first retrieved material.

Table 1. Relative melting points of core constituents (McCardell, 1990)

Melt Constituent	Melting Temperature (K)	Formation Temperature (K)
$UO_{2.0}$	3120	
$ZrO_{2.0}$	2960	
$UO2_{.+x}$	2900	
$(U,Zr)O_2$ liquid ceramic phase		2810
$(U,Zr)O_2$-Fe_3O_4 ceramic phase	2695	
a-Zr(O)/UO_2 and U/UO_2 monotectic		2670
α-Zr(O)	2245	
α-Zr(O)-UO_2 eutectic		2170
Zircaloy-4	2030	
Stainless Steel	1720	
Inconel	1650	
Inconel-zircaloy	1500	
Liquid U from UO_2-Zircaloy interaction		1400
Fe-Zr and Ni-Zr eutectic		1220
Ag-In-Cd	1073	

The progression of catastrophic melting when the core became uncovered was led by reaction of the Inconel grid spacers with exposed zircaloy cladding, followed by eutectic reactions between the stainless-steel control rod cladding and the zircaloy guide tubes. When the control rod tubes failed, the silver-indium-cadmium neutron absorber had already melted. The cadmium evaporated from the alloy, leaving the silver and indium to join the iron-zirconium/nickel-zirconium metal flowing at 1220K to the bottom of the vessel. This flow solidified at intact grid spacers, interfering with coolant flow, further complicating the problem of circulating water in the core. As temperatures continued to rise, the zirconium oxide external surface began to break down allowing a steam-zirconium metal reaction to progress exothermically, further driving the heat load. A similar exothermic reaction occurred between steam and the stainless-steel components. Metallic zircaloy began melting as temperatures exceeded

2030K, and at 2170K partially-oxidized alpha-phase zirconium oxide and uranium oxide began to have a eutectic relationship, leading to a fully liquid ceramic at 2810K. Core reflooding solidified the majority of the melt and shattered some previously intact fuel. (Akers, 1992)

Table 2.TMI-2 Grab Sample Peak Temperature Estimates (GEND-INF-075, Pt 1 p 60, 1986)

Particle	Temperature Range[a] (K)	Comments
1A	2170-2245	No melting of UO_2; ballooned α-Zr(O); eutectic Zr-U interaction.
1B	2170-2600	No melting of UO_2; slight grain growth; eutectic Zr-U interaction.
1E	2810-2960	No melting of ZrO_2; melting of α-Zr(O) cladding; prior molten (U,Zr) O_2.
1H	>2810	Dissolution of $(U,Zr)O_2$ by porous heterogeneous U-Zr-O melt.
3L	>2850	Above the liquidus temperature for U-Zr-O ceramic.
3M	>2850	Areas of $(U,Zr)O_2$ melt; contains trace Cr, Ni, Fe.
4A	~2810	Foamy U-Zr-O molten ceramics contacting UO_2; may be slightly lower due to impurities.
4B	~2810	Foamy U-Zr-O molten ceramic contacting UO_2 fuel; may be slightly lower due to impurities.
4D	>2850	Molten $(U,Zr)O_2$; dense.
5E	~2810	Foamy U-Zr-O molten ceramic contacting fuel.
6B	<2245	No melting of α-Zr(O).
6C	2170-2960	No melting of ZrO_2; UO_2-Al_2O_3 eutectic interaction.

An image of ballooned clad described in the first entry (Particle 1A) of Table 1 is shown as Figure 16. It is a multi-phase sample that illustrates some of the different reactions that occurred at fuel-clad interface. It includes metallic zircaloy with uranium and zirconium oxides at one surface and apparent uranium dissolution into the zircaloy at the lower surface.

Figure 16. Cross-section of partially intact fuel-clad section. (GEND-075 Pt. 1, 1986)

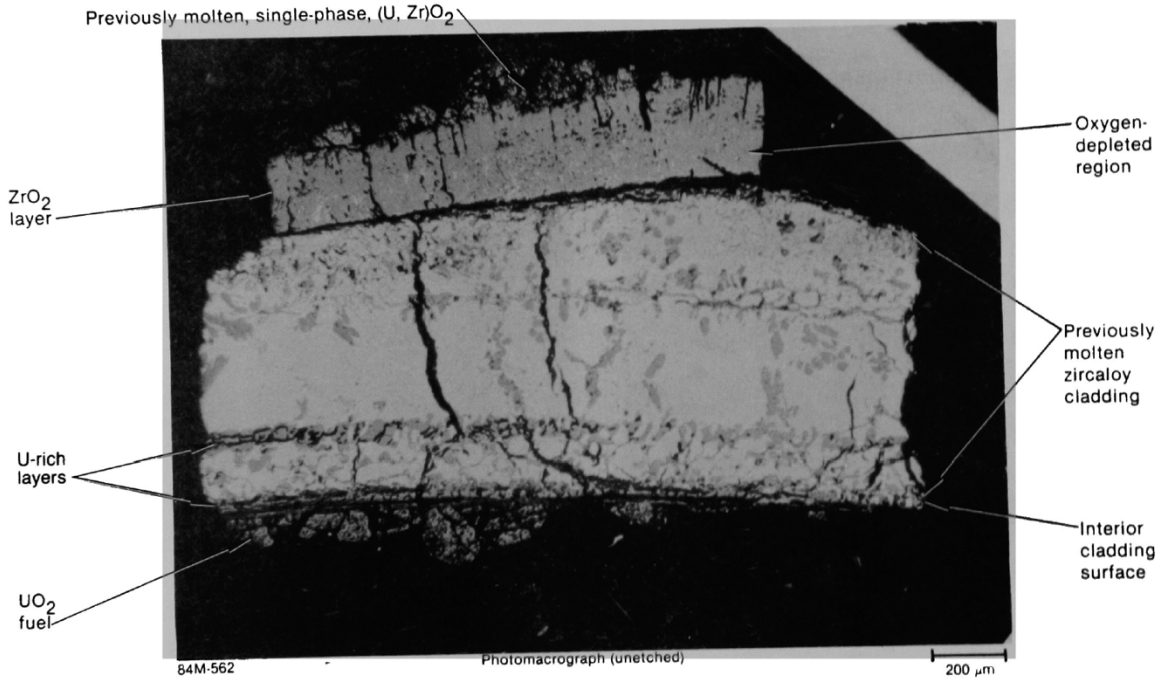

Figure 17. Macrograph of grab sample showing uranium diffusion into cladding. (GEND-INF-075 Pt 2, 1986)

Optical and electron micrographs show example grain structures and phases of the uranium-zirconium grab sample melt fragments in Figure 18.

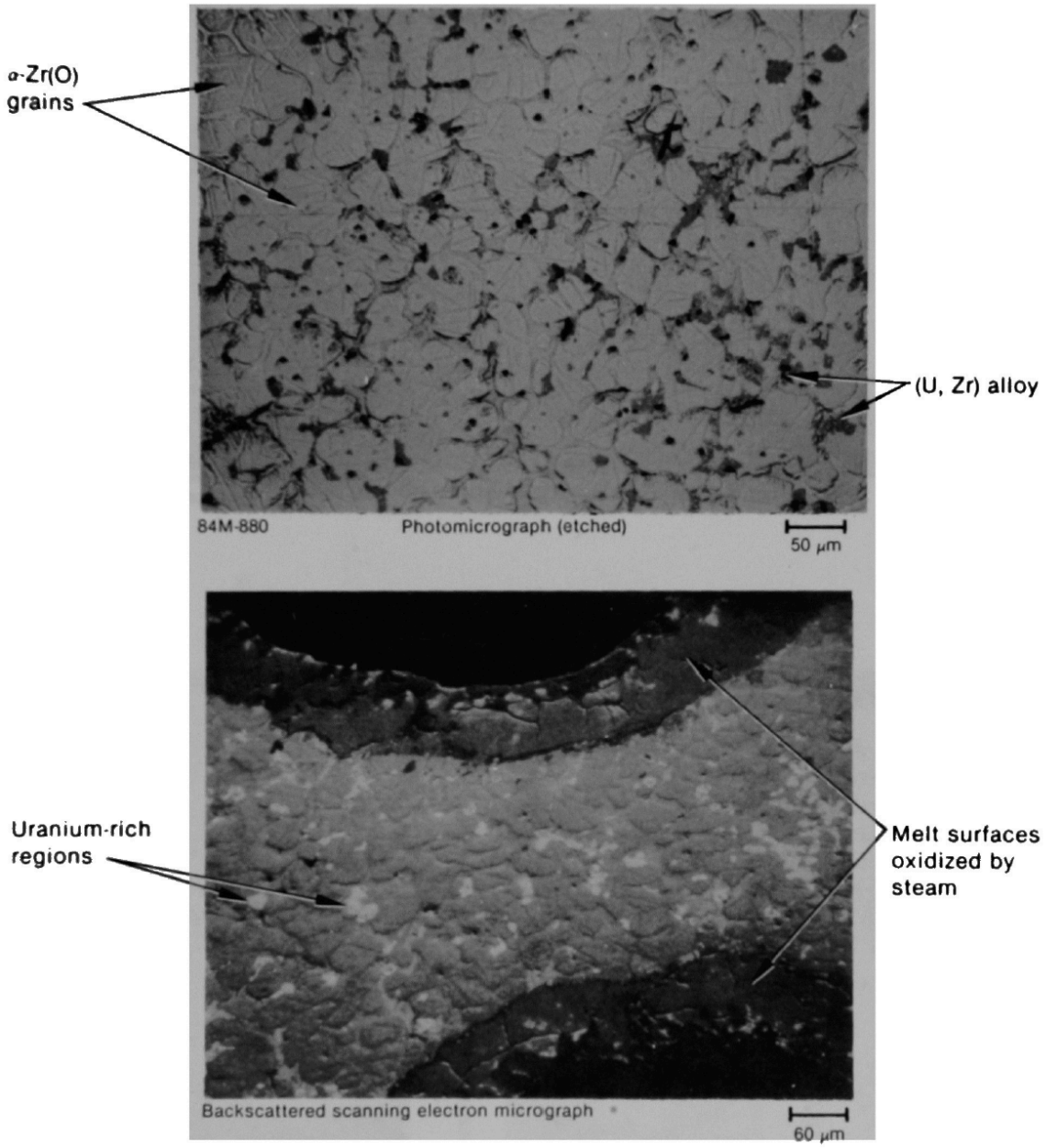

Figure 18. Photomicrographs displaying grain type and phases present. (GEND-INF-075, Pt. 2, 1986)

Radionuclide Data

Gamma-ray spectra were used to identify and quantify primary fission products in the grab sample and to extrapolate the relative quantities as an indication of retention in the core. Due to the extreme high temperatures, fission gases such as ^{85}Kr and several xenon isotopes were released quite uniformly, having negligible retention in the samples. Cesium and iodine species are among the most readily released, having relatively low vapor temperatures, and being highly soluble in water, both in the elemental form as well as in the form of oxides and other compounds.

^{137}Cs is a direct fission-product with a single 662 keV gamma emission and a 30-year half-life, which is consistently produced in a reactor, making it a dominant isotope in nuclear evaluation. The grab samples taken at the center of the core had ^{137}Cs values varied only approximately 5% from the mean

value of the group. Those taken at the mid-radius had as much as a five-fold range, and were as much as 85% higher than the center sample location.

^{90}Sr is produced by fission at a rate nearly directly proportional to that of ^{137}Cs with a similar 28-year half-life, but its mobility is much less, due to a higher melting and vapor temperature (1050K/1655K) as a pure substance, and lower solubility as an oxide. Comparison of the types of samples indicated that ^{90}Sr was more selectively found in relation to the uranium phase. ^{125}Sb was generally retained at approximately 21 percent of the predicted value.

As the core melted, multiple reactions occurred between the ceramic and metal components in the fuel and core structure. The actions taken to stabilize the melt included flooding the core with water. Between the initial loss of primary coolant to the containment and the later injection of cooling water into the core, as much as 80% of the cesium that was predicted to be in-core inventory was leached out of the debris. This estimate was developed by comparing the core inventory calculated using an ORIGEN-2 model against the average values of nuclides found in the grab samples. From this comparison, only approximately 22% of ^{137}Cs was retained while at least 98% of the ^{90}Sr was retained. A tabulated reporting of the data taken from Table 25 of GEND-INF-075 Pt. 1 (Akers, et.al, 1986) for the two locations is shown as Table 3.

Table 3. Retention of radionuclides in TMI-2 based on grab sample gamma spectra data

Nuclide	Total Core Inventory (Ci) calculated by ORIGEN-2	H8 (Central Location) Average Concentration (uCi/g) Decay corrected to Apr 1, 1984	Fraction of Inventory Retained (%)	E9 (Mid-Radius Location) Average Concentration (uCi/g) Decay corrected to Apr 1, 1984	Fraction of Inventory Retained (%)
^{90}Sr	6.62E5	5.55E3	105	5.82E3	110
^{106}Ru	1.15E5	4.97E2	54	6.97E2	76
^{125}Sb	3.7E4	9.2E1	31	6.23E1	21
^{129}I	2.29E-1	4.7E-4	26	4.17E-4	23
^{134}Cs	3.7E4	5.99E1	20	7.23E1	24
^{137}Cs	7.6E5	1.32E3	22	1.7E3	28
^{144}Ce	2.75E5	2.95E3	134	2.8E3	127
^{154}Eu	6.38E3	6.03E1	98	4.12E1	81
^{155}Eu	1.61E4	9.02E1	70	9.16E1	71

Based on these data, it is clear that strontium, cerium and europium are retained in the sample material at values in excess of that expected. The values in excess of 100% are assumed to be due to higher core burnup at the sample locations. The higher burnup anomaly was compared against the initial ^{235}U enrichment values for the fuel that would have been at the sampling locations. The measured sample enrichment for the center core location was consistent with the expected value, but the mid-radius sample enrichment was higher than the original value. This difference at the mid-radius was presumed to indicate that higher-enriched fuel had relocated and become mixed with the debris from the expected value.

With regard to ^{154}Eu and ^{155}Eu, the ORIGEN-2 model of the time had a large uncertainty in calculating the rate at which these isotopes were produced. Although ^{106}Ru retention in the core is less than 100%, specific metallic samples with high nickel content were observed to have disproportionately high ^{106}Ru concentrations. To a lesser extent, the same nickel affinity phenomenon was noted for metallic samples with higher-than-expected concentrations of ^{125}Sb.

Sample Crushing Tests

To evaluate the potential for increased release as a result of mechanically pulverizing the debris, 50 g of the combined bulk material from one sample were crushed to reduce the particle size and expose a greater surface area. The crushed material was then placed in deionized water to simulate conditions expected during debris removal. One result was that the ^{137}Cs concentration in the water increased by nearly an order of magnitude, indicating that increased surface area allowed more effective leaching.

The other concern for crushing was the possibility that an increase in airborne contamination would result. Based on the test procedure, exposure of nearly dry pulverized sample resulted in an increase in airborne activity, but if the sample was fully wetted, no increase occurred. For defueling operations, it was recommended that controls be applied to prevent drying of the core debris.

Sample Pyrophoricity

The potential presence of pyrophoric zirconium fines was tested by attempting to ignite samples using spark ignition and direct flame. Neither wet, nor dry samples were found to be ignitable, much less pyrophoric.

Leadscrew Analysis

The control rod drive mechanism leadscrews that were removed from core positions H8 and B8 to allow insertion of the Quick Look camera and grab sampling operations were examined in depth to determine what temperatures were achieved at those locations and evaluate the presence of fuel on the drive rod surfaces. Visual examinations and chemical and radiological measurements were made with the purpose of estimating the maximum temperature to which the leadscrews were subjected. Hardness and microstructure analysis showed that the H8 leadscrew from the center of the core had a temperature range of 700 to 1255K, while the B8 mid-radius leadscrew temperature was from 755 to 1116 K. Uranium oxide and zirconium surface deposits were present with a concentration highest at the end nearest the core. Due to solubility issues, not all of the nuclides identified on the H8 leadscrew were removable in 40% nitric acid at near boiling temperature. Presumably due to different temperature conditions and durations the B8 deposits were almost completely soluble in acid. Gamma spectrometry and active neutron measurement with delayed neutron counting was done to detect fuel presence in the leach solutions from the surface residue. Using the measured concentrations of nuclides, an estimate of the core inventory that might be plated out on the plenum assembly surfaces was made, indicating that that value amounted to less than 2 wt% of the total. (Vinjamuri, EGG-TMI-6685, 1985)

Containment Building General Radiological Conditions

Because it was possible to keep the reactor pressure vessel filled with water for shielding, at the time that the video inspections and grab sampling were performed, general body fields within the containment building had dropped from approximately 430 to 150 mR/hr (4.3 to 1.5 mSv/hr)at the entry level and to approximately 60 mR/hr (0.6 mSv/hr) at the top of the reactor vessel as shown in Figure 19. Multiple cycles of flushing, scrubbing and scabbling with a variety of remote vehicles and manual efforts were required to achieve these values. Several components were shielded with lead blankets to meet the desired levels.

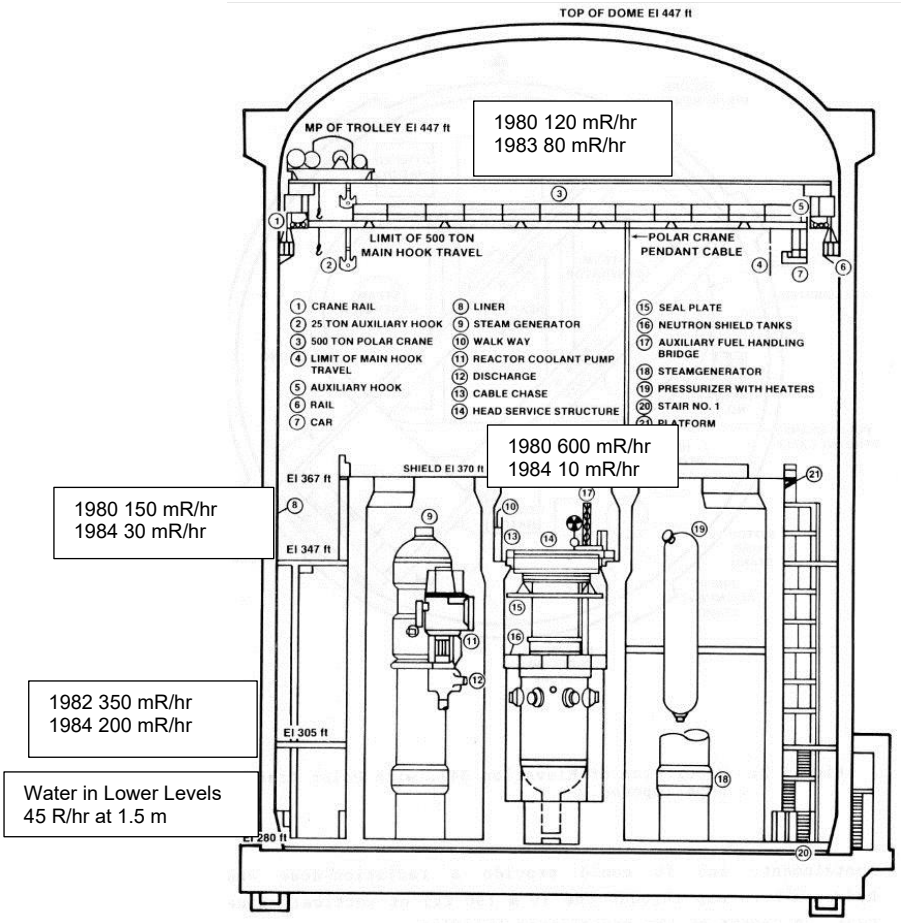

Figure 19. Containment Building Dose Rates, 1980 and 1983. (Courtesy of INL)

3.3 Ultrasonic Core Topography Mapping

A multiple-transducer underwater ultrasonic system was developed at INEL to provide a detailed survey of the contours of the irregular melt structure. The system was deployed in 1983 and collected data from two downward facing 2.25 MHz transducers that were positioned using a 13 m-long tool. The transducers were lowered to within 15 cm of the surface and then raised in 2.5 cm increments. At each increment, a horizontally oriented transducer was rotated 360 degrees, providing a range indication of the contour as shown in Figure 20.

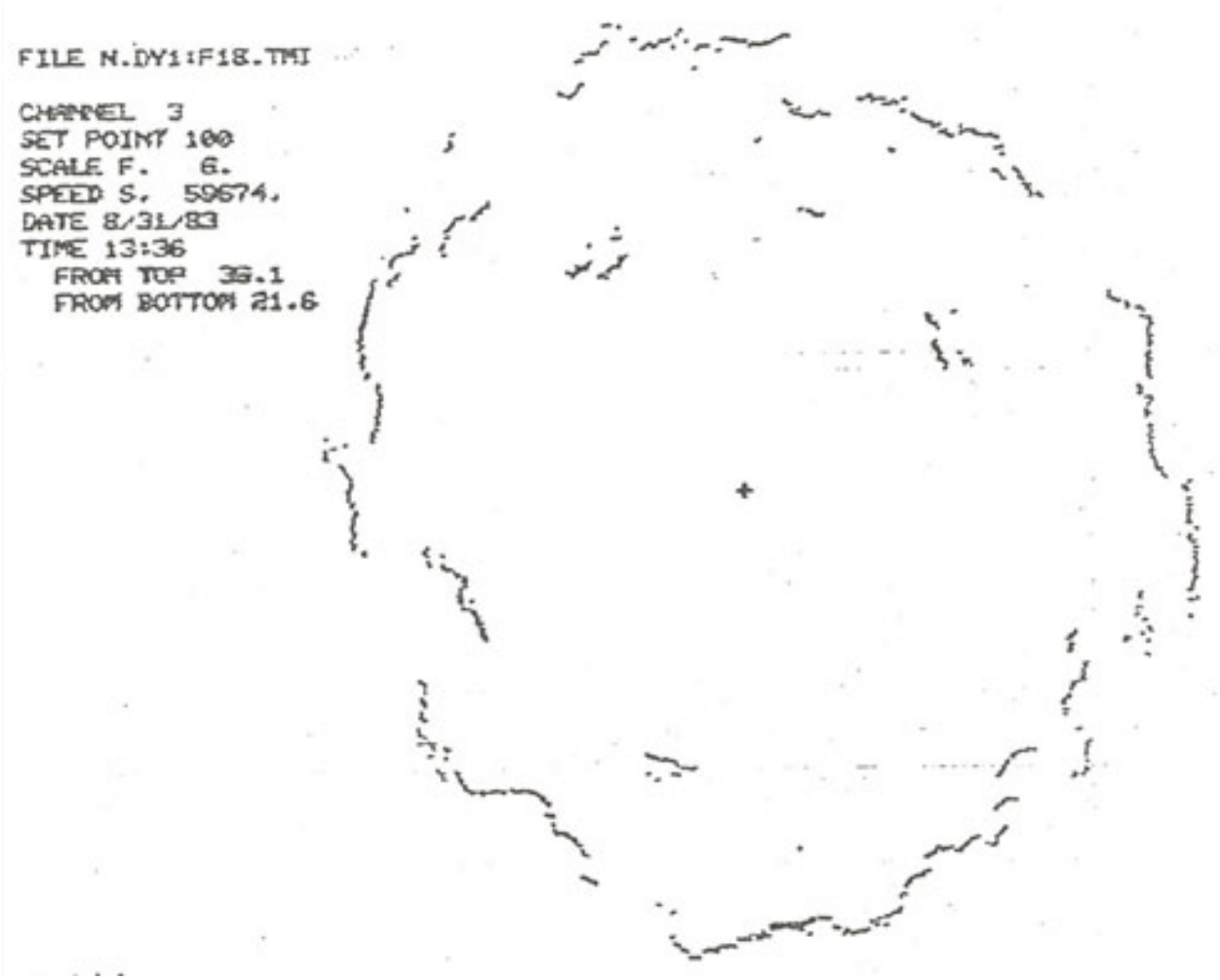

Figure 20. Range-bearing plot from Ultrasonic Survey. (GEND-INF-012, 1984)

Compilation of the various elevation plots allowed the plots to be converted into an isoheight map (Figure 21) and then three-dimensional physical model (Figure 22) that was used to evaluate recovery options.

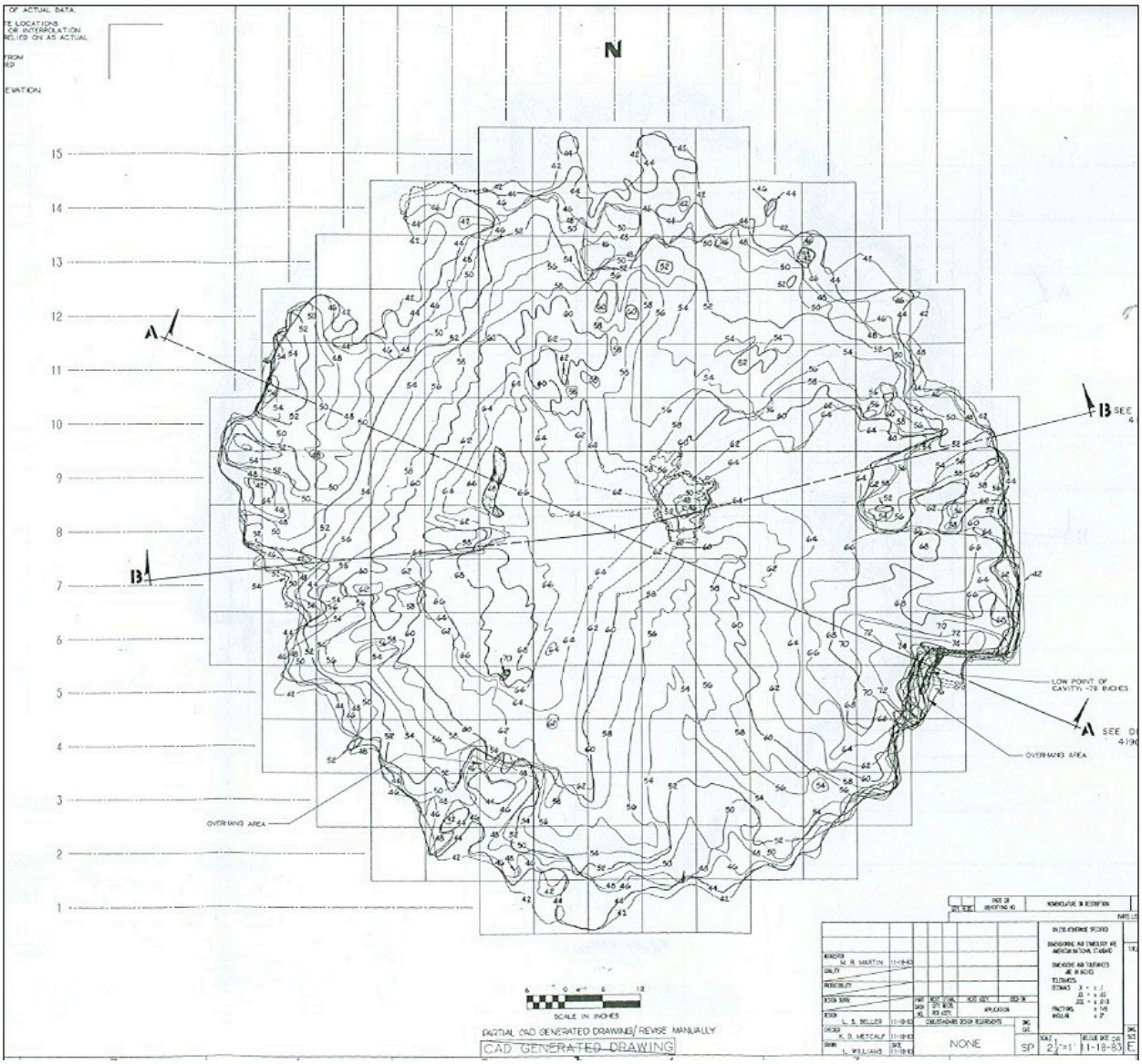

Figure 21. Isoheight Map of Core Melt Contour. (GEND-INF-012, 1984)

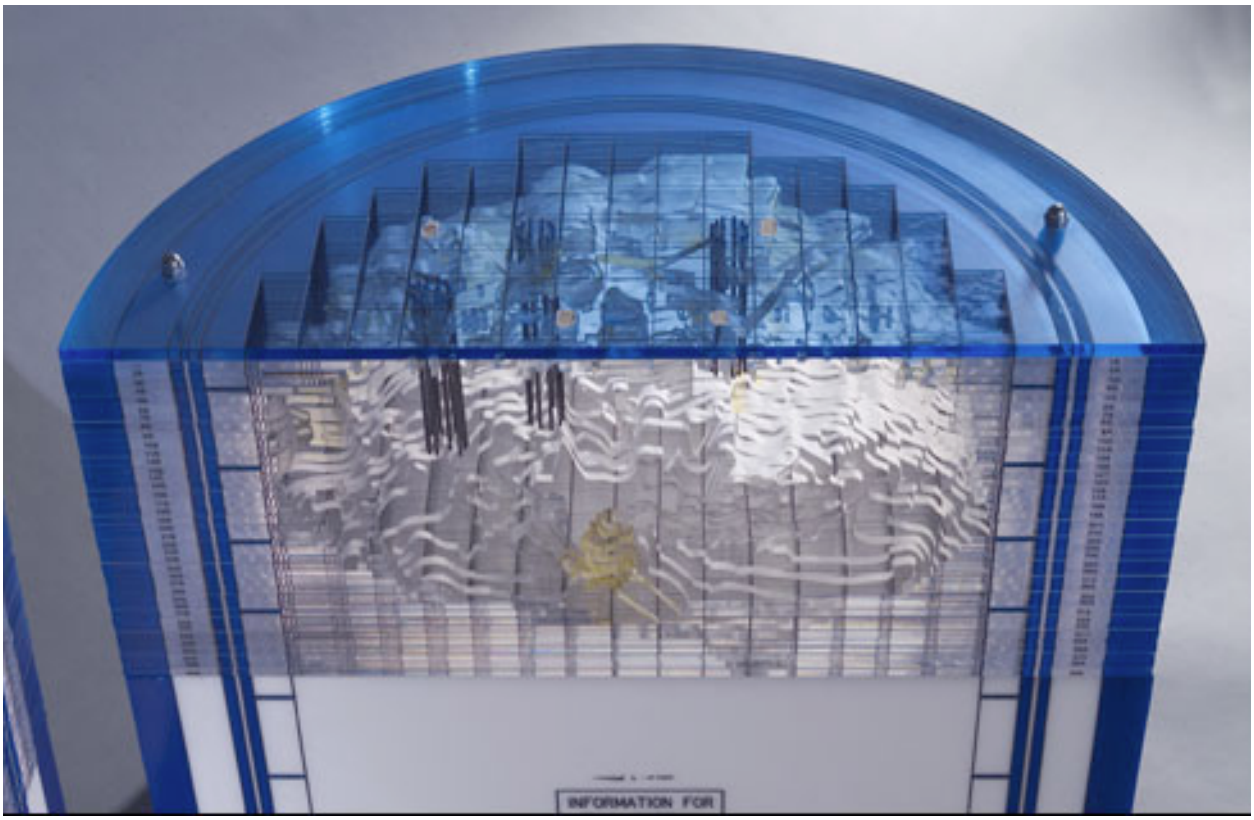

Figure 22. Acrylic Layer 3D Model Reconstruction Cross-Section. (Courtesy of INL)

3.4 Reactor Pressure Vessel Head and Plenum Removal

One of the most significant efforts in the process of recovery was to gain access to the internals of the Reactor Pressure Vessel (RPV). Large-scale efforts went into planning, engineering and training to remove the reactor vessel head. A shielded location for storing it was constructed, a special shielded control booth for the crane operations was build, and monitoring and control systems were engineered. As part of the stabilization efforts, the system was completely filled with water, including the pressurizer, which is substantially higher than the top of the pressure vessel. The water level needed to be lowered to allow the head to be removed. By mid-1984, the polar crane certification was completed; the reactor pressure vessel (RPV) head could be jacked up a small distance, allowing conditions to be evaluated. One of the most significant efforts in the process of recovery was to gain access to the internals of the RPV. Large-scale efforts went into planning, engineering and training to remove the reactor vessel head. A shielded location for storing it was constructed, a special shielded control booth for the crane operations was build, and monitoring and control systems were engineered. The water level was lowered to allow the head to be removed. By mid-1984, the polar crane certification was completed; the RPV head could be jacked up a small distance, allowing conditions to be evaluated. The head was carefully removed and stored, allowing the internals indexing fixture to be installed so that the plenum could be removed while underwater. The upper plenum was inspected, and it was determined that it had only sustained a small amount of damage. The upper plenum was inspected, and it was determined that it had only sustained a small amount of damage. By late 1984, the plenum was raised and inspected, and by mid-1985, it was removed, allowing inspection of the bottom side of the upper spacer grid. The upper spacer grid had remnants of fuel elements stuck in it, requiring operators to push the stubs back into the vessel prior to removing it. A view of the underside of the upper spacer grid fuel bundle removal is shown in Figure 23. Some melting of the highest temperature central area of the grid is visible.

Figure 23. Underside of Upper Fuel Grid showing Evidence of Melting. (Courtesy NRC/INL https://tmi2kml.inl.gov/)

Figure 24 shows a diagrammatic view of the grid plate of areas where fuel assembly top temperatures caused melting by exceeding 1750K.

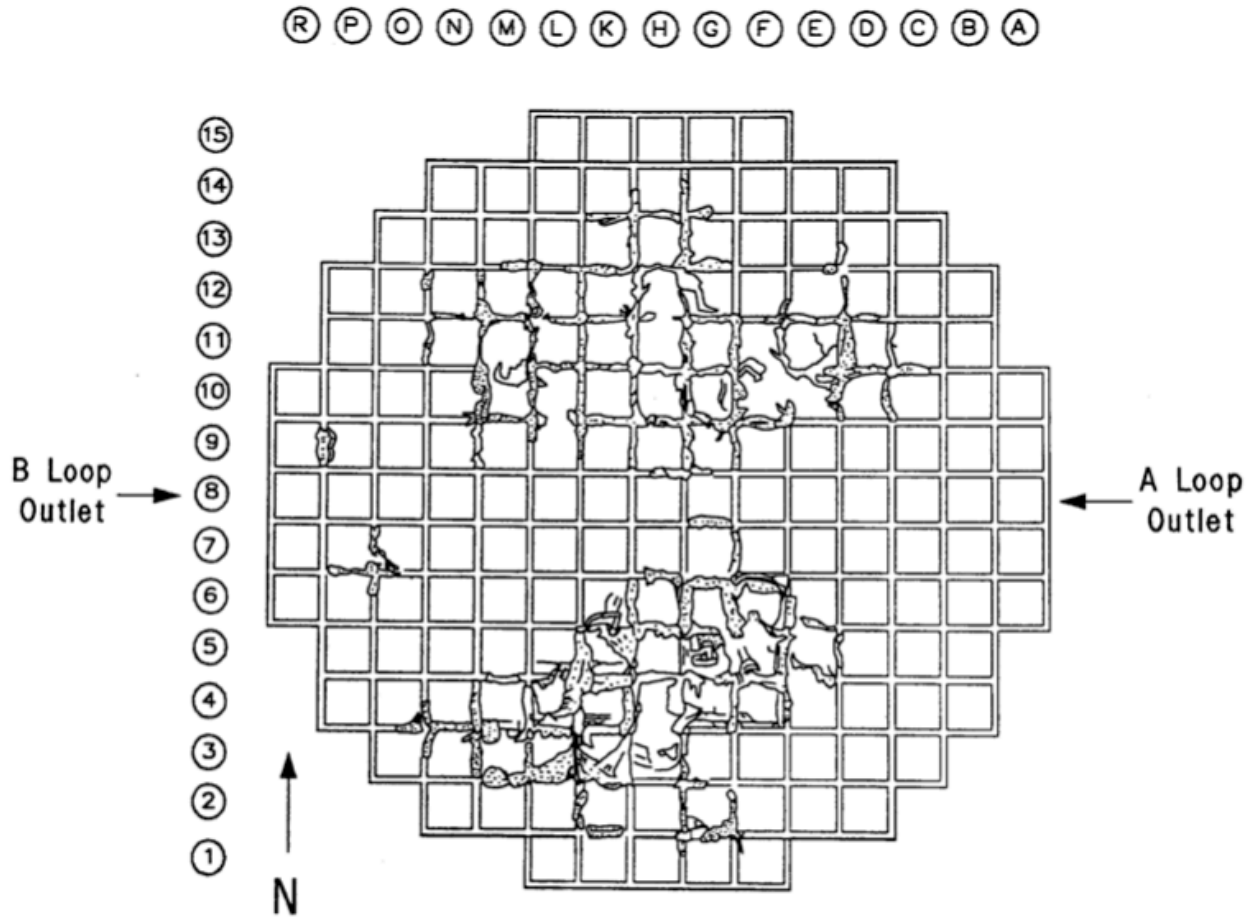

Figure 24. Areas of upper fuel grid plate where melting occurred. (GEND-INF-082, 1987)

Once the RPV upper head and plenum assembly were removed, it was possible to more completely evaluate the degree of damage. Around the perimeter of the vessel, forty-two percent of the 177 fuel assemblies were recognizable. Of the standing assemblies, all were damaged, with two that had damage to only ten percent of their rods. Various views of damaged fuel rods are shown as Figure 25.

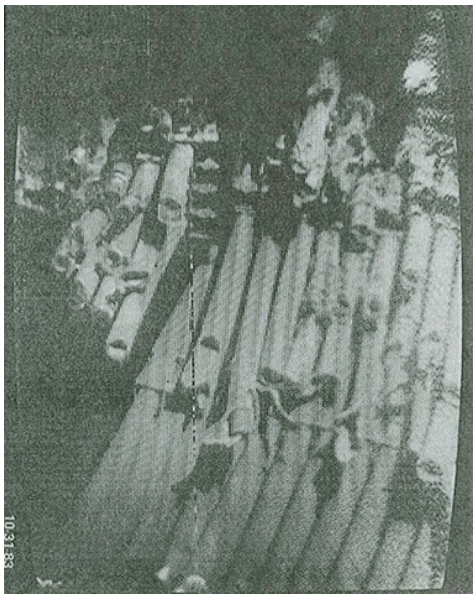

Figure 25 Remains of fuel assemblies (Upper view, hanging rods; lower view, rods fallen into debris bed, Courtesy NRC/INL https://tmi2kml.inl.gov)

3.5 Training

All of the activities involved with the head removal process were put through trial exercises with equipment assembled to reflect expected conditions to the extent possible to minimize potential for unnecessary personnel exposure, environmental release, or further equipment damage. Earlier activities including the initial reactor building entries also involved careful planning and contributed to development of processes for improved radiological control.

Containment Re-entry Training

As in an ideal situation where emergency response is required, the first re-entry teams that went into the TMI-2 containment building were well-rehearsed in the tasks they needed to perform. The personnel involved went through 100 hours of classroom training to familiarize them with the facility details and the concerns of interest in the initial forays into the building.

Classroom training was supplemented with 50 hours of practice exercises working through the TMI-2 companion reactor, TMI-1 which had been shut down at the time of the accident. The personnel were taken through as many scenarios as possible to make clear the recommended responses in the event of emergency conditions.

The practical exercises at TMI-1 included being able to make egress from the building in lights-out conditions. All personnel were trained to perform radiation surveying regarding air sampling, general beta-gamma body fields, taking loose contamination smears and photographing general conditions. Although this radiological control process is considered routine in present day nuclear facilities, the term ALARA had only been coined three years prior to the accident, and radcon practices were less well defined.

Numerous critical audits and reviews of the TMI-2 program led to development of a more rigorous radcon organizational structure and radcon program guidelines that were issued by Institute of Nuclear Power Operations (INPO) four years later.

Quick Look Inspection and Vessel Head Removal

Prior to attempting the removal of CRDM leadscrews from the top of the reactor vessel to insert cameras for the Quick Look inspection, teams worked through the process using mockup tools and equipment. Verification of clearances for tools and extraction of the leadscrews was done using the TMI-1 reactor. Each individual had a rehearsed role in which they had demonstrated their ability to perform their assigned tasks safely and efficiently to minimize personnel dose.

Mockup structures assembled for training and logistic validation included the following:

1. Control rod Drive Mechanism service structure (constructed as a full-scale wooden model and using a full-length CRDM) Used for multiple inspection task walk-throughs.
2. Plenum Head Mockup (constructed as a full-size wood and plastic structure that represented the head flange area). Used to verify camera positions
3. IIF (Internals Indexing Fixture) and Platform Mockup (constructed as a precise dimension full-scale steel cylinder) Used for lifting and positioning the indexing fixture on the vessel upper flange and testing rigging and latching devices. Also used to check out level monitoring equipment.
4. Reactor vessel Stud Detensioning Mockup (constructed with full-length studs and testing of techniques for loosening the reactor vessel head bolts)
5. Auxiliary Fuel-Handling Bridge Mockup (used a spare crane bridge to practice disassembly and removal of the mast and trolley from the AFHB)

Each of the inspection activities was walked through by personnel using the various mockups to confirm their procedures. These included the camera insertion crew that put the first video cameras into the reactor vessel in the Quick Look program, as well as the grab sampling team that acquired numerous kgs of loose debris for the first steps of characterization. Likewise, the group that performed the ultrasonic surveys of the core topography had gone through the necessary actions multiple times prior to deploying their equipment.

The teams that lifted and removed the RPV head had worked through the tasks thoroughly prior to reducing the tensile stress on the studs and rigging the head for removal.

The process of first jacking up the reactor plenum, doing video and radiological measurements and then removing it worked through their process according to the procedures and ultimately clearing it of debris and removing it.

Groups that installed the shielded work platform on the reactor upper flange had worked out the rigging and positioning requirements as well as verified platform dimensions to assure that it would fit.

Offsite teams including those developing the core boring equipment were working with full-height mockups and surrogate material to test equipment that was intended to be able to bore through a large mass of material of unknown composition. Metals, ceramics and agglomerated materials were tested. The equipment was tested regarding disassembly of the parts to be able to make it fit through the available doorways into the work area and then reassemble it on the reactor head platform. A full walkdown of the task had been done before bringing the equipment into the containment building.

Ultimately the process used at TMI-2 was directed to training

- On equipment installation
- On equipment of operations
- On lifting and rigging operations
- For anticipated upset condition response
- For contingency operations

Classroom work covered basic theory on operation of the equipment, and instruction on operation of equipment within the design limits.

Hands-on training followed using the mockups and actual equipment as appropriate.

Further development involved coordination of a group for complex actions like lifting of large components. The group training actions were directed by lift control supervision. (GEND-044, 1985)

Over time, the process was developed to the point that even that routine work used prejob briefings to verify conditions using data and information from each prior day's experience to define their tasks and minimize dose. Videotape reviews were used to familiarize the workers with the area where work was to be performed and identify areas of concern including high radiation areas.

Because TMI-2 operated under NRC license, all of the procedures, tools, techniques and training were reviewed and approved by the regulatory organization prior to use. (NUREG-KM-001)

Defueling was performed by certified reactor operators, whose training included fissile material handling controls that were specific to packaging the debris as is was recovered. In at least one instance, additional training was developed due to high extremity exposures that resulted from operators unknowingly manually handling a piece of corium during decontamination activities. Due to the potential for criticality, the procedures and training were reviewed and approved by NRC.

3.6 Distinct Component Recovery

After removal of the upper head, the plenum assembly was removed. To achieve this result, the upper end fittings from numerous fuel assemblies had to be dislodged from the upper grid. Fourteen of the end fittings were melted to such a degree that four could not be removed and ten could only be partially removed. The plenum was also washed down using a water jet, which was able to displace fines and pieces that were approximately the size of fuel pellets.

The first material removed from the RPV included 110 upper-end fittings as well as control rod and burnable poison rod components. Five partial fuel assemblies were included in the eighteen debris canisters that were shipped to INEL for examination.

Distinct Component Examination

Distinct components were shipped to the TAN Hot Cell and opened in specialized handling fixtures that facilitated controlled removal of items for inspection and selection for analysis. Figure 26 shows a view of the handling carriage that was used to receive, open and sort through the various parts that were forwarded to Idaho for examination.

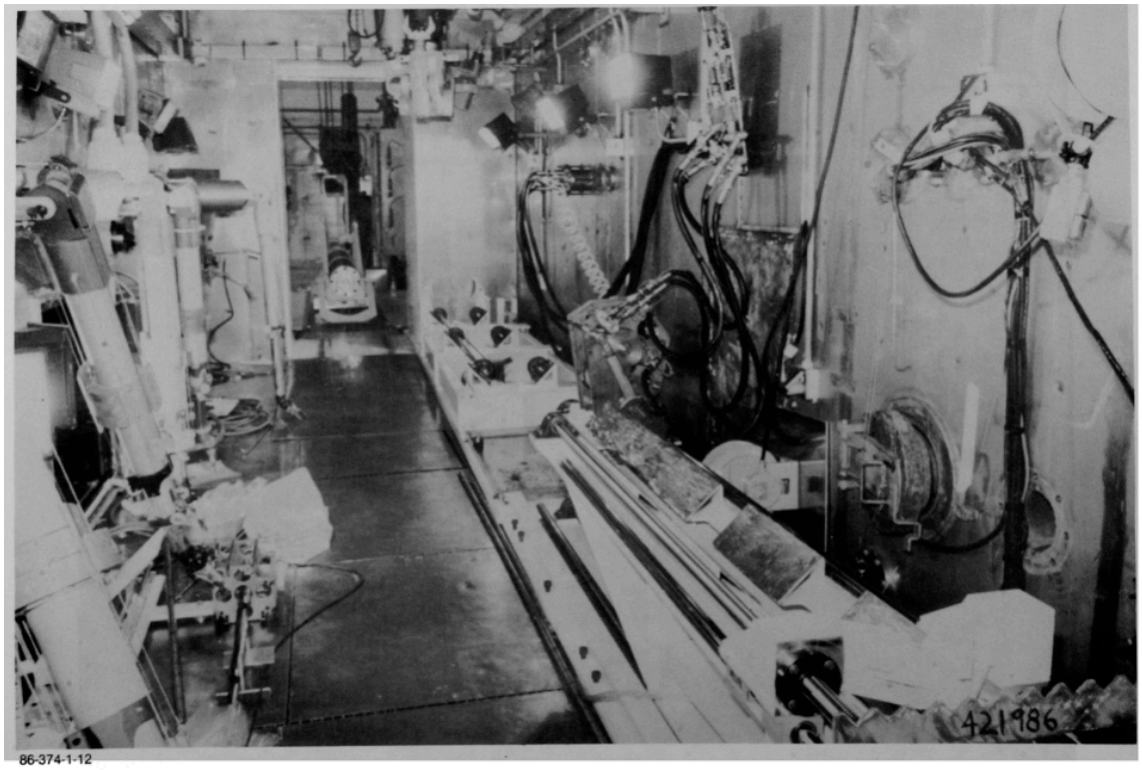

Figure 26. Canister unloading table in TAN Hot Cell (GEND-INF-082, 1987)

Once the canisters were unloaded in the TAN Hot Cell at INEL, the various distinct components were

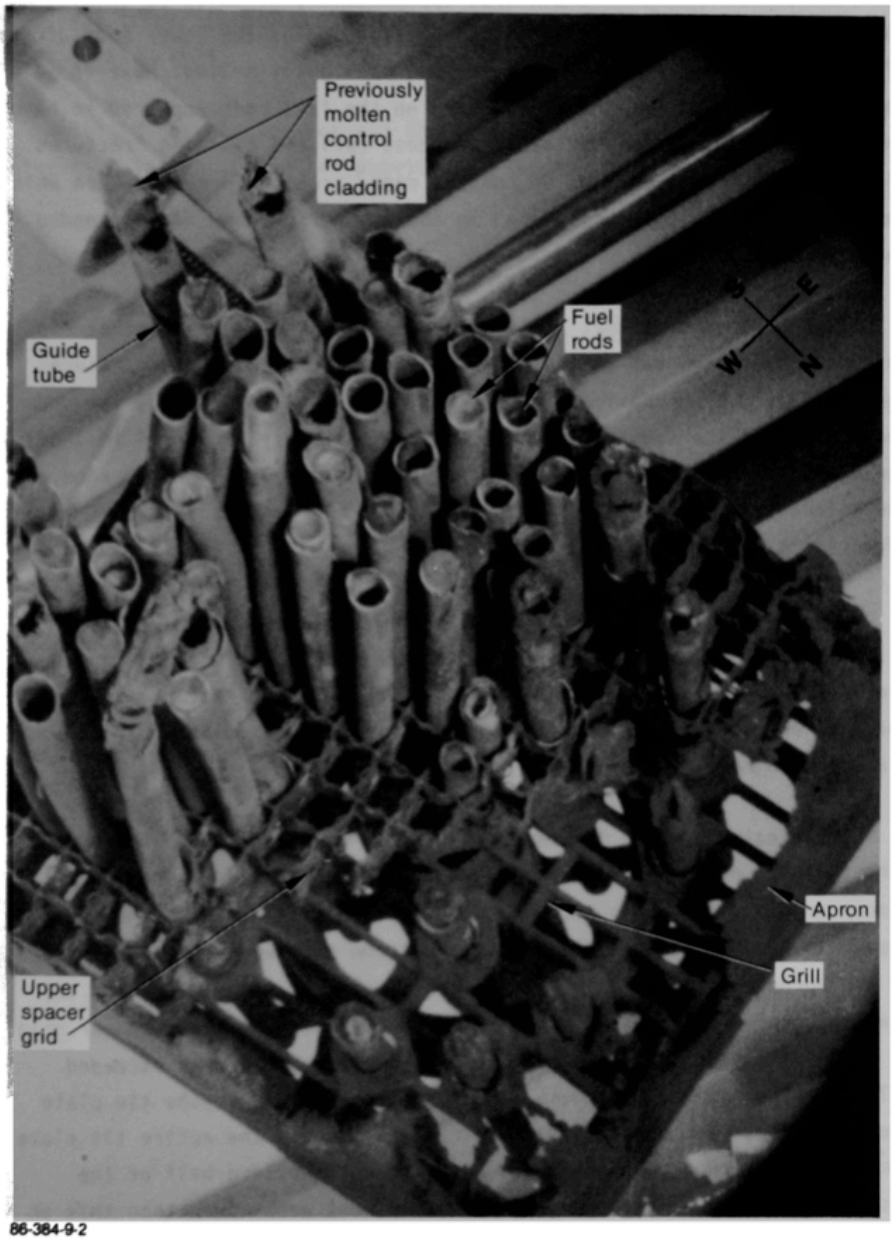

photographed, subjected to neutron radiography, and gamma spectroscopy. An example of an upper end fixture with retained fuel rods is shown in Figure 27. (GEND-INF-082, 1987) Stubs of melted control rods and guide tubes were recovered and photographed as seen in Figure 28. Note that the silver-indium-cadmium neutron control material has melted and drained out of the rod. Figure 29 shows metallographic images of cross-section and axial mounts of a control rod section that retained a portion of its control medium at the level of the plenum spring at the top of the rod. A partially melted control rod spider is shown as Figure 30.

Figure 27. End fitting recovered from Debris Canister D-153 photographed in the INEL TAN-607 Hot Cells (GEND-INF-082, 1987)

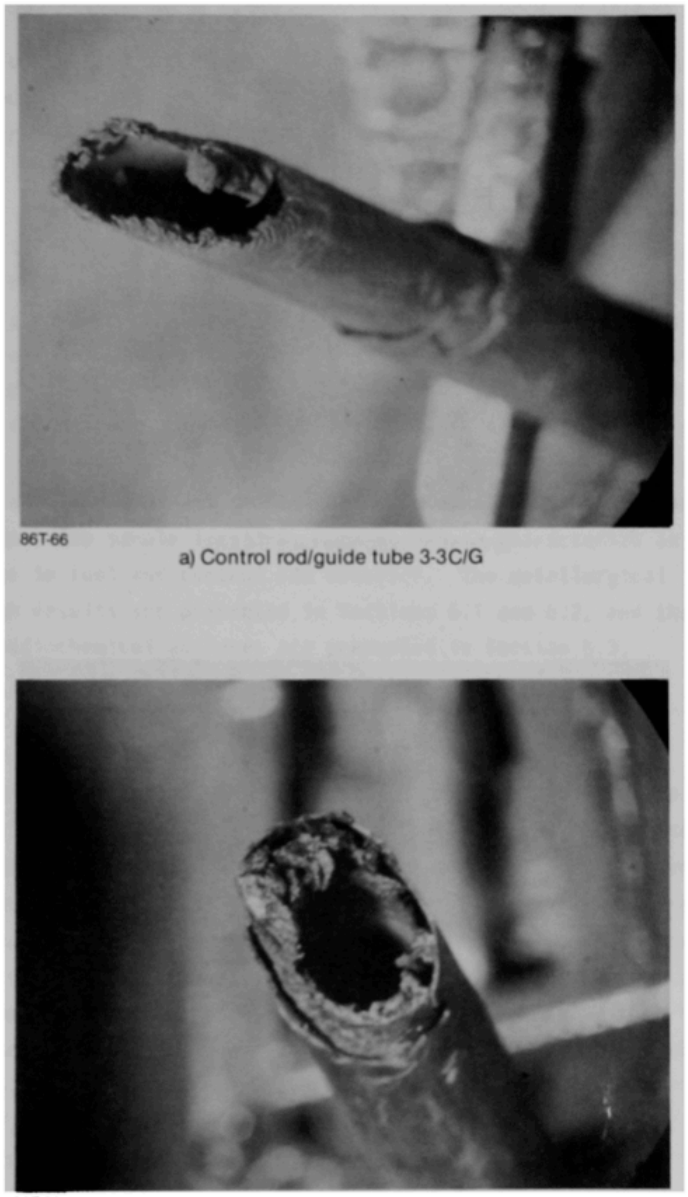

Figure 28. Melted stubs of control rods and guide tubes (GEND-INF-082, 1987)

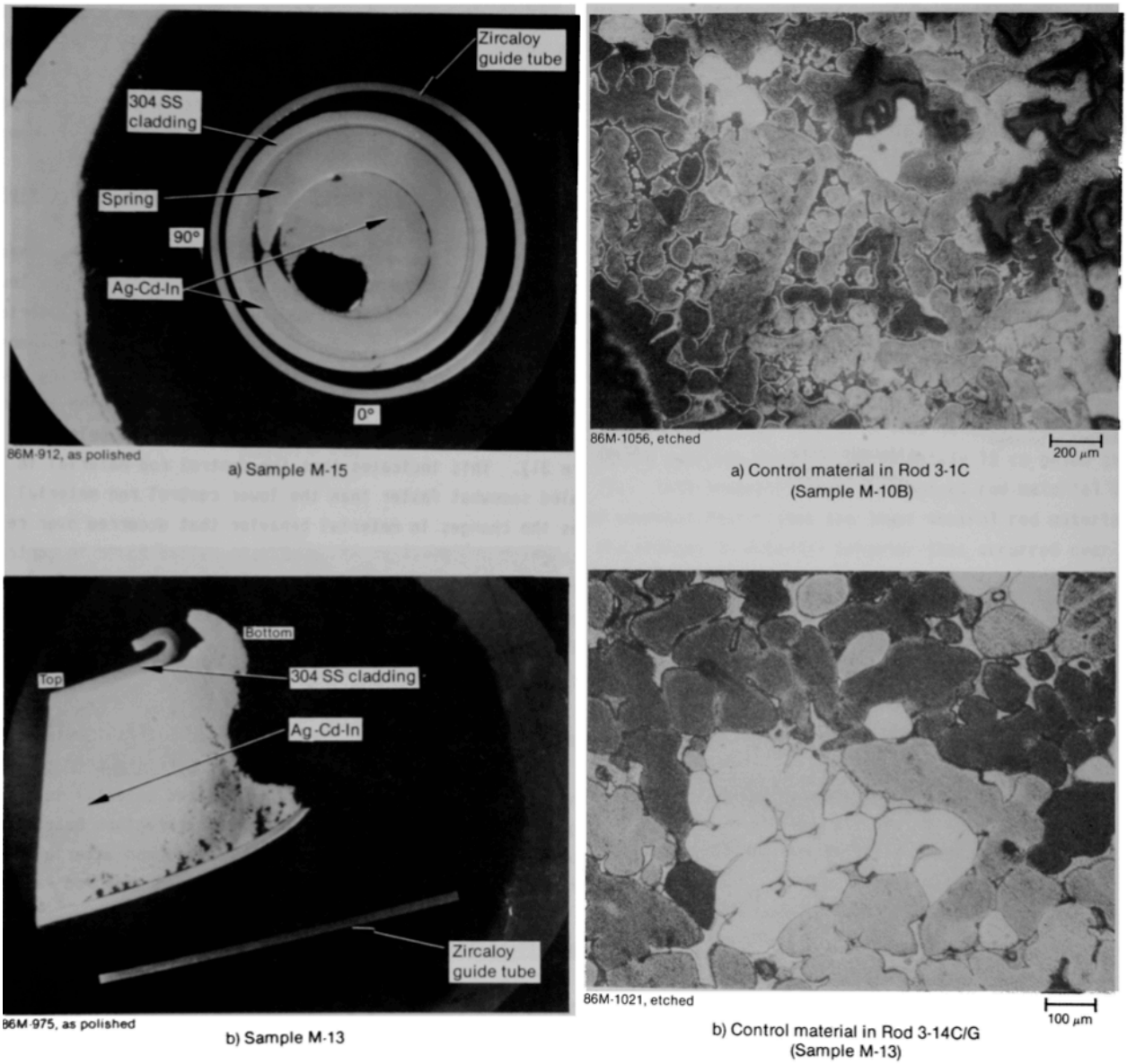

Figure 29. Metallographs of control rod 3-14C/G showing partially retained silver-cadmium-indium alloy, right; Dendritic structures in micrographs of etched mounts (GEND-INF-082, 1987)

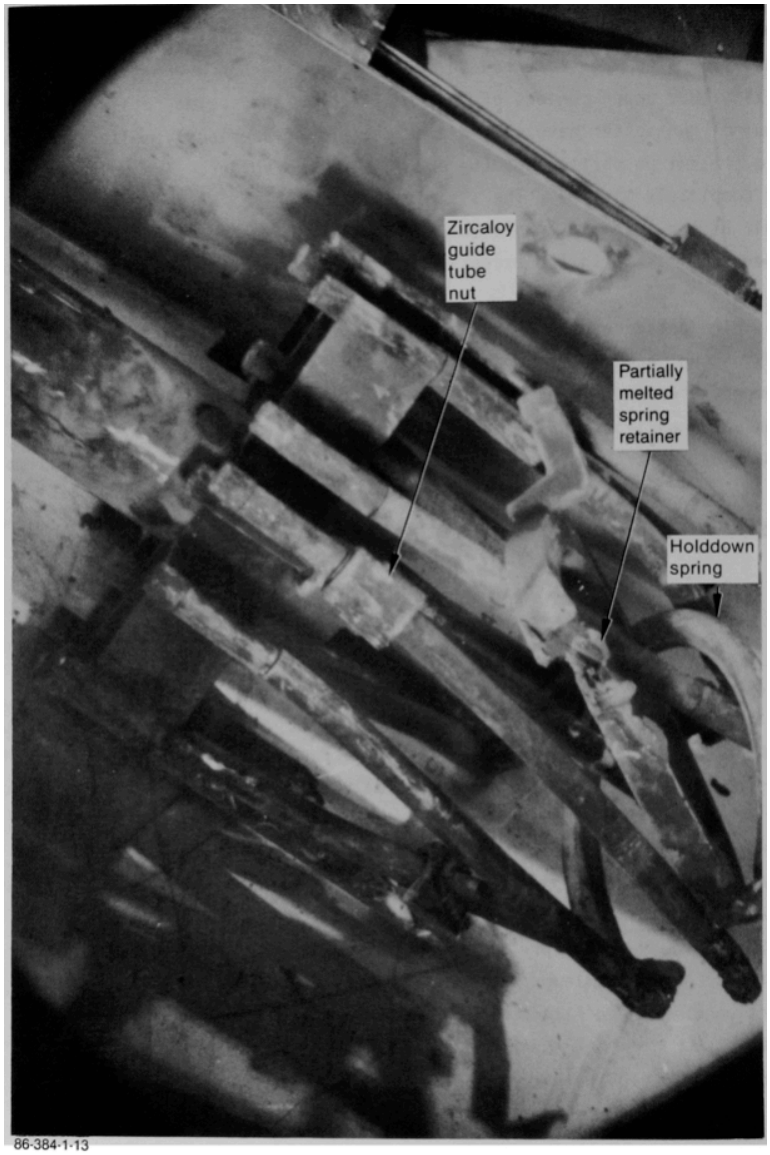

Figure 30. Partially melted control rod spider (GEND-INF-082, 1987

3.7 Core Stratification Sampling Program

The Core Stratification Sampling Program adapted a commercial core boring machine—typically used for geologic operations such as oil exploration—for the job of confirming the composition of the melt below the upper surface. In 1986, ten cores were bored at selected locations in the core. The drilling machine was instrumented to monitor changes in drive-motor torque as an indication of changes in material composition. The core samples were shipped to INEL to be analyzed for chemical and radiological composition. From the core data, it was possible to determine that the melt varied in thickness from 1.5 m in the core center to 30 to 60 cm toward the outer edge of the core. The solidified melt amounted to approximately 10% of the core.

To accommodate materials ranging from metallic to ceramic, the core boring system was based around a bit that used a combination of industrial diamond and tungsten carbide, silver-soldered into the drill body. The drill bit type is shown in Figure 31. This type of bit is hollow and creates a hole with a

cylindrical center core that is removed with the drill, resulting in an elevation-representative section of the material it bores through. In this case, it is a sample core that was extracted by boring through the formerly melted reactor core.

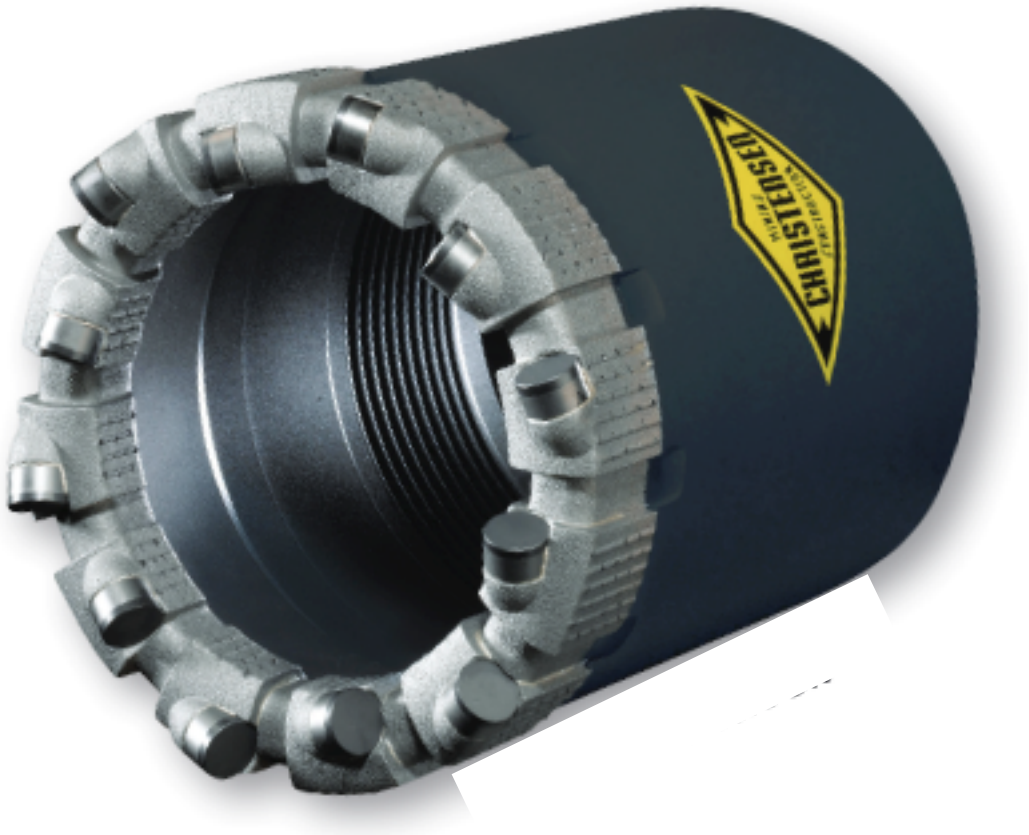

Figure 31. Core sample core drill bit (Croft, 1986)

The drive unit for the core boring system used a hydrostatically driven spindle and hydraulic-drill-string raising-and-lowering mechanism. A 50-hp electric motor drove a hydraulic pump that ran the spindle as well as the hydraulic pump for raising and lowering. Drill operations were monitored for rotational speed and torque applied, as well as vertical force applied to the bit. The drill could operate from 0 to 500 rpm, with a torque from 0 to 3000 ft-lb (4067 N-m) and a vertical force of up to 10,000 lb (4535 kg) applied to the bit. The system was designed to work with the shielded defueling platform and reach any position within the central 8-ft (2.4 m) of the core diameter. The system was constructed in modules to allow it to be transported into the containment via the 1 m × 1.9 m airlock doors.

The core bores were acquired using a 3.5-in. (89 mm) OD core barrel attached to a sectional drill-string that allowed the bit to be driven to the full depth of the reactor vessel to extract a 2.5-inch (63.5 mm) OD core. During operation, the drill bit was cooled, and chips flushed by using a six gpm flow of the borated water that filled the reactor vessel. The selected equipment was a Longyear Corporation 38EHS unit, and used a Megalo head spindle, which allowed for adjustment of the jaw diameter to the required diameter of the drill-string casing. A 4.5-in. (114 mm) OD casing was inserted into each hole that was bored to provide stability for the drill string and keep the hole open if video viewing was to be performed. The core barrel length was 132 in. (3.35 m) to assure that it would be able to fit inside the debris canister.

Due to preinstallation testing using mock materials, the spindle torque and vertical force values provided an indication of whether the drill was running through standing fuel arrays, loose rubble, metal,

or ceramic debris.

The system was mounted to the defueling platform in a manner that allowed radial and rotational position of the drill location to be precisely controlled. That position was confirmed by use of a surveyor's theodolite. Figure 32 shows an elevation view of the drill orientation on the platform and its position in the vessel. Figure 33 shows a plan view of the locations in the core where samples were taken and visual inspection performed.

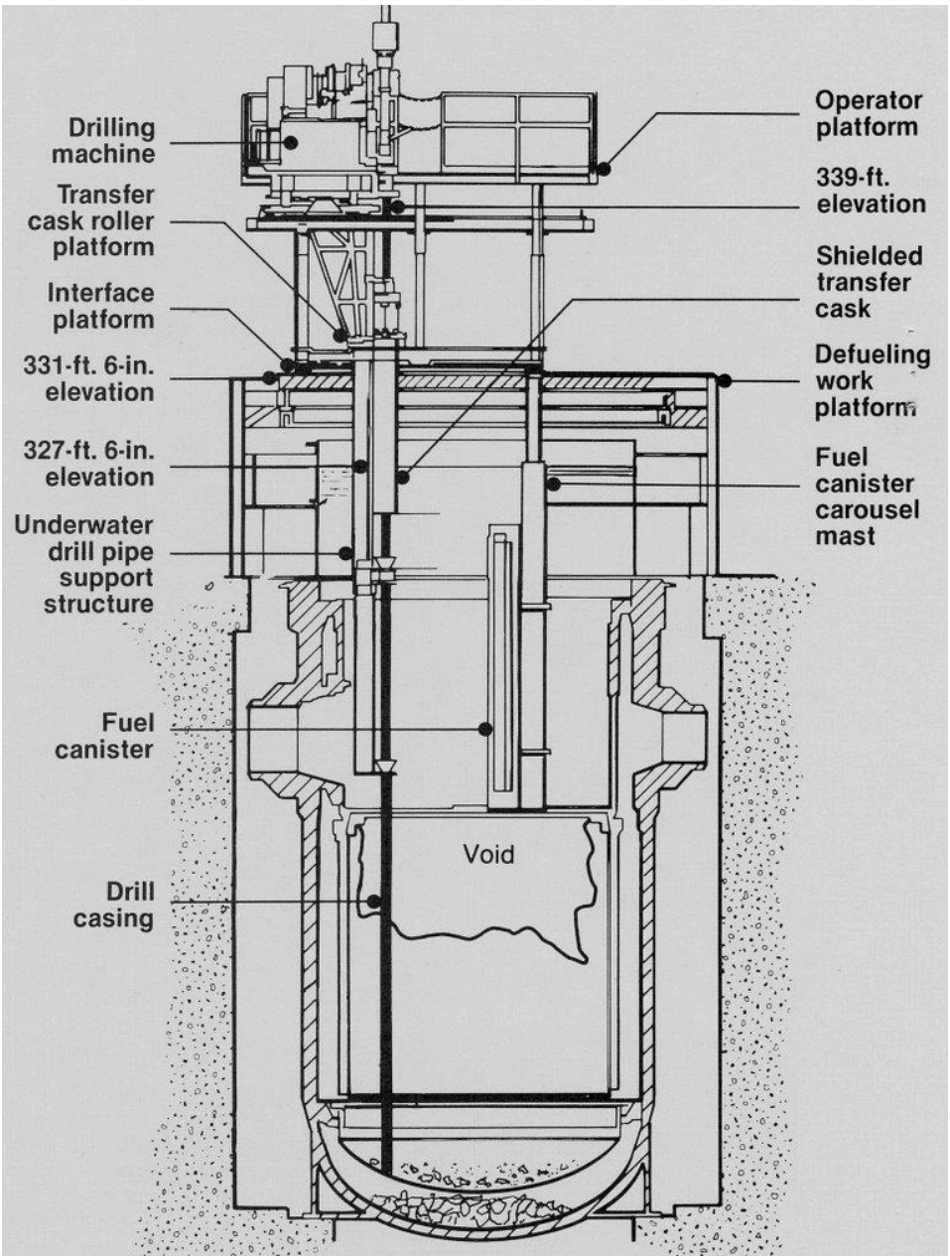

Figure 32. Elevation view of core stratification core bore system. (Courtesy of NRC/INL tmi2kml)

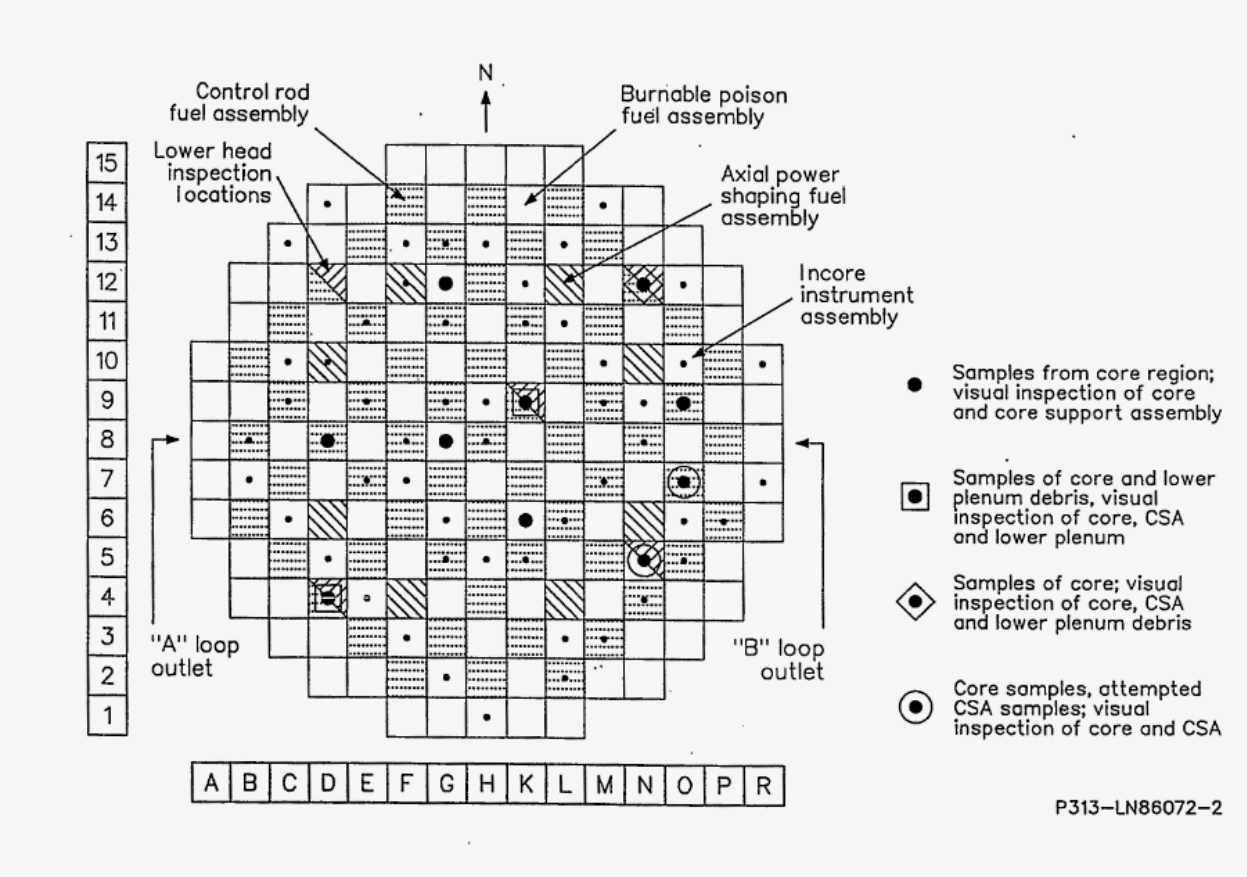

Figure 33. Plan view of core boring locations. (GEND-049, 1985)

3.8 Core bore Characterization

As with the loose debris samples, analysis of core bore samples included density measurements, gamma spectrometry, chemical composition by mass spectrometry, metallographic mounting with optical and electron microscopy to identify grain structure and chemical distribution and X-ray diffraction to establish crystal structure. These analyses yielded the identification of the various ceramic and metallic phases, which produced a basis for correlating control room temperature indications with timing of the materials that melted, relocated, solidified, remelted or fractured. The primary melt located below the loose debris field was evaluated according to its composition, being the upper crust, the central region, peripheral crust and lower crust. Figure 34 shows the range of material types and encountered and observations from a core bore from the periphery of the main core region.

Samples were selected for examination by U.S. DOE operators as well as multiple international laboratories, including ones in Japan, Germany, Canada and France. The analysis included inductively-coupled plasma, optical emission spectroscopy as well as microprobe to determine elemental chemical composition, scanning electron microscopy to determine surface topography, and transmission electron microscopy and X-ray diffraction to identify chemical constituents and crystalline structure (Russell, EGG-TMI-7992, February 1988). Other testing included furnace tests to measure the release of volatile fission products from the various samples. Some of those involved were D.W. Akers, S.M. Jensen and L.A Niemark, INEL-US; G. Bart, PSI-Switzerland, P.D Bottomley, M. Cocherelle, P. Hofmann and H. Kleykamp-JRC Karlsruhe-Germany, A. Brown Sweden; A.J. Manley UK, D.S. Cox, Canada and J. Duco, M. Trotabas, G. Geoffroy, M. Robin and G. LeMarois CEA-France.

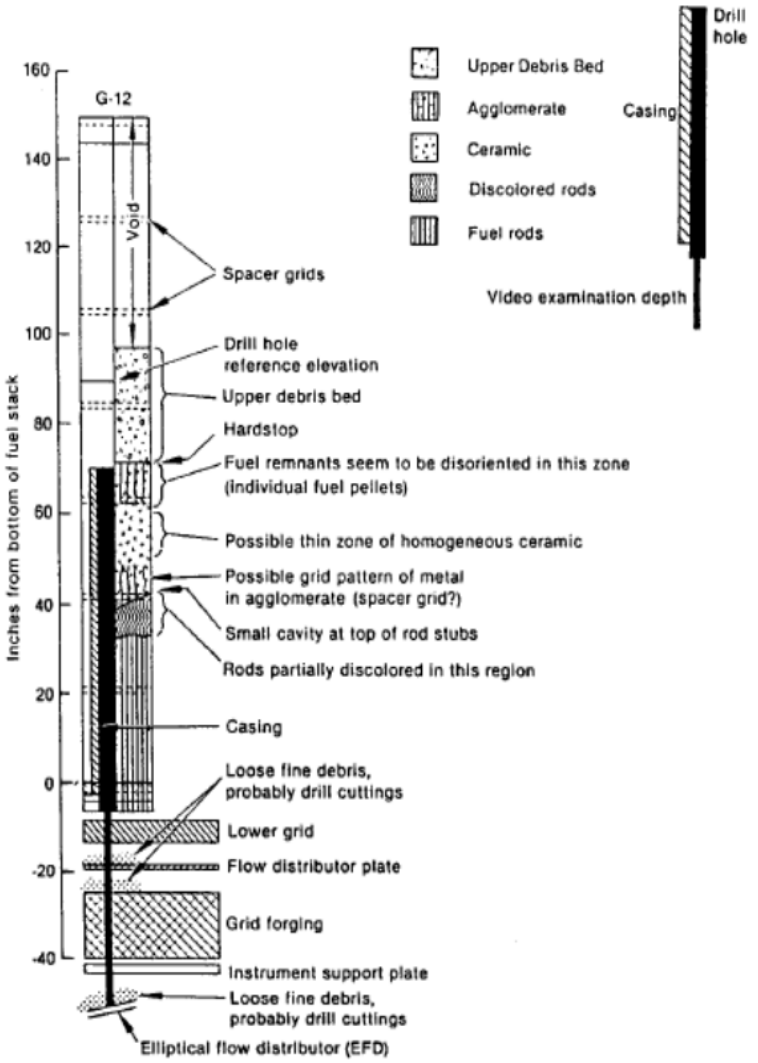

Figure 34. Example of core bore material diversity. (EGG-TMI-7385, 1987)

Upper Crust

The upper crust of the central melt contained ceramic and metal phases, with the ceramic consisting of various fuel material ratios of uranium-zirconium oxide and the metallic phase being primarily iron-nickel-aluminum from melted structural components and control rods. Metallic phases were present in cracks within the ceramic phases. This suggested that the ceramic phase had solidified and low melting temperature metal filled the cracks, flowing from above into the established ceramic. Approximately one-fourth of the upper crust was metallic in nature.

The upper crust samples were examined using scanning electron microscopy and optical metallography. Distinct phases of high-uranium $(U,Zr)O_2$ and high zirconium $(Zr,U)O_2$ were identified. FeCrO spinel crystals were found at grain boundaries in the ceramic phases. By X-ray diffraction, crystal structures identified included cubic UO_2, and monoclinic and tetragonal ZrO_2. The presence of these phases indicates that the melt cooled relatively slowly, allowing the multiple crystalline phases to form. Rapid quenching would have been expected to leave the $(U,Zr)O_2$ cubic form as a single phase.

Metallic phases that had penetrated cracks in the ceramic melt included 1) silver and indium from control rods, 2) iron, nickel and tin from structural steel and zircaloy, and 3) inclusions of silver, indium, nickel and tin as individual elemental constituents. One investigator found nickel-tin alloy precipitates that were approximately 40% tin, and iron-nickel phases, both of which have specific formation temperatures of 1500 and 1700K, respectively. Some of the melt material broke up into granular fragments that can be seen in the core bore tube as Figure 35.

Figure *35* Core Bore Section with loose U-ZrOx gravel (Courtesy INL)

Central Melt

The central region of the melt was composed primarily of relatively homogeneous uranium-zirconium (U, Zr) O_2 ceramic or metal-ceramic agglomerates. A section of the core bore indicating the progression of particles melting together into an integrated melt is shown in *Figure 36*.

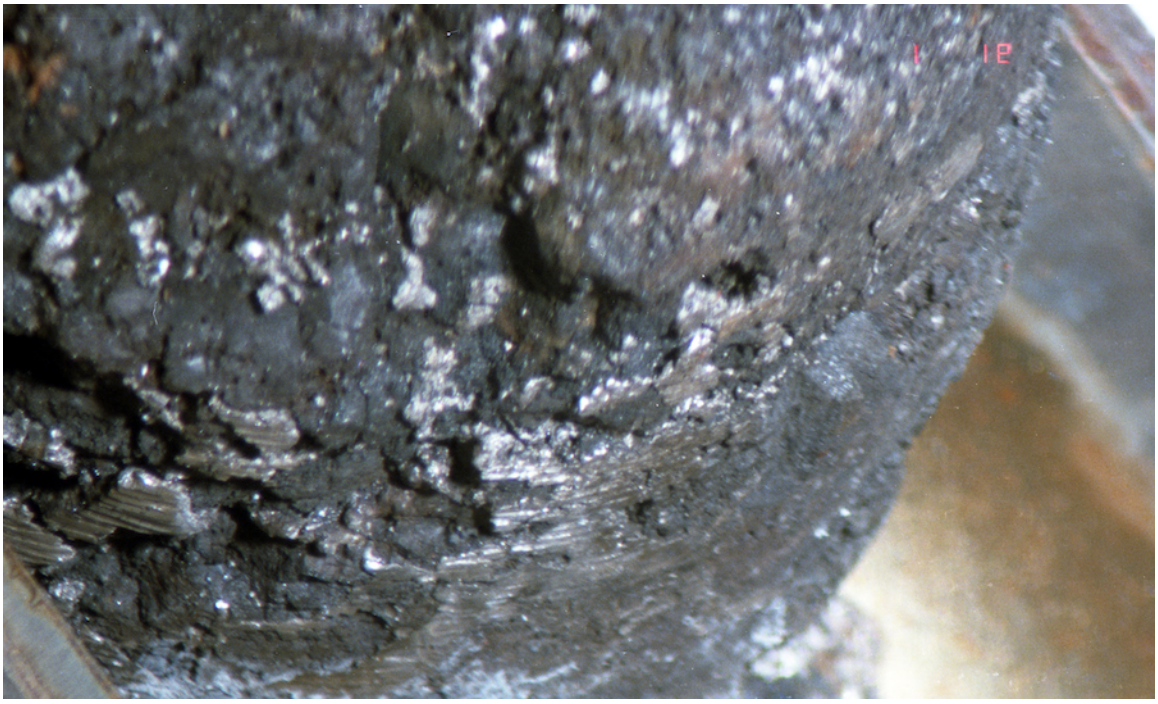

Figure 36 Core bore section consolidated melt material (Courtesy INL)

Variations in composition resulted in phases with higher uranium as well as those with higher zirconium. The “homogeneous” ceramic types were predominately uranium-zirconium oxide, the relative concentrations varied widely (UO_2 62–82 wt%, ZrO_2 18–53 wt%) over the melt volume. Confirmation of the ceramic characteristics was done by X-ray diffraction; this showed the fluorite face-centered cubic form of UO_2 and the monoclinic of ZrO_2. Cubic spinel phases containing iron, nickel, chromium, aluminum and tin in the homogeneous melt material appear at the grain boundaries and, in some cases, as discrete inclusions in void spaces. In other cases, silver spheres were identified within metallic phases. In general, it appeared that the central melt remained at a high temperature for a longer period than the upper crust, allowing the various constituents to become more uniformly mixed. The presence of aluminum in the central melt is indicative that the aluminum-boron oxide burnable poison rods had melted at an early stage in the process, prior to the formation of the upper crust. A scanning electron micrograph of a sample from the central portion of the melt (Core bore G12-P9-B) with iron-nickel and iron-chromium inclusions is shown in *Figure 37*. (Bottomley, 1989) Some of the silver-indium control rod material alloyed with tin from zircaloy appeared as discrete metallic inclusions in which chromium oxide particles were present in voids. (McCardell, 1989) *Figure 38* is an SEM image of a spherical silver inclusion within a multi-phase material.

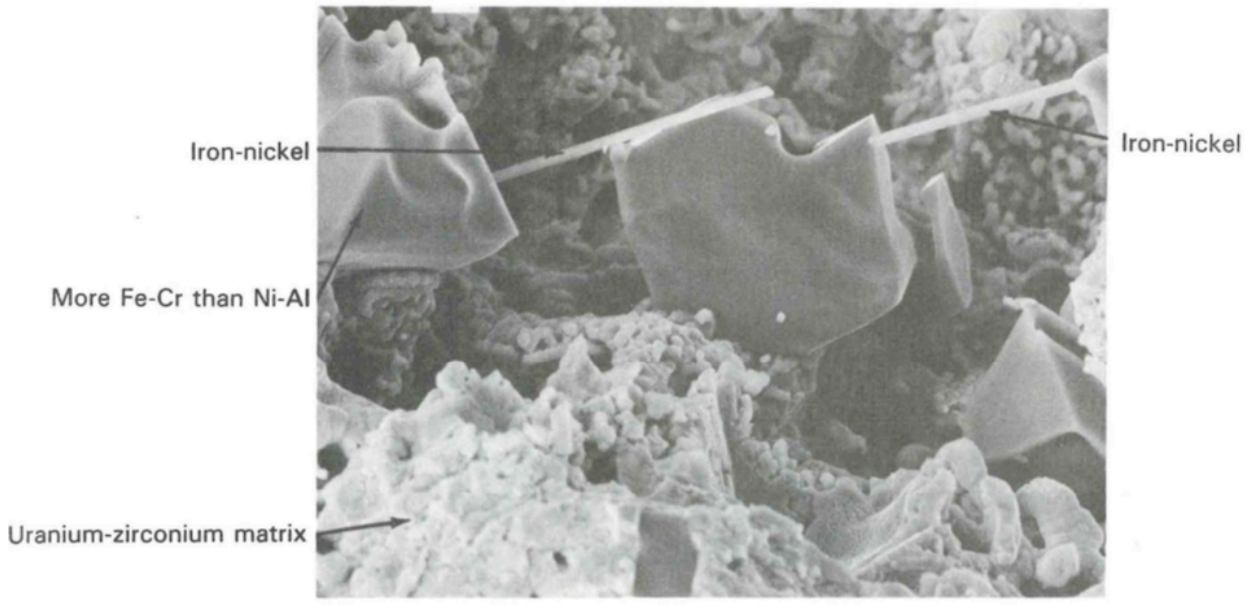

Figure 37. Iron-nickel crystals in uranium-zirconium central melt sample (Bottomley, 1989)

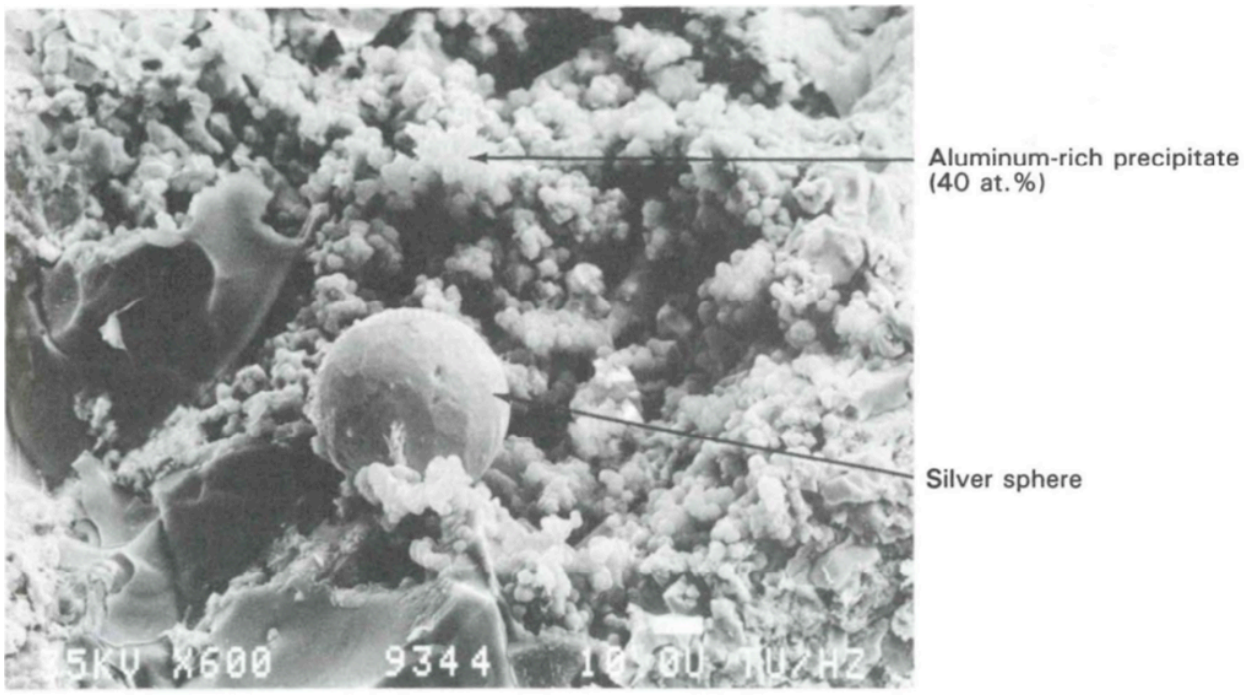

Figure 38. SEM image of spherical silver inclusion (Bottomley, 1989)

Volatilization tests were performed by Bottomley were unable to detect krypton, xenon or iodine, but the expected cesium, europium and ruthenium isotopes were released after heating a core sample to 2273K. An unusual observation of this testing was the higher release of ^{134}Cs relative to ^{137}Cs. Partial volatilization of the fission products was noted at 2273K, with complete release at 2773K.

Lower Crust

The lower crust of the central melt included stacks of fuel pellets that were encapsulated in a metal phase. The metal composition included three alloys that had a high percentage of zirconium, primarily Zr-Fe-Ni-Cr and Zr-Ni-In, as well as silver-indium. (McCardell, 1990) A cross-section image of the lower crust sample showing the fuel-rod stacks is Figure 39. (Hobbins, 1989) This image graphically illustrates how lower melting point materials such as Inconel (rod spacers) and control rod stainless steel melted when the core became uncovered and flowed to a lower level to solidify when sufficient heat was absorbed by the cooler bulk material at the depths of the core. In some cases, a thin shell of zircaloy remained surrounding the uranium dioxide fuel pellets, while in other cases, the zircaloy had either dissolved into the metallic phase or reacted with the UO_2.
Figure 40 is a photomicrograph of a previously molten, primarily uranium oxide sample with Cr, Al, Fe, and Ni accumulation at grain boundaries. A graphic illustration of materials encountered at various depths is Figure 41.

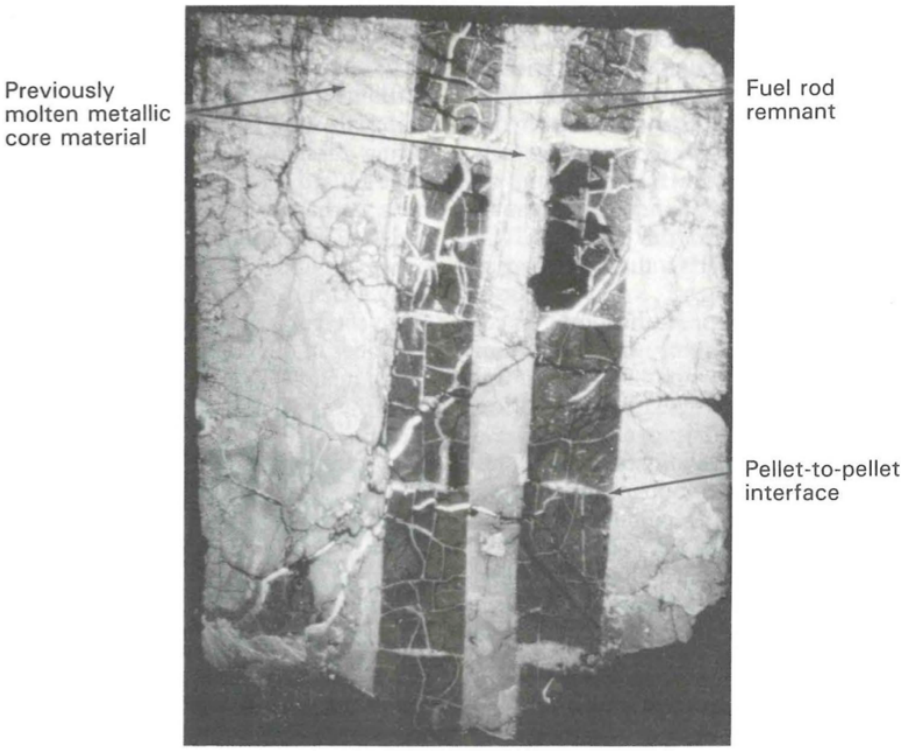

Figure 39. Encapsulated fuel-rod pellets in sample from lower crust core bore. (Hobbins, 1989)

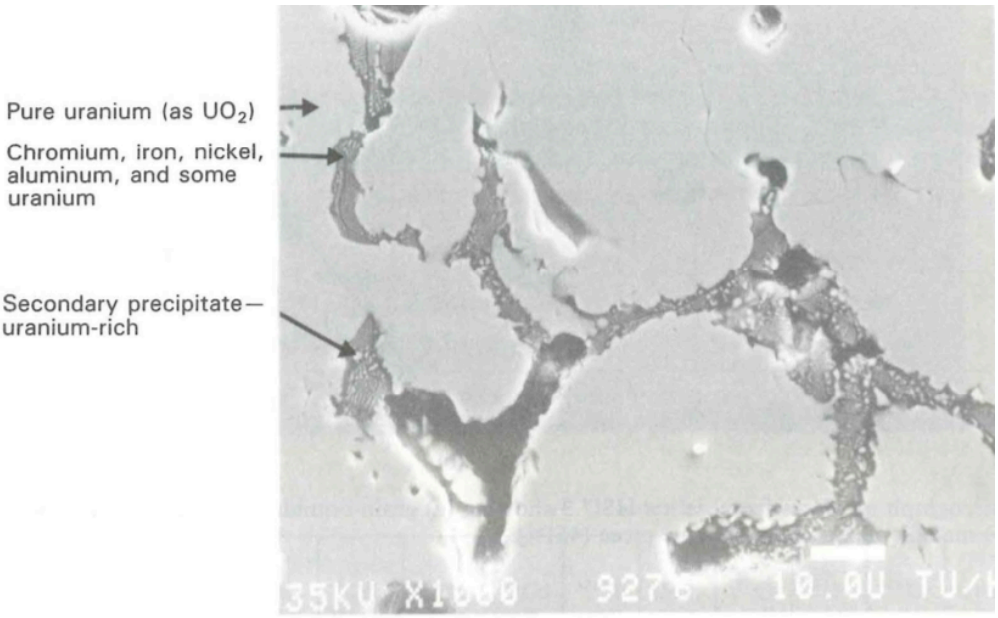

Figure 40. Uranium phase with metallic inclusion (Bottomley, 1989)

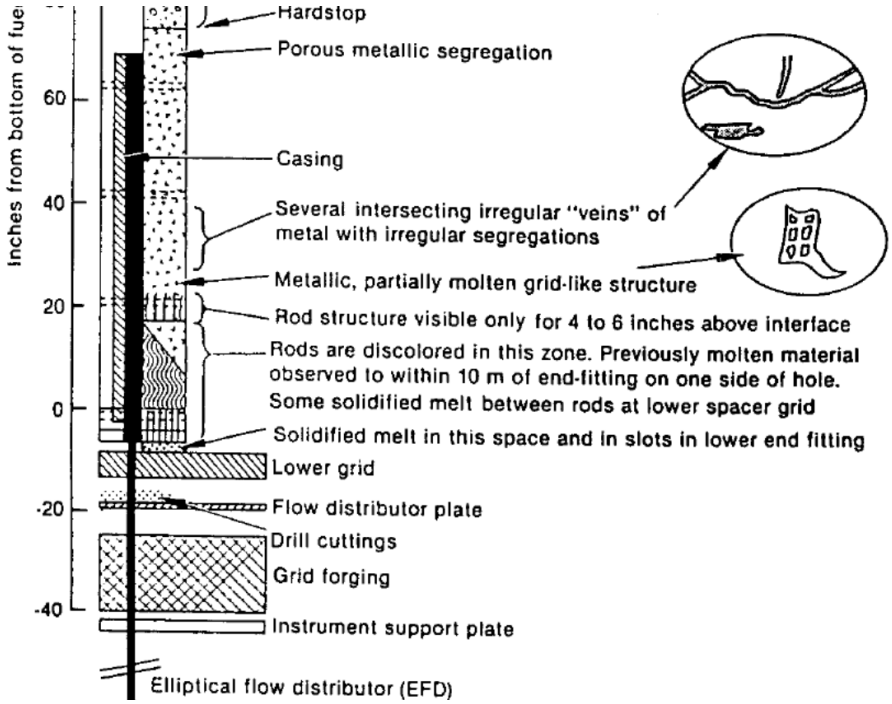

Figure 41. Section of core bore K9. (McCardell, EGG-TMI-7385, 1987).

For fuel-rod sections immobilized in the lower level of the melt, such as that taken from position K9, nearly in the center of the core, significant alteration of the zircaloy clad at the location of the melt partition, with a wide range of zirconia thicknesses observed. Hydride formation was noted as relatively uniform, with a circumferential uniform hydride surface.

Sections of clad that did not undergo gross oxidation exhibited the expected beta-phase of zirconium. In the highly oxidized zones, alpha-phase zirconium oxide (Zr[O]) was overlaid by a 14–52-micron layer of zirconia (ZrO_2). The large variation in zirconia thickness is indicative of the effect of a large thermal gradient. The oxygen ratio measured at the alpha-zirconium oxide/zirconium beta-phase interface indicated that temperatures may have exceeded 1370K. (Trotabas, 1989)

Fission-product ^{137}Cs and ^{134}Cs, and activation product ^{125}Sb and ^{60}Co-deposition were detected by gamma-ray spectrometry. Surface scrapings showed ^{238}U that may have been deposited during the samples' years-long exposure to uranium-containing water in the reactor vessel. (Jensen, GEND-INF-082, September 1987).

To establish these characteristics, core bores were subjected to axial gamma-ray spectrometry to identify the concentration and distribution of gamma-emitting fission products. The cores were examined for chemical content to determine what constituents had reacted to produce the melt.

Chemical analysis was performed to establish chemical composition, radionuclide content, and provide a basis for nuclear material accountancy. Several approaches were used to dissolve the samples for analysis. These included grinding the samples to get a sample mass that could be readily dissolved, dissolution with sequential application of nitric acid to dissolve metal and uranium, followed by hydrofluoric acid to dissolve remaining silicates and oxides of niobium, tantalum, titanium and zirconium, then any remaining undissolved material was melted in a pyrosulfate fusion, which was used to provide a solution for to be used for mass spectrometry and scintillation counting analysis.

An example of a metallographic image of mounted debris showing ZrO_2 as a separate phase as well as a uranium-aluminum-zirconium oxide phase appears in Figure 42.

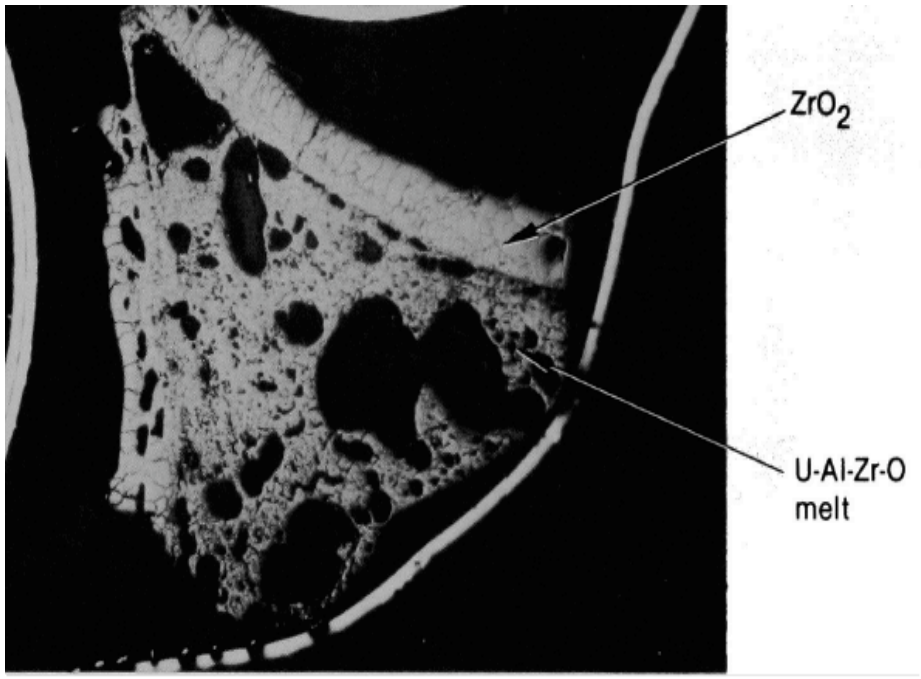

Figure 42. Optical metallograph of melted core sample. (Akers, GEND-INF-075 Part 1, 1986)

In those zones of the core where the lower sections of the fuel assemblies were largely intact, the core bore samples retained that configuration with some distortion due to the twisting action of the core bit passing through that material. A section of the intact rod structure is shown as a composite image in Figure 43, and detailed views in Figure 44 and Figure 45.

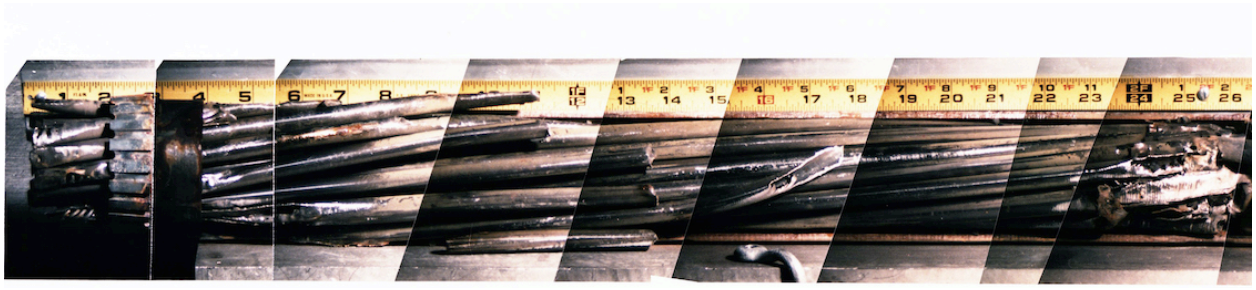

Figure 43 Composite Image of Intact Rods Core Bore (Courtesy INL)

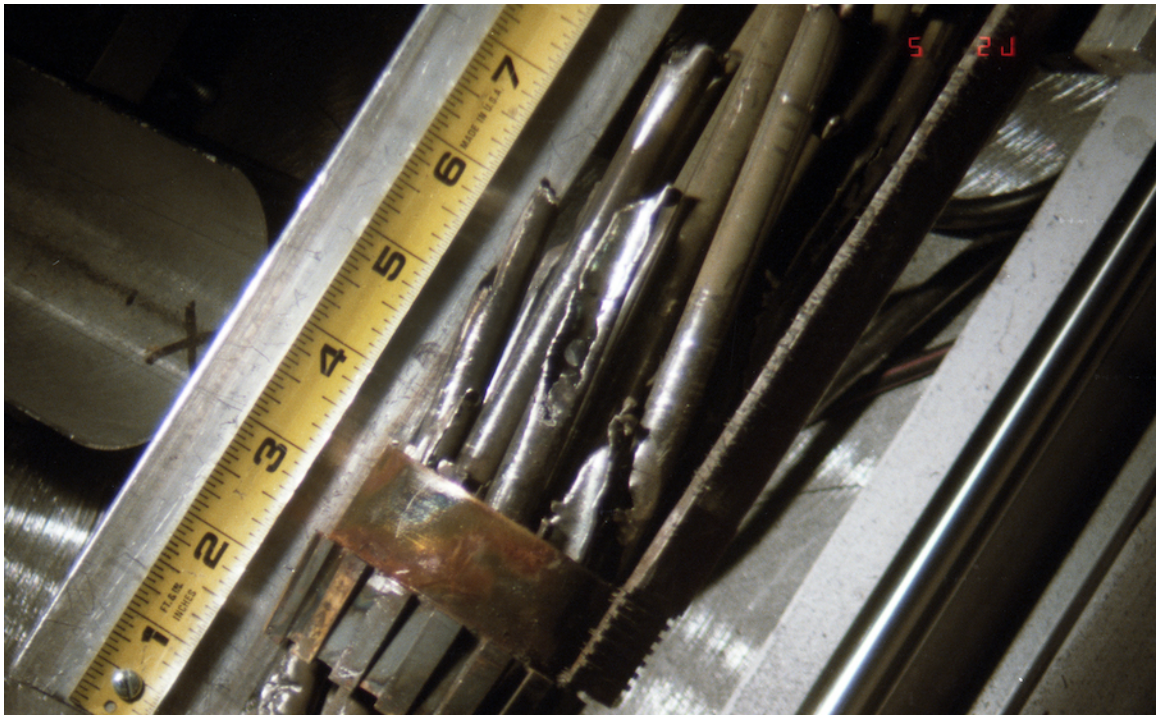

Figure 44 Individual Image of Partially Intact Rods Core Bore (Courtesy INL)

Figure 45 Rods Showing Discoloration and Melted Ends (Courtesy INL)

Following the receipt and analysis of the grab samples and the core bore samples, it was possible to combine that information with the video and ultrasonic probe data to reconstruct the post-accident melt profile. Additional information regarding the material that accumulated in the lower plenum was the result of removal of the lower core support structures. The reconstructed melt image has been included in nearly every general explanation of the melt outcome, and to follow suit, it is included in Figure 46.

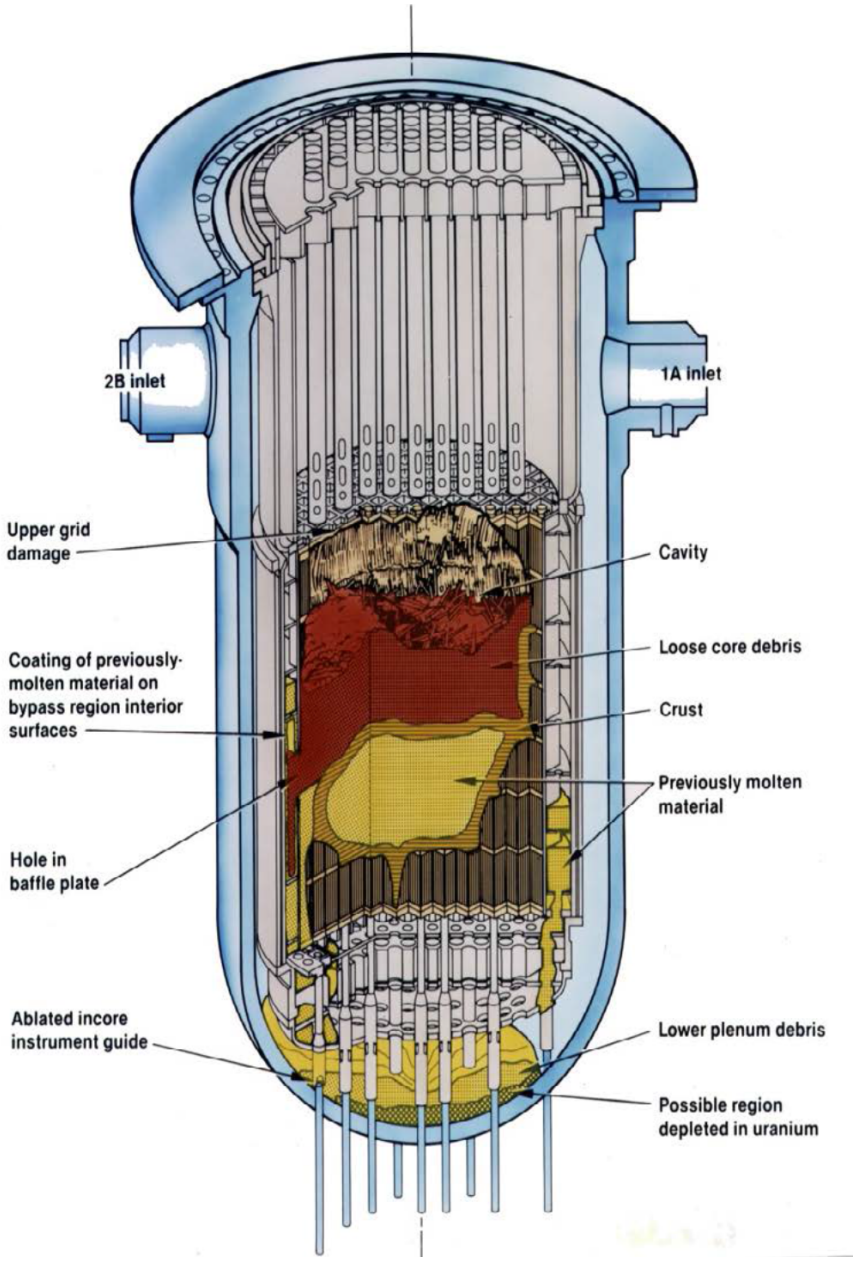

Figure 46. Final reconstruction of post-accident in-vessel debris configuration. (Courtesy of INL, 2022)

By combining the composition averages from the core bores and recovery actions, it was possible to develop a tabular inventory of where fuel ultimately resided at the point the melt was stabilized. The general mass inventory is shown in Table 4.

Table 4. Debris Composition and Distribution (Akers, 1990)

Core material repositories	Core material distribution of fuel material [a]			Core material distribution of control rod materials [a]		
	Uranium	Zirconium	Tin	Silver	Indium	Cadmium
Upper reactor plenum	(b)	(b)	(b)	1.0	(b)	(b)
Upper core debris	24	13	(c)	1.8	(c)	(c)
Upper crust region						
Ceramic	1.3	1.2	2.3	1.2	3.6	0.65
Metallic	--	0.3	6.1	2.4	3.3	0.39
Consolidated region						
Ceramic	12	18	--	10	27	6.1
Metallic	--	0.2	5.8	1.6	2.1	1.1
Lower crust region						
Ceramic	3.6	2.8	9.3	7.3	7.2	1.4
Metallic	--	5.6	26	11	16	2.9
Intact fuel rods (d)	33	33	33	11	11	11
Lower reactor vessel head	15	11	(c)	(c)	(c)	(c)
Lower core support assembly	4.6	3.3	(c)	(c)	(c)	(c)
Upper core support assembly	3.3	2.4	(c)	(c)	(c)	(c)
TOTAL	97	91	82	47	70	23

(a) Percentage of the total amount of the element originally present in the core
(b) Insignificant amount (<0.1 wt%) based on the upper plenum measurements
(c) Elemental constituent not detected based on detection limits of approximately 0.1 wt%

Characterization of the various sampled materials provided an indication of the distribution of radionuclides that were retained in the core according to their relative volatility as shown in Table 5.

Table 5. Reactor System Fission-Product Distribution (Akers, 1990)

Fission Product Repositories	Fission-product distribution Low-volatility fission products Percent of inventory [a]			Fission-product distribution Medium-volatility fission products Percent of inventory [a]			Fission-product distribution High-volatility fission products Percent of inventory [a]		
	Ce-144	Eu-154	Eu-155	Sr-90	Ru-106	Sb-125	Cs-137	I-129	Kr-85
Ex-vessel	0.01	(b)	(b)	2.1	0.5	0.7	(b)	(b)	54
Containment atmosphere, basement, and tanks							47	(47) [c]	(b)
Reactor coolant system	(b)	(b)	(b)	1	(b)	0.2	3	1	(b)
Auxiliary building	(b)	(b)	(b)	0.1	(b)	0.7	5	7	(b)
In-vessel									
Upper reactor plenum	(b)	(b)	(b)	(b)	(b)	(b)	(b)	(b)	(b)
Upper core debris-A	26	30	24	23	14	13	5.3	5.9	6

Fission Product Repositories	Fission-product distribution Low-volatility fission products Percent of inventory [a]			Fission-product distribution Medium-volatility fission products Percent of inventory [a]			Fission-product distribution High-volatility fission products Percent of inventory [a]		
Upper core debris-B [c]	20	19	19	19	16	24	4.3	5.3	(b)
Upper crust region Ceramic Metallic	1.4	2.0	1.6	 0.73 (b)	 0.8 3.8	 0.5 7.8	0.41	0.27	(b)
Consolidated region ceramic metallic	24	32	22	 8.3 (b)	 2.2 9.0	 3.1 6.9	0.77	2.1	(b)
Lower crust ceramic metallic	5.9	7.9	5.1	 4.5 (b)	 5.7 24	 7.4 36	1.4	3.5	(b)
Intact fuel rods	30	30	30	30	30	30	30	30	30
Upper core support assembly	3.4	4.5	(d)	3.9	0.23	0.22	0.46	0.12	(b)
Lower core support assembly	4.7	6.3	(d)	5.3	0.32	0.30	0.63	0.16	(b)
Lower head-reactor vessel	16	21	(d)	18	1.1	1.0	2.1	0.54	(b)
TOTAL	105	122	110 [d]	93	94	119	95	97	91

(a) Percentage of total amount of the fission-product inventory calculated from comparisons with ORIGEN2

(b) Insignificant amount (<0.1 wt%) based on the upper plenum measurements

(c) Two sets of bulk sample measurements were performed on the upper debris bed. The A series was performed on 16 cm^3 sample from near the center of the core at a variety of depths whereas the B series were bulk samples from near the bottom of the debris bed. The data provide a range. For the totals, the B series data were used.

(d) Measurements not performed for this radionuclide at this core location. The total shown value in parenthesis is a total which assumes the same distribution as Eu-154 for the repositories where measurements were not performed

3.9 Vessel Investigation Project

As a result of the determination that a significant part of the melt had relocated to the lower head of the reactor pressure vessel, a separate effort was organized to evaluate its effects. Fifteen samples of the head material were acquired with reach tools from the top head work platform after the solidified core material had been removed. Other samples included sections of instrument guide tubes. The steel samples were analyzed using tensile, microhardness, Charpy V-notch impact and creep testing. Analysis of the samples' chemical composition was also performed. Temperature effects were evaluated using optical metallography. The estimated temperatures from several locations ranged from a local maximum of 1100C to a general maximum of 727C. Some cracking was observed around instrument nozzles, but no through-wall penetration occurred. It was concluded from various calculations that the vessel could have sustained the local maximum temperature for thirty minutes if heat could be dissipated to relatively cool sections of the vessel. (Wolf, 1994)

Evaluation of the fuel debris material recovered from the lower head was done according to the protocol used for characterizing the loose grab sample debris and the core samples. Radiological, chemical and physical properties were measured. The data indicate that all of the samples were uranium-zirconium oxide which had solidified in the lower head. The investigation identified both uranium-predominant and zirconium-predominant phases, which suggested a relatively slow cooling process with fully oxidized zirconium. The average elemental composition was generally 70 wt% uranium and 13.75 wt% zirconium. Approximately 3 wt% of the melt was stainless steel and Inconel from core structural materials. Porosity identified in the material was presumed to result from trapped steam or metal vapor.

3.10 Core Removal

Multiple approaches for core removal were considered prior to receipt of the first characterization data. Five official predictions of the degree of core damage were compiled into a single report known as GEND-007.

The GEND-007 report was used as a basis for development of design concepts for defueling. These were the dual telescoping tube/manipulator system, the manual defueling-cylinder system, the indirect defueling-cylinder system, the flexible-membrane defueling system, and the dry defueling system. The dual telescoping-tube system would have mounted two telescoping tubes on the TMI-2 defueling bridge and remotely operated them by closed circuit video. The manual defueling system was a design with a rotating cylinder supported on the top flange of the reactor vessel with a slot through which operators would perform manual removal of the core. The indirect defueling-cylinder system was to have inserted an X-Y bridge with a telescoping tube in place of the manual tools of the previous design. The flexible-membrane defueling system would have incorporated an X-Y bridge using a single telescoping tube operating through a conical contamination control membrane and used a separate tank whose support arms were to have pivoted out over the reactor vessel to hold manipulators canisters, buckets, and tools in support of the manipulation function of the telescoping tube. The dry defueling system was to insert an indexable shield ring on the top flange of the reactor vessel that used an access port to remove debris via a heavily shielded transport cask (Sec. 8.2.2 EPRI NP 6931).

Considerable discussion about the merits of manual versus automated core removal included the possibility of using the Westinghouse remotely operated service arm (ROSA) to shred the melted core and transfer the result by vacuum to canisters outside the reactor vessel. One of the negative aspects of this approach was the dispersal of the core nuclides, increasing the dose potential and placing a greater demand on the water-cleanup systems. Several variations of the remote and manual core recovery systems were proposed, but all had the problems of complexity and delays due to development and testing of tools to size materials that were poorly understood and not well characterized.

Due to the expected delay in the automated-tool system development and the cost and availability of the polar crane, it was decided that the manual defueling approach was the most expedient. The manual shielded defueling platform was fabricated and installed on the top of the Internals Indexing Fixture, which was mounted to the top flange of the reactor vessel as part of the plenum removal process. The platform was a shielded turntable with slots through which extended reach tools could be used to pick up individual pieces of debris and accumulate them in baskets that were used to fill the fuel debris canisters. The platform also supported the canister handling system and included specific ports for canister removal. An isometric view of the platform is shown in Figure 47. The work elevation was nine feet above the upper flange of the reactor vessel, as seen in Figure 48. Figure 49 is a photograph of the deployed system from above.

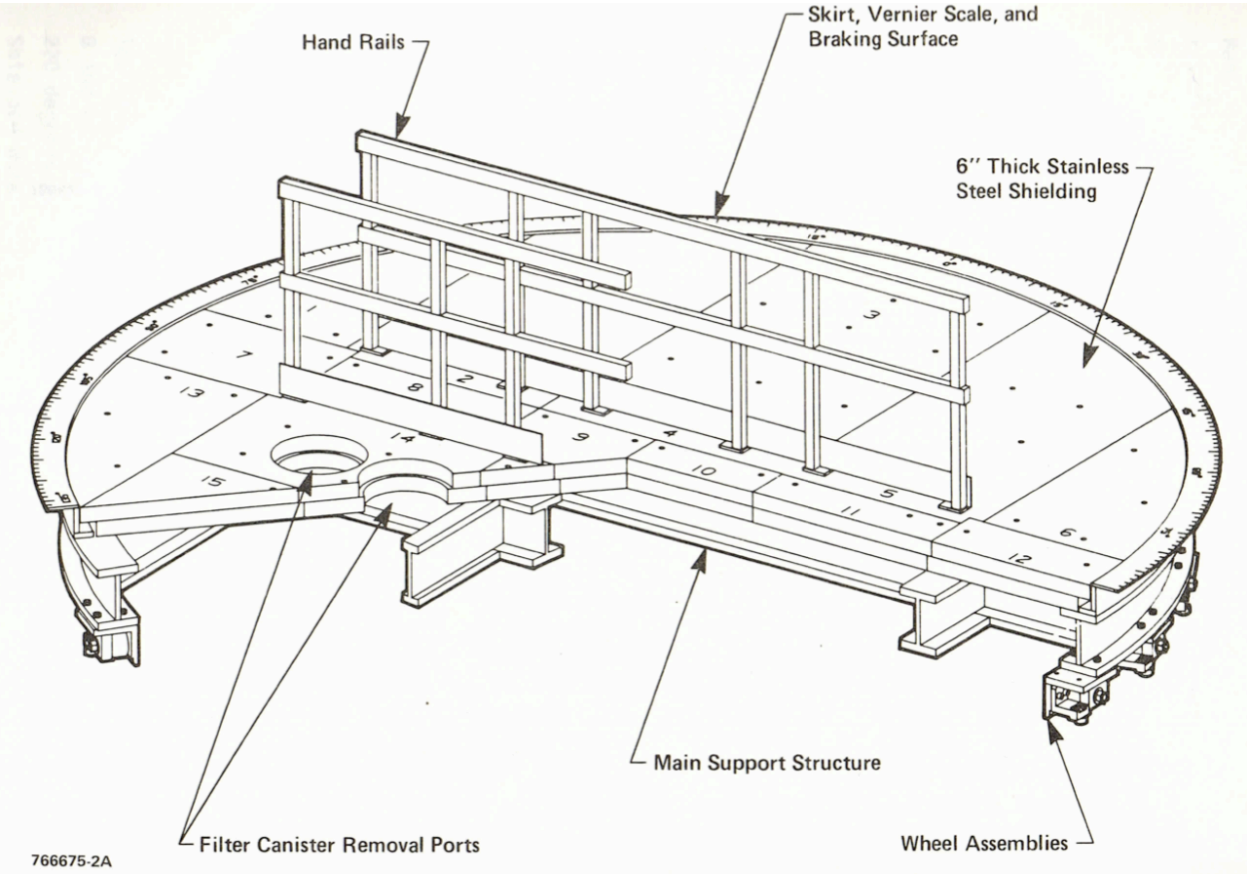

Figure 47. Manual shielded defueling platform. (Falk, 1985)

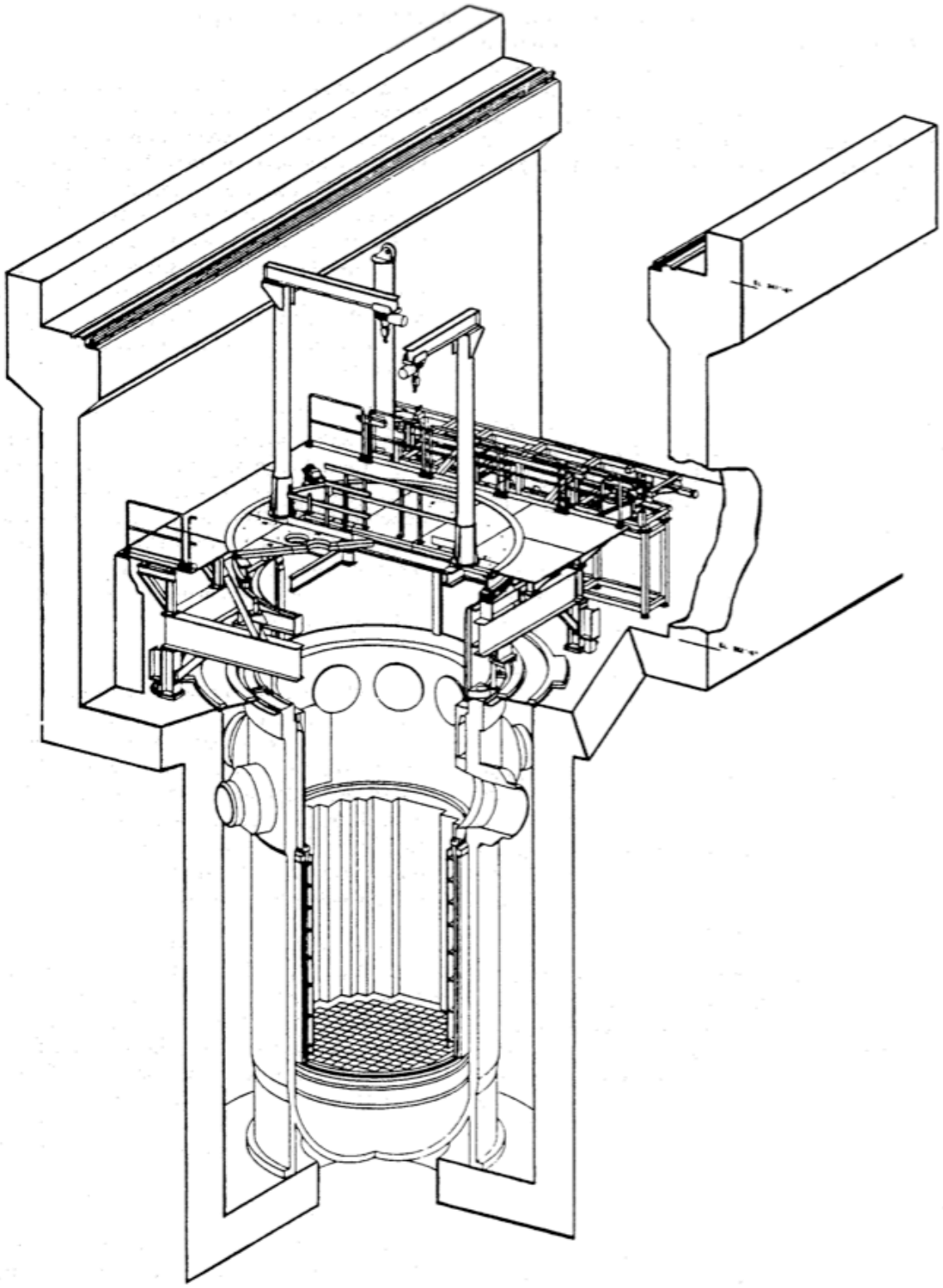

Figure 48. Defueling platform schematic in position on reactor vessel. (Holton, 1990)

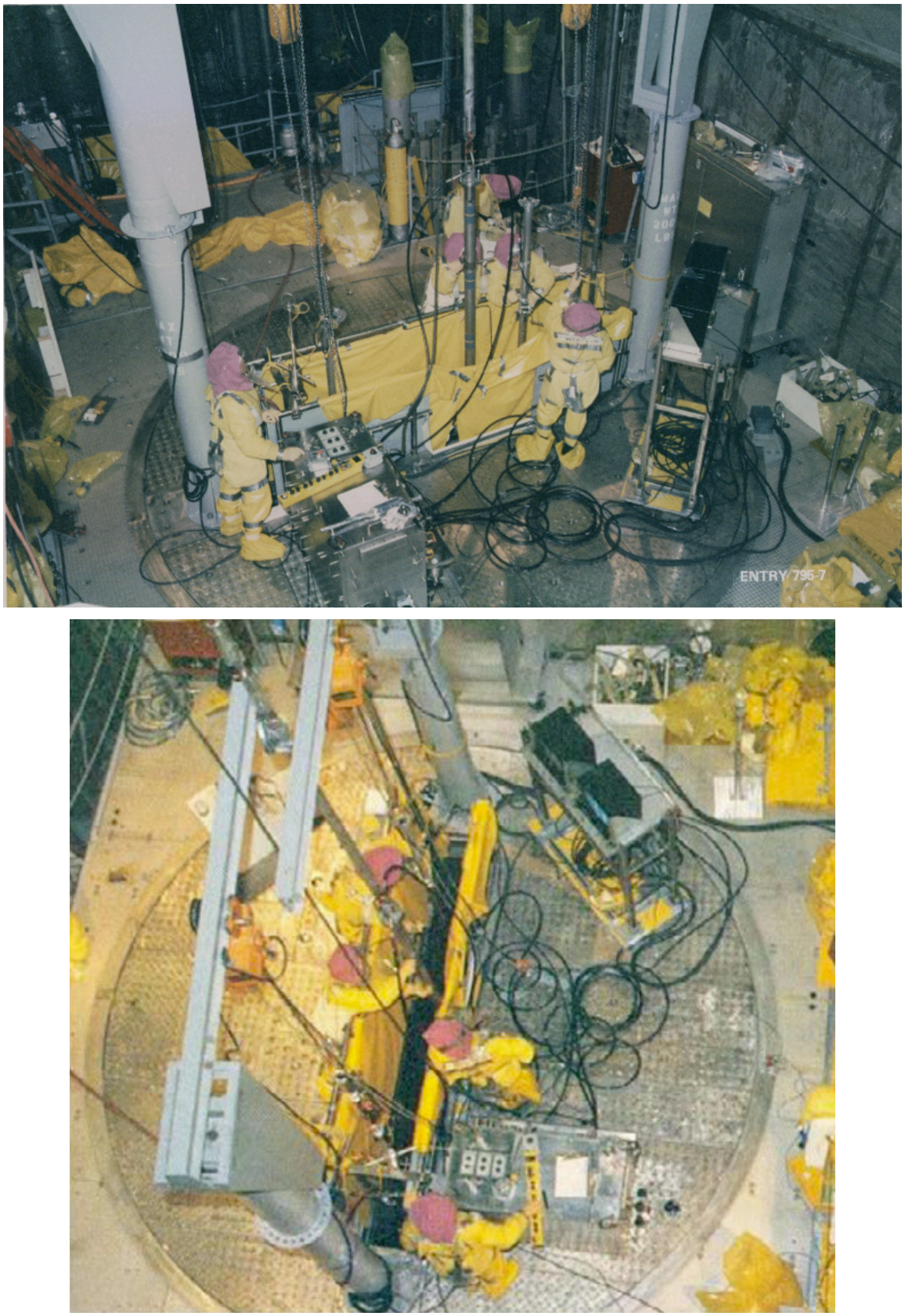

Figure 49. Photos of shielded defueling work platform. (Courtesy of NRC/INL tmi2kml)

The platform also supported a five-canister turret system that allowed multiple canisters to be loaded, as shown below in Figure 50. Once loaded, the canisters were weighed and then selectively transferred to the fuel pool for dewatering prior to loading into the transport cask.

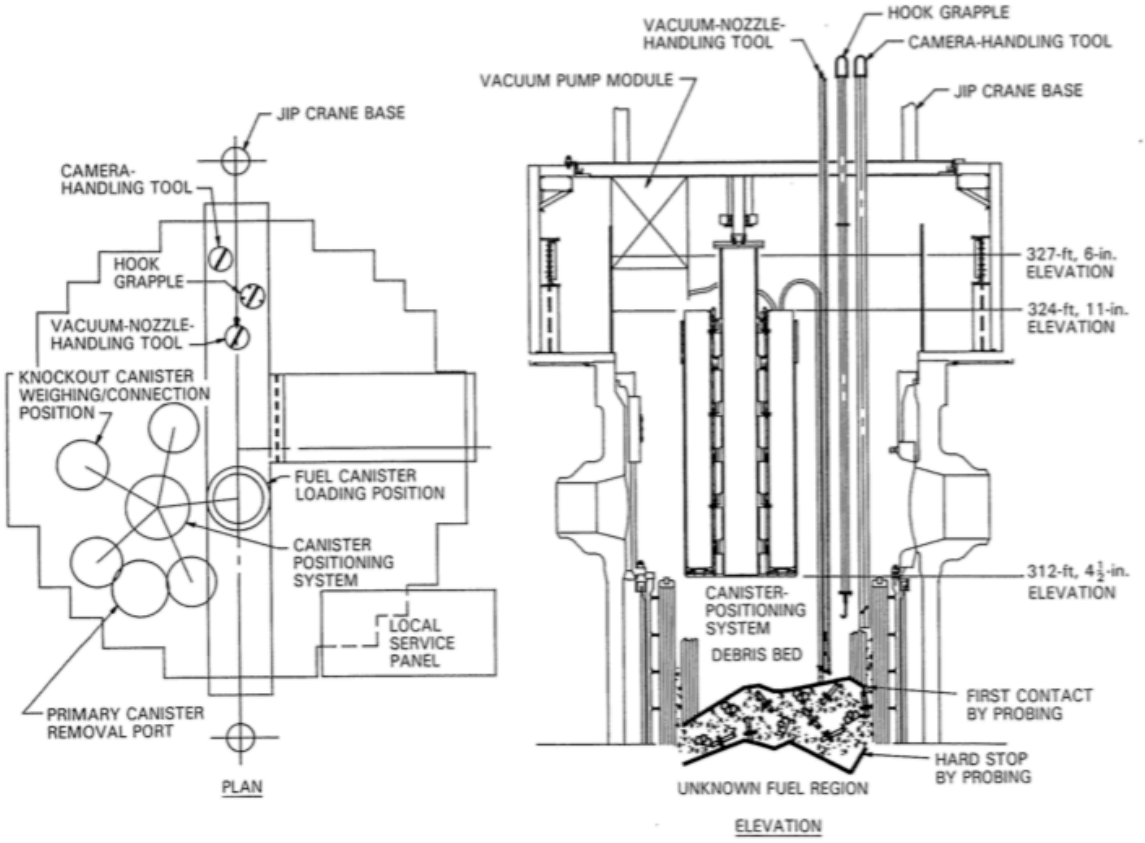

Figure 50. Canister-positioning system. (GEND-INF-073, 1986)

Once a canister had been filled to the desired limit, it was closed, lifted out of the reactor vessel through the penetration in the defueling platform, wiped down, and raised into the shielded transfer device, which then transferred the canister to the refueling canal within the reactor building. As shown in Figure 51, the canister would be loaded into an upender that rotated it to the horizontal orientation, allowing it to be moved through the fuel-transfer tube to the fuel-handling building pool.

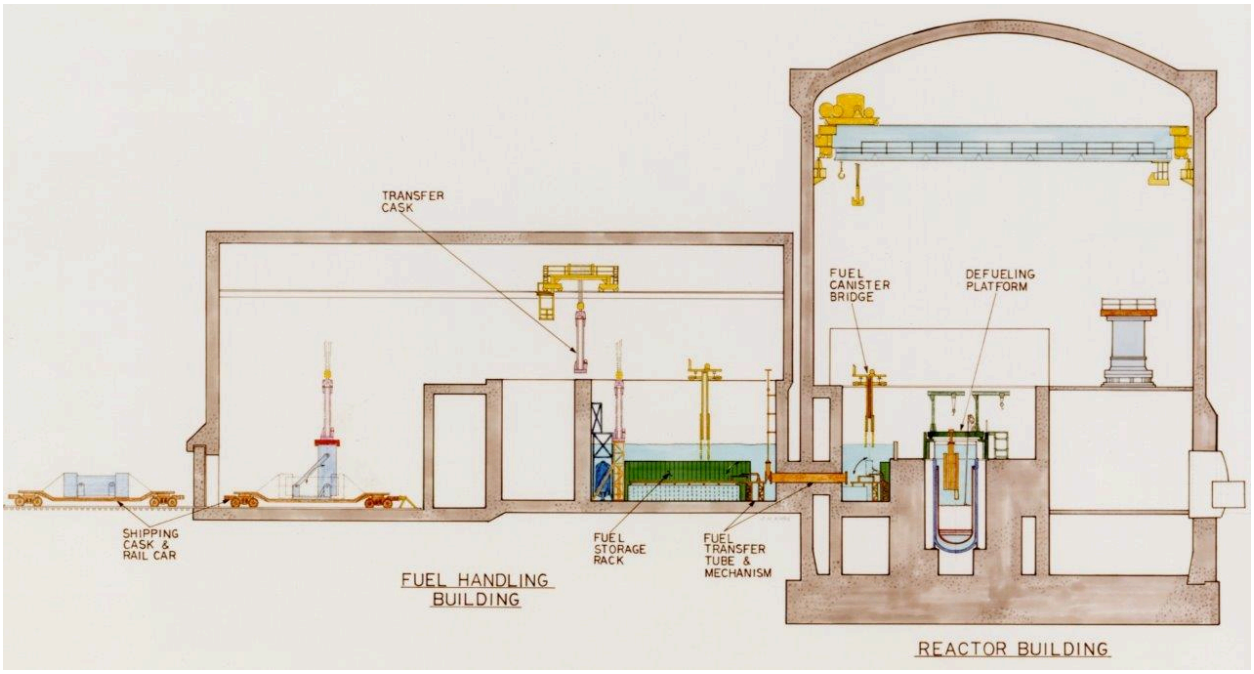

Figure 51. Schematic of canister transfer from reactor to fuel-handling building. (Courtesy NRC/INL tmi2kml)

Debris canisters were filled piecewise by filling buckets, which were then transferred to the canisters. A graphic (Figure 52) shows operator notes on filling a canister, including the location from which material was retrieved (shown as depth from the platform and radial position as well as the type of material added to Canister D-188). (In this example all material is identified as loose debris.)

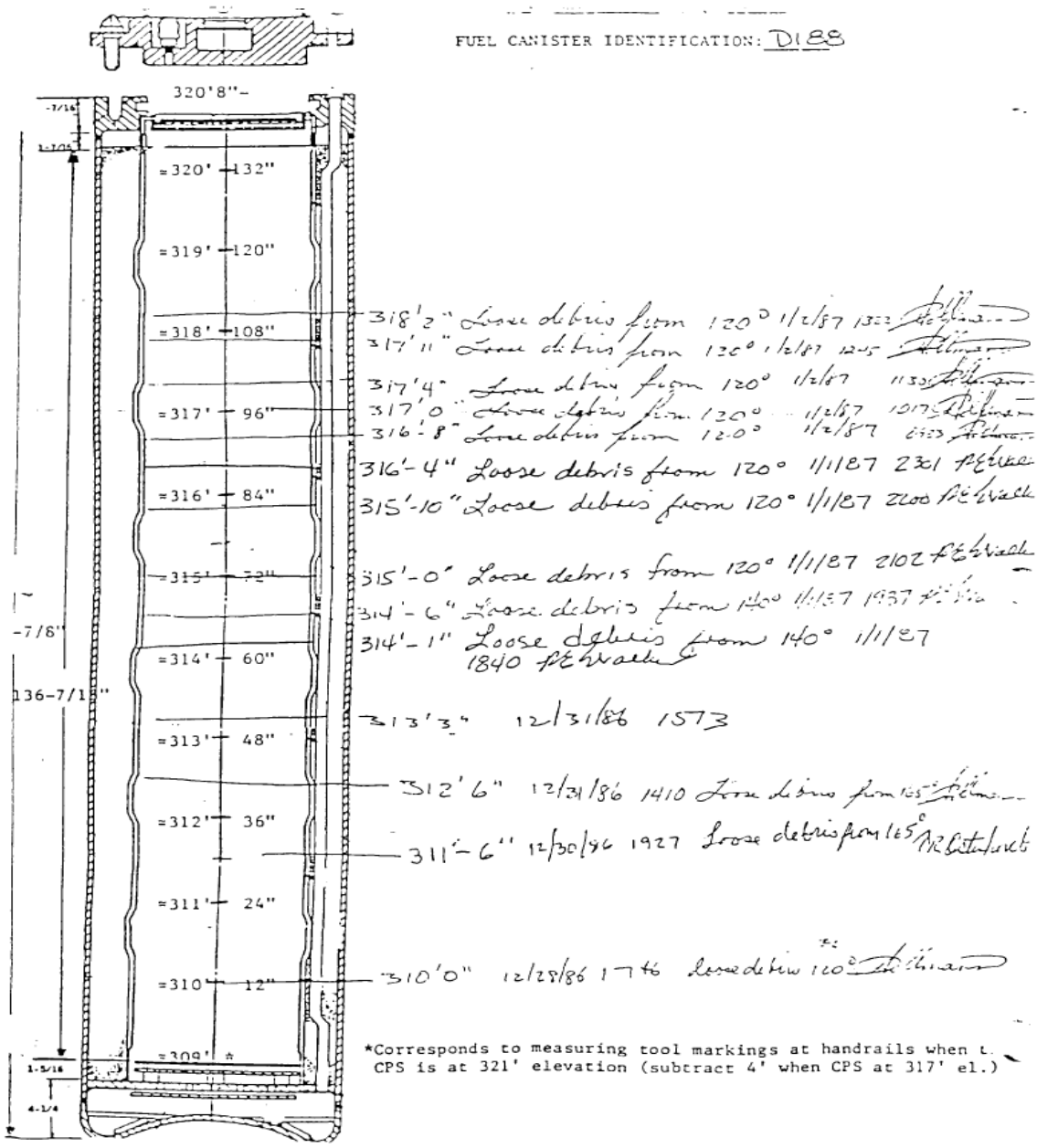

Figure 52. Operator log graphic of Canister D-188 loading. (Pincock, 2013)

Defueling Tools

More than 20 specialized tools were developed for debris retrieval and sectioning of the melted core, including a water jet cutter, an abrasive saw, bolt and bale cutters, hooks, pliers, (GEND-INF-065) and an underwater plasma torch. Numerous changes in tool design occurred as the core conditions became better understood. Early design bases assumed a degree of consistency in the material to be retrieved when, in fact, the diversity of melted, broken, and shattered material was significant. Only 15% of the fuel retained a recognizable rod and assembly configuration. Examples of the tools, including a clamshell tool, a spade-bucket tool, a spike tool, and a gripper tool, are shown in Figure 53.

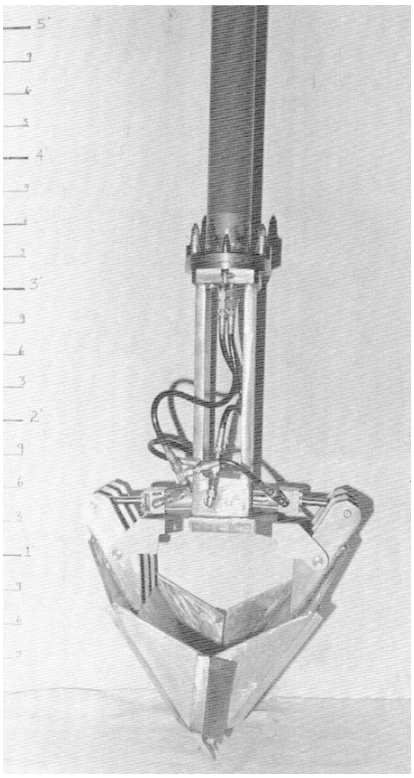

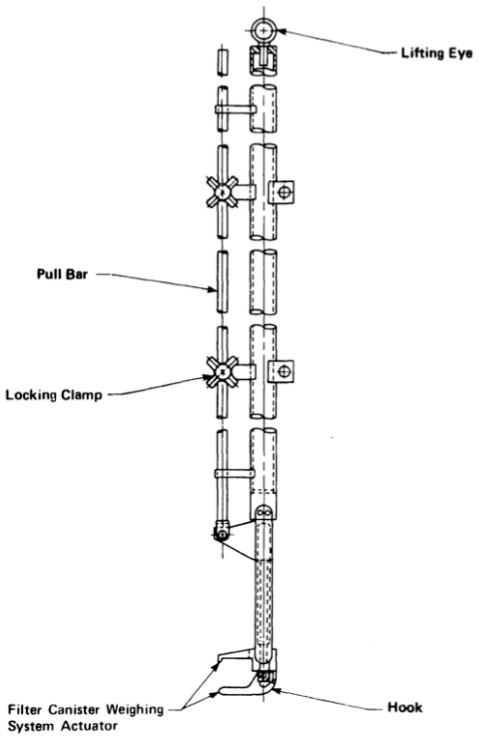

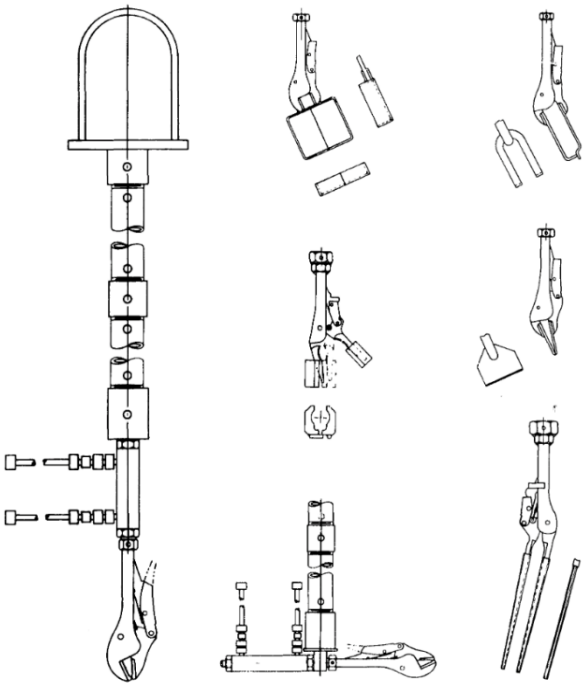

Figure 53.Clamshell tool, spade-bucket tool, spike tool, gripper tool, vise grip tools (GEND-INF-065)

The debris was recovered by manual tools, including scoops, pliers, and hook tools. The material was collected in reusable buckets or baskets, which were transferred to the debris canisters using a funnel.

The canisters were weighed during loading to assure that the design weight limit was not exceeded as well as to provide a running total of fuel recovered for material accountability.

Debris Removal

Primary fuel-removal operations began on October 30, 1985 and concentrated on making room for installation of the canister-positioning system. Much initial effort amounted to removal of fuel end fittings. The process of loose debris removal using a spade-bucket tool proceeded until April 1986 when the hard layer of formerly molten fuel was reached. Several tools, including a hydraulic impact chisel and a 135 kg impact tool, were tried on the crust, but none was able to penetrate it.

The core boring machine developed for the purpose of taking ten characterization cores was fitted with a 11.4 cm solid face bit with Stratapax cutter inserts for cutting through the ceramic melt (Kirkland, 1987), and in October 1986, it was used to begin the process of boring 409 holes to break up the center of the solidified melt. This operation was made more difficult by poor visibility conditions due to a loss of water clarity that resulted from microbial growth and small particulates that plugged the water-cleanup sintered-metal filters. The microbial bloom was attributed to the introduction of river water during the early recovery response.

Following breakup of the central monolith, water clarity was improved by using an additional water-filtration system. At that time, it was possible to see that there was a ring of large pieces that had been only partially broken up. These pieces were estimated to weigh as much as 1200 kg. Thus, they weighed too much to be handled with the manual long-reach tools. Because the pieces were overlaid on debris, hammering and chiseling them in place was ineffective; the loose material absorbed most of the impact energy. A special thick-walled funnel was designed for the canister top. Large chunks were placed in the funnel and broken up using a 198 kg jackhammer fitted with a 3.6-meter-long chisel.

Pieces as large as 5 cm were retrieved using an underwater suction system that used an air-driven diaphragm pump connected to a 10-cm-diameter suction pipe. The schematic and isometric sketches of the configuration are shown in Figure 54. This suction system worked with the knockout and filter canister system to recover pieces too small to be easily picked with manual grab tools. The system had a maximum flow rate of 288 L/min. A flow rate of 227 L/min was demonstrated to be sufficient to pick up 9.5 mm OD × 16 mm long UO_2 fuel pellets. Operator care was needed to prevent plugging of the suction uptake due to the random size and geometry of the material that could be moved. Using this system, as much as 14,500 kg of debris was removed in a single month. (GEND-INF-073) This system was operated from late 1986 to mid-1987.

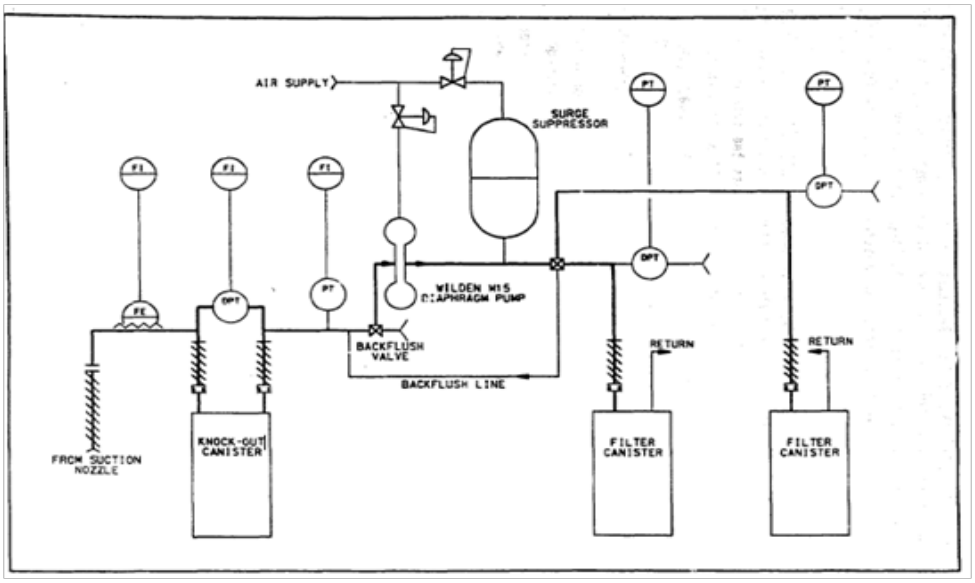

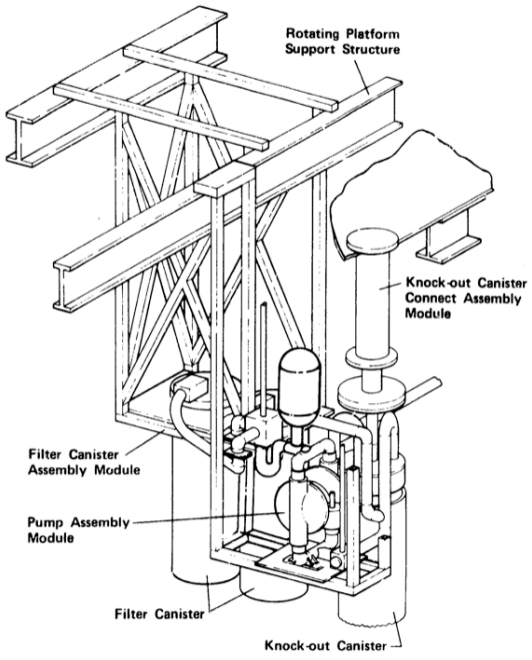

Figure 54.Suction System Schematic (GEND-INF-073 and GEND-INF-062)

For recovery of particulate from the area below the LCSA, an airlift system was developed by EG&G Idaho. This system uses entrained air injected into a vertical pipe that has a specific submergence to create a density differential that causes lower density (due to air entrainment) liquid in the lift leg to flow up that pipe to a separation chamber that allows solids to be collected and the liquid returned to the vessel while venting the air through a filter. Airlifts are used in highly hazardous chemical and radiological process plants because there are no moving parts and the motive force is remote from the material being transported, allowing maintenance without risk to personnel. An image of that design is shown in Figure 55. (EG&G, 1987)

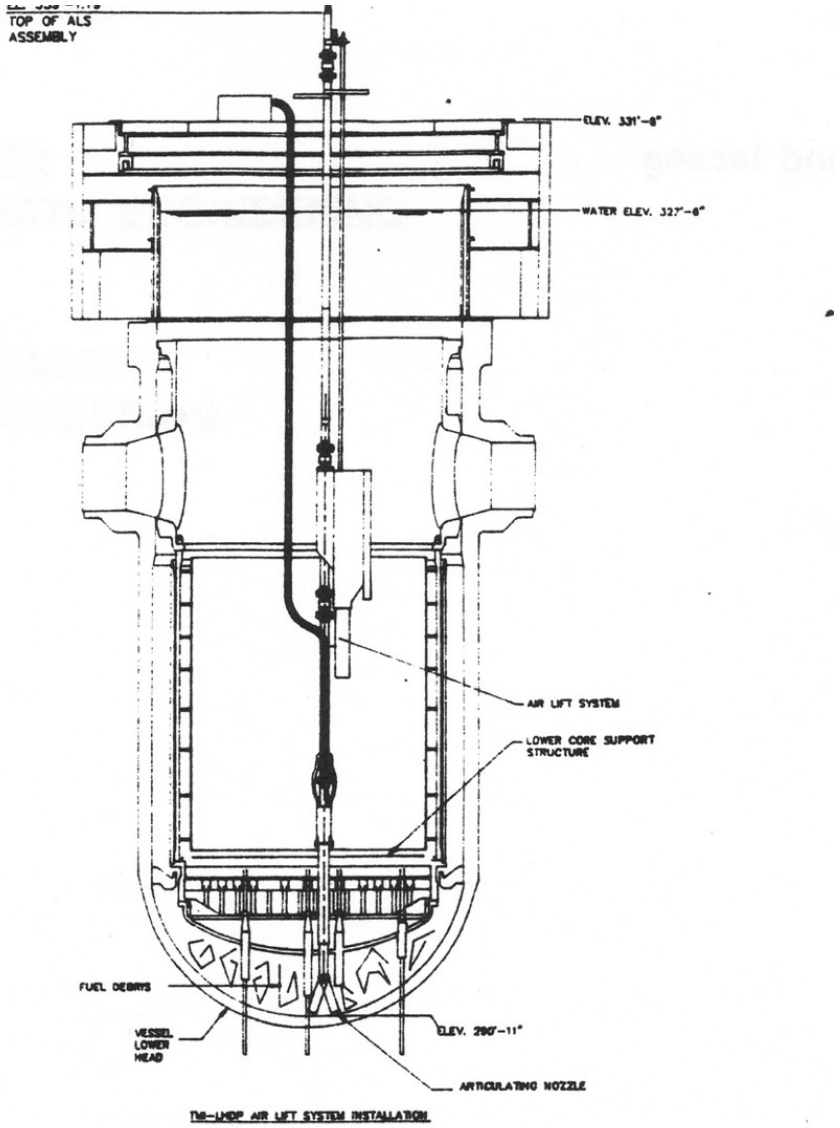

Figure 55. Airlift System Schematic. (EG&G 1987)

Due to distortion of the end fittings of some assemblies, a decision was made separate those discrete non-fuel components to the extent possible and dispose of them separately from the fuel debris that were placed in canisters. The separated end fittings were shipped to the U.S. DOE site at Hanford, Washington, and buried as low-level waste.

Stub or Partial Assemblies

The next type of fuel debris remaining after the central monolith and perimeter melted zones were removed was the partial or stub assembly region around the periphery of the reactor vessel and the pieces remaining below the melt. Some sections were partially stuck together. Most of this material was removed using long-handled tools that screwed into the top, attached as a clamshell, and then using pry tools to tilt partial assemblies away from each other. In some cases, largely intact assemblies could be removed after a spike was pressed into the top of the assembly and a tool with two fingers grasped it at the base. Except for two significantly melted locations, the stub assemblies were removed by November 1987.

Lower Core support Assembly (LCSA)

Once the stub assemblies were removed, it was possible to see that between 9,000 and 18,000 kg of debris had fallen through the lower core support framework. Initial design assumptions had been that only easily suctioned pieces would be present under this structure. Video revealed that, in addition to the debris that fell through during the stub assembly and nozzle removal, a substantial quantity of melted, solidified core mass was present under the LCSA.

Because its purpose was to support the entire core, the LCSA was massive: 3 m in diameter and fabricated in five stainless steel plates, 90 cm deep. The components included the lower-grid top rib, lower-grid distributor plate, lower-grid forging, in-core guide support plate, and in-core guide tubes, as shown in Figure 56.

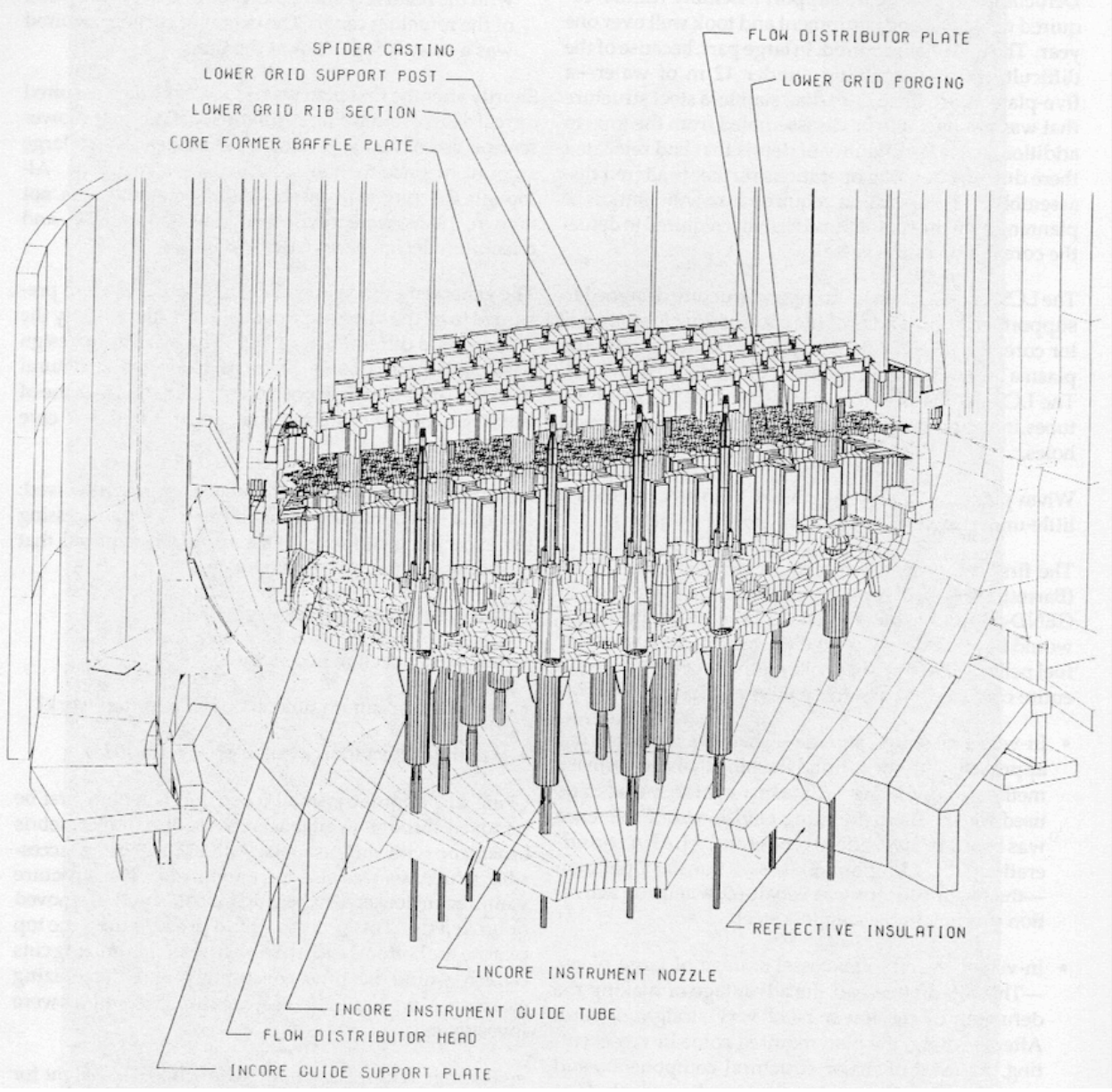

Figure 56. Lower core support assembly model. (Holton, EPRI-NP-6931, 1990)

Multiple alternatives were considered for the removal and sizing process, ranging from sawing and shearing to thermal, abrasive, plasma, and explosive cutting. After additional demonstration testing, the plasma-arc cutter was applied for the primary portion of this task. The work was performed under 12 m of borated water. It was estimated that opening an access hole with an area of 1.2 m^2 would require 890 cuts. Because of the large number of cuts necessary to create an opening through which the debris could be removed, an automated cutting system (ACES) was developed to deploy the plasma torch. The ACES system is shown in Figure 57. One alternative design included a multi-axis dual-arm system (MANFRED) that ultimately was not used due to its complexity and the expected problems of decontaminating the multitude of hoses and cables that operated the arms. The plasma torch was deployed using an X-Y bridge, which was lowered into the reactor vessel to a short distance above the lower core support to position the torch. (McGough, 1989)

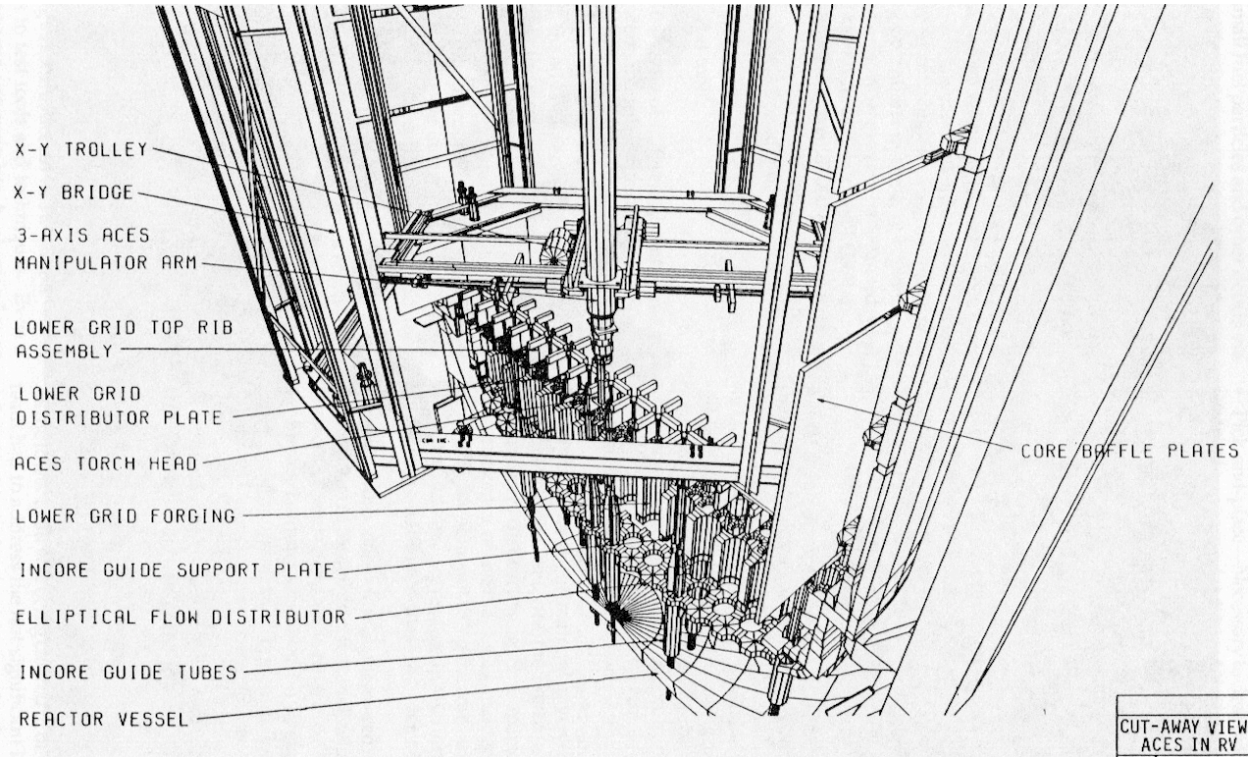

Figure 57. Automatic cutting equipment system (ACES). (Holton, EPRI-NP-6931, 1990)

Prior to deployment of the plasma-arc torch, numerous concerns were raised, including problems of maintaining subcritical, potential for hydrogen evolution, pyrophoric reaction of zirconium in water, the potential to damage the reactor vessel lower head, and unexpected spread of contamination. Through analysis, these concerns were discounted, and the torch was deployed.

Prior to using the plasma torch, the plan was that the core boring machine would be used to drill out fifteen of the 52 in-core guide tubes and all 48 distributor plate support posts. The core bore drill was fitted with two different types of bits (trepanning and junkmill) to perform this task (see Figure 58). Due to problems discharging drilling chips, the bits became fouled, and not all of the in-core tubes were able to be cut. Despite that setback, core boring machine was able to cut the lower-grid rib plate into thirteen pieces.

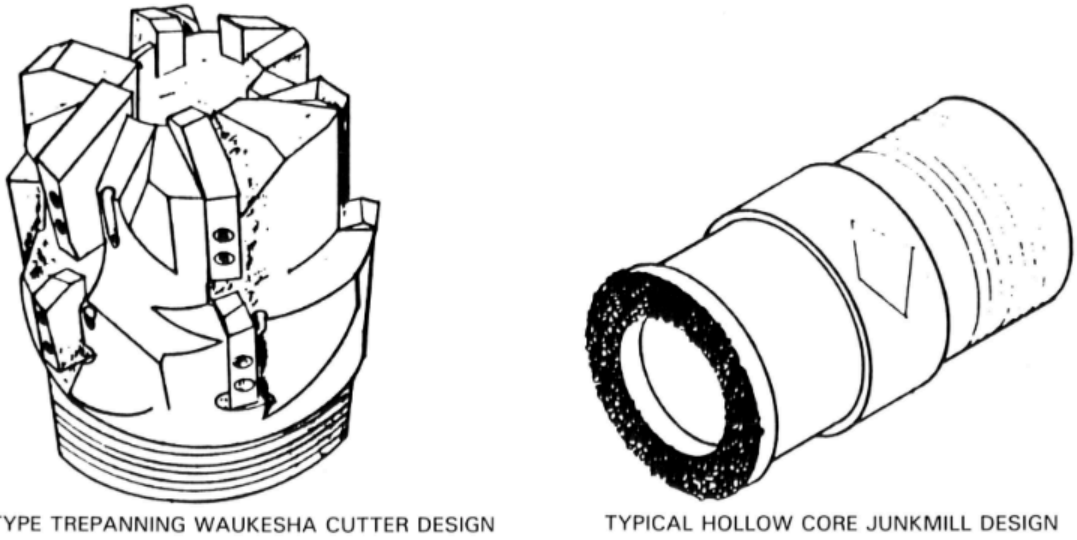

Figure 58. Trepanning and Junkmill Bits (Kirkland, 1989)

The lower-grid distributor plate was disassembled and removed in four pieces in June and July 1998. Due to problems with torch failures attributed to adherent debris, the torch controls were redesigned. Cutting the 34-cm-thick lower-grid forging plate required the use of an abrasive saw to perform vertical cuts while the plasma torch completed the horizontal cuts. The forging was removed during the period from August to December of 1988.

The in-core guide-support tube plate was removed in four pieces between December 1988 and February 1989.

The flow distributor plate was removed as 26 pieces during the period from February through April of 1989.

Prior to removal of the core former baffle plates, it was necessary to remove debris generated by previous defueling activities.

Lower Head Debris Removal

The primary tools used for core removal were long-handled grippers, scoops, and tongs. Between pick-and-place actions with these tools and vacuuming using the airlift, 12,400 kg of debris were removed from the lower head in May 1989. This cleanup revealed a formerly molten monolithic mass on the bottom head of the reactor vessel. Although this mass was as much as 0.6 m thick at the center, it was determined to be brittle as it was fractured using an impact hammer. Figure 59 is a schematic view of the melt.

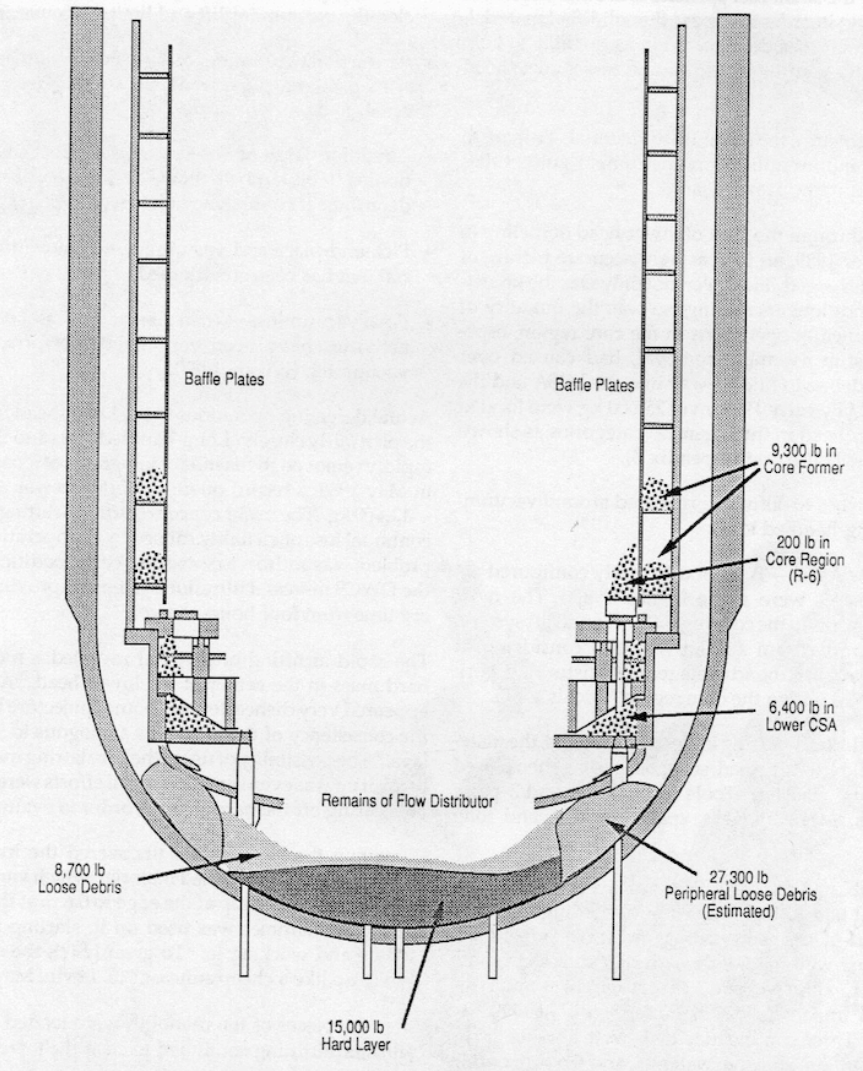

Figure 59. Debris located below the lower core support assembly. (Holton, EPRI-6931, 1990)

It had been estimated that 4000 kg of debris was located behind the core former baffle plates. Removing the 4-m-long baffle plates involved removing the bolts that held them in place and moving the eight pieces out of position to allow vacuuming of the debris. An airlift and cavitating water jet were used to recover the debris.

In all, the debris at the bottom of the vessel were tabulated as follows: 4218 kg behind the core former plates, 2903 kg was found in the lower core support area, and 3946 kg of central and 12,383 kg of peripheral loose debris, and 6804 kg of previously-molten monolithic hard layer, adding up to 30,254 kg.

4. Canister Design

As a matter of system integration, the common component from the reactor to the current storage configuration was the canister. The canisters function as a discrete fuel-handling unit, provide confinement of fission and activation products, and maintain subcriticality. Design-requirement specifics are provided in Appendix A.

The canisters were designed by a team from B&W and fabricated to American Society of Mechanical Engineers (ASME) Section VIII pressure vessel standards. The canisters were central to the retrieval process at the reactor, needed to be compatible with the INEL interim storage pool, and were initially

expected to be a confinement barrier in transportation.

Canisters for general debris, granular material, and filtered water were designed to be handled by the fuel-handling equipment at the reactor while being compatible with the interim storage pool at INEL.

The fuel debris canister was designed to accommodate partial fuel assemblies as well as debris. Some initial design assumptions considered the possibility that a significant fraction of assemblies were intact. The original approach was to use 457-mm-diameter canisters, but that was reduced to 456 mm due to handling limitations within the reactor vessel.

The knockout canisters were used to receive pieces suctioned from the reactor vessel that were too small for remote manual pick-and-place recovery; these ranged from fuel-pellet size to 140 microns.

The filter canister was designed to remove particulate as small as 0.2 microns from the suction stream. Cross-sectional views of the canister types are shown in Figure 60–Figure 62. The canisters were designed to allow remote dewatering and prevent hydrogen buildup resulting from radiolysis of retained water during transportation.

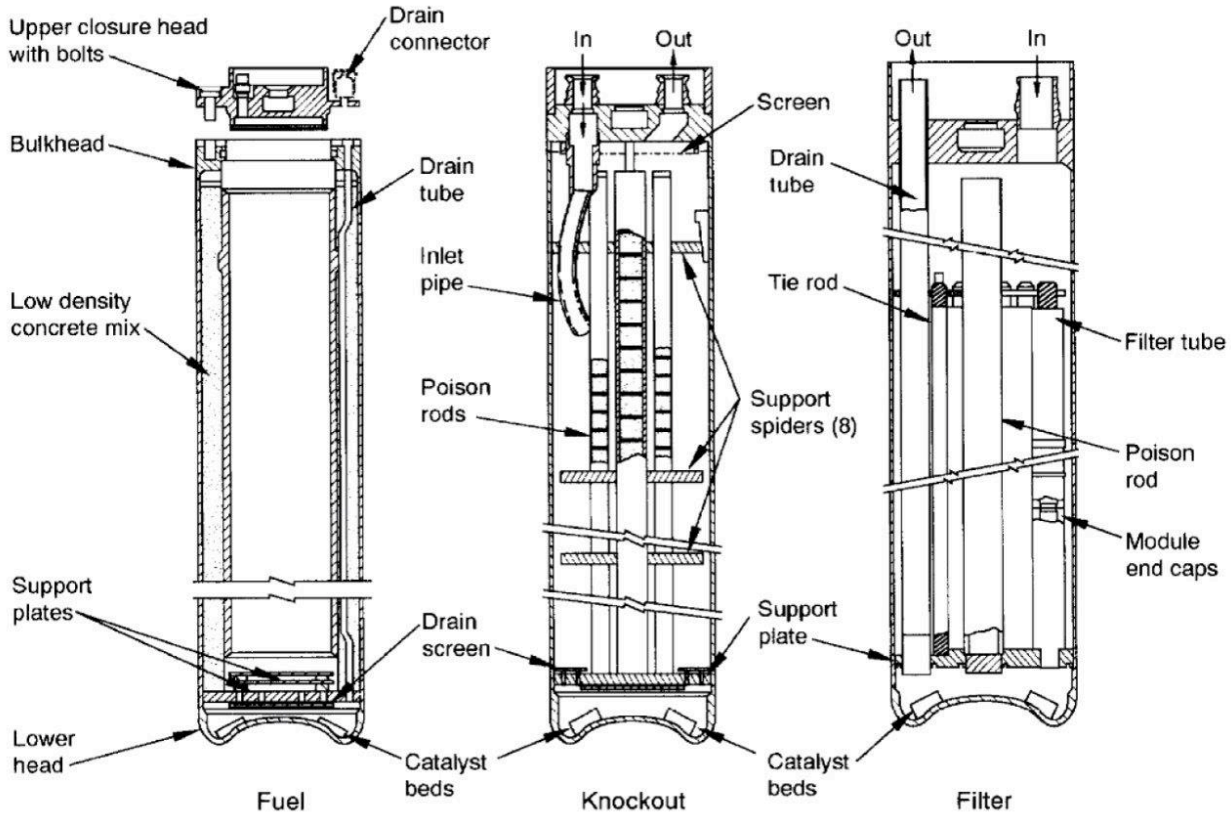

Figure 60. Fuel debris, knockout, and filter-canisters elevation view. (Courtesy NRC/INL tmi2kml)

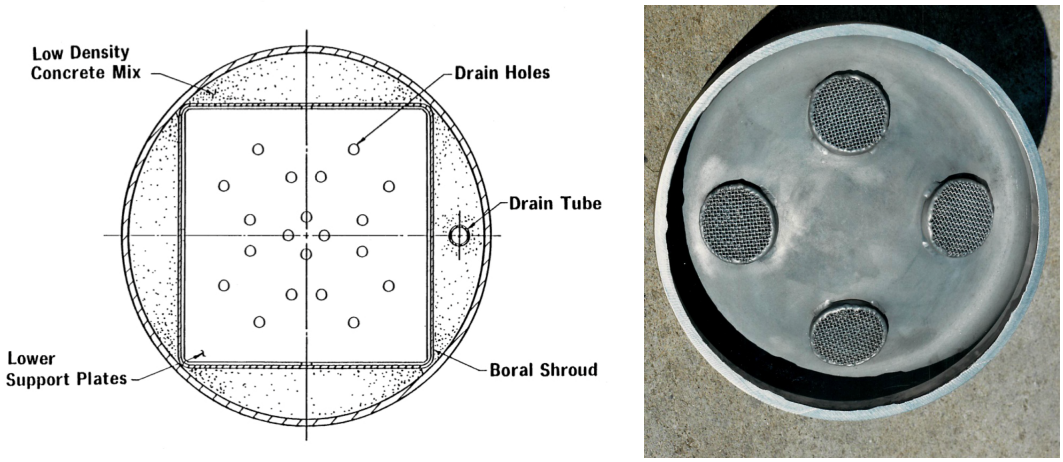

Figure 61. Cross-section view of fuel debris canister and lower head with catalyst bed. (Courtesy of INL, 2012)

Figure 62. Internal structure of knockout canister. (Courtesy of INL, 2012)

Concerns were raised regarding the properties of the debris being recovered. One uncertainty was the potential for pyrophoric reaction of unoxidized Zircaloy in air. This was determined to be unlikely

because the debris were submerged in water, which would oxidize any zirconium surface immediately. To address this as a transportation issue, the canisters were backfilled with argon during dewatering. There was also the possibility of achieving a flammable concentration of radiolytically produced hydrogen. Numerous alternatives were suggested, but the choice was a platinum-palladium catalyst recombiner material that would convert hydrogen and oxygen back into water.

Assuring subcriticality (k_{eff} less than 0.95) in the nonhomogeneous mass of debris, whether as a single canister or in an array, was achieved by use of boron neutron poisons in several configurations. The square tube of the fuel debris canister was constructed by sandwiching a layer of stainless steel over plates of borated aluminum. The structure of the filter canister includes a center rod that is filled with B_4C pellets. In the knockout canister, four rods arranged around a large central rod, all filled with B_4C pellets function to prevent criticality (Babcock & Wilcox 1985).

4.1 Reprocessing as a Treatment Disposal Option

Alternatives considered other than long-term storage and disposal included the possibility of shredding the debris to 0.5 to 2 cm^2 particles and dissolving it in acid to recover uranium and plutonium using variations of the standard UREX/PUREX flowsheet. This process would have used gadolinium-containing nitric acid to achieve dissolution of the uranium and plutonium oxides with a design capacity of 140 kg per day. The resulting solution would have been processed through two cycles of relatively conventional extraction operations using 30% tributyl phosphate in light diluent flowing through multiple stages of mixer-settlers or centrifugal contactors to eliminate fission products and yield separated uranium and plutonium solutions. First-cycle extraction was designed to have 16 stage extraction and 24 stages of stripping, followed by concentration of the product in a critically safe-by-geometry evaporator. Second-cycle would have also used 16 stages of extraction, the products of which would be processed with a ferrous partitioner to reduce plutonium to +3 ionization state prevent its extraction into the uranium stream. The plutonium-containing aqueous stream would have been processed separately using ion exchange, elution and oxalate precipitation. (Evans, Hammer, EGG-TMI-6130, 1982)

Alternatives included partial dissolution as well as complete dissolution. Centrifugal filtration was proposed for separation of undissolved solids. Uranium solutions were to be converted to solid by fluidized-bed calcination. Parallel operations would be maintained for uranium and plutonium processes. Complete dissolution would have allowed a high level of recovery for accountable material quantitation. Unfortunately, process designs were based on the assumption that the debris would be the result of a partial melt that left damaged fuel that was largely soluble in nitric acid. Given the challenge that was later encountered in dissolving the debris from grab samples for characterization, the proposed process would likely have needed to use a different means to get the uranium into solution for extraction. (GEND-INF-075, 1986)

Waste solutions were to be treated at the Idaho Chemical Processing Plant by calcination to a granular oxide solid waste form which would be melted into a borosilicate (BS) glass or iron-enriched basalt analog. If the dissolution and separations processes were to be performed at the Idaho Chemical Processing Plant, significant modifications and expansion would have been required. (Evans, Hammer, EGG-TMI-6130) Processing this commercial fuel debris would have required new construction or significant modifications to existing federal facilities. In 1982, these modifications and facility construction were estimated to cost $75 million, relative to the projected direct disposal cost of the debris at $32 million.

5. Canister Shipping Process

As part of the defueling, it was decided that a sort of post-mortem examination of the fuel needed to be performed. The core needed to be removed and stored to allow completion of the reactor-building cleanup.

To achieve a resolution of the final destination for the debris, negotiations in 1981 between NRC and DOE led to a memorandum of agreement under which DOE would take a portion of the debris for research, and the balance would be retained onsite. In 1982, the decision was made to transfer the entirety of the core to DOE for research and storage until the national high-level waste repository was operational.

It was determined that the then-INEL had the requisite combination of facilities that could store the core debris and do the necessary research on the materials that were recovered. The laboratory also had experience doing research on severe accidents for the NRC and the nuclear industry.

To move the core and debris the 3540 km from Pennsylvania to Idaho, it was decided to design and construct two specialized rail casks. Rail as chosen to limit the number of shipments, allowing seven canisters to be shipped at once, versus one in a legal-weight truck cask. The shipping cask was designed and fabricated by Nuclear Pacific.

Because the fuel cladding was damaged or absent, the debris canisters were initially designed to be the primary barrier to dispersal. Due to concerns about the ability to achieve adequate sealing with the bolted-head canister design, it was concluded that the cask would need to provide double containment. The cask design provided two barriers in the form of internal and external cask modules, complete with individual impact limiters for the canisters. Double containment was mandated because the primary fuel-clad barrier was no longer present, and the transportation regulation requires double containment for Pu-containing materials. Three casks were fabricated for rail service. Forty-nine cask loads were transferred in 22 shipments. An elevation view of the general facility configuration for transfers to the shipping cask is shown in Figure 63.

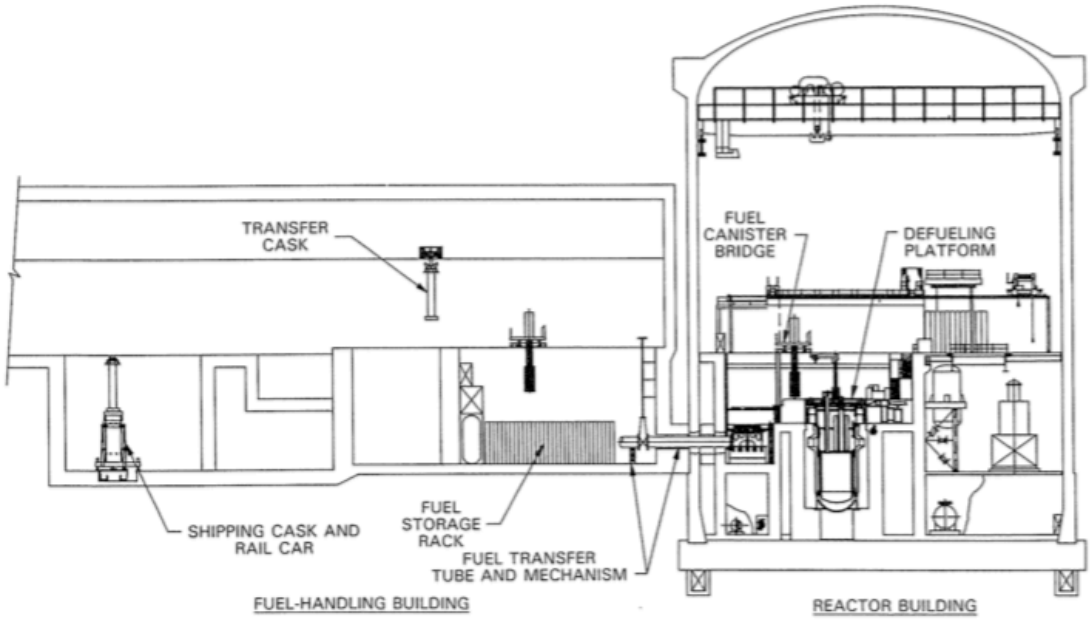

Figure 63. Reactor and fuel-handling building arrangement for canister shipping. (Courtesy NRC/INL tmi2kml)

Once a canister was identified for shipping, it was dewatered using argon purge gas and loaded into the fuel transfer cask. The cask was moved to the fuel-handling building loading area, where the shipping cask was staged. The shipping cask was rotated from its horizontal transport position, and a loading collar was installed. A mini-hot cell was mounted to the loading collar and used to remove the shield plug from the shipping cask position designated to receive the canister that was ready for shipping. The fuel-transfer cask was mated to the loading collar, the canister was lowered into the position in the shipping cask, and the shield plug was replaced. The loading collar and mini-hot cell configuration are shown in Figure 64, and the upended rail shipping cask with the fuel transfer cask attached is shown in Figure 65.

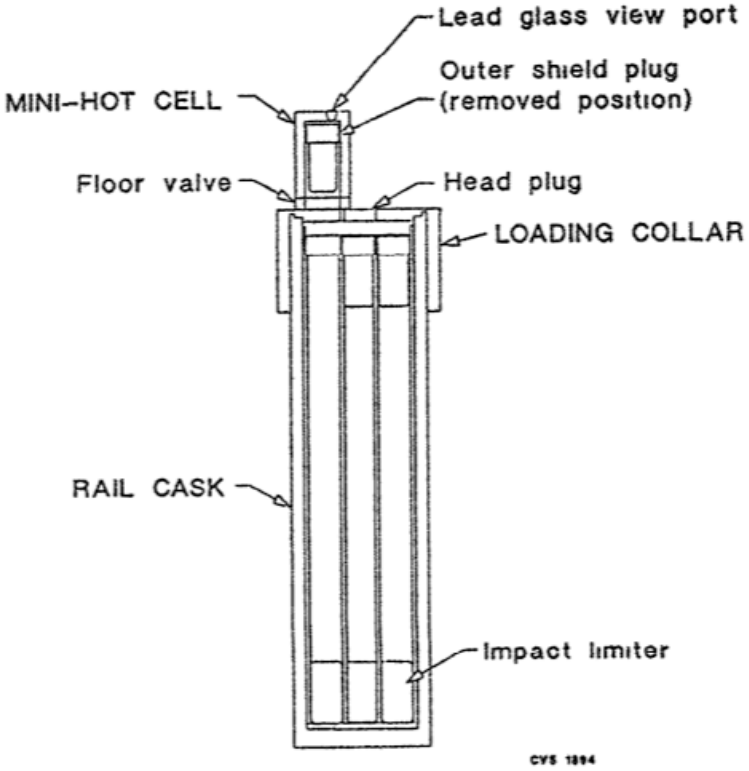

Figure 64. Schematic of mini-hot cell with rail cask and loading collar. (Reno, 1986)

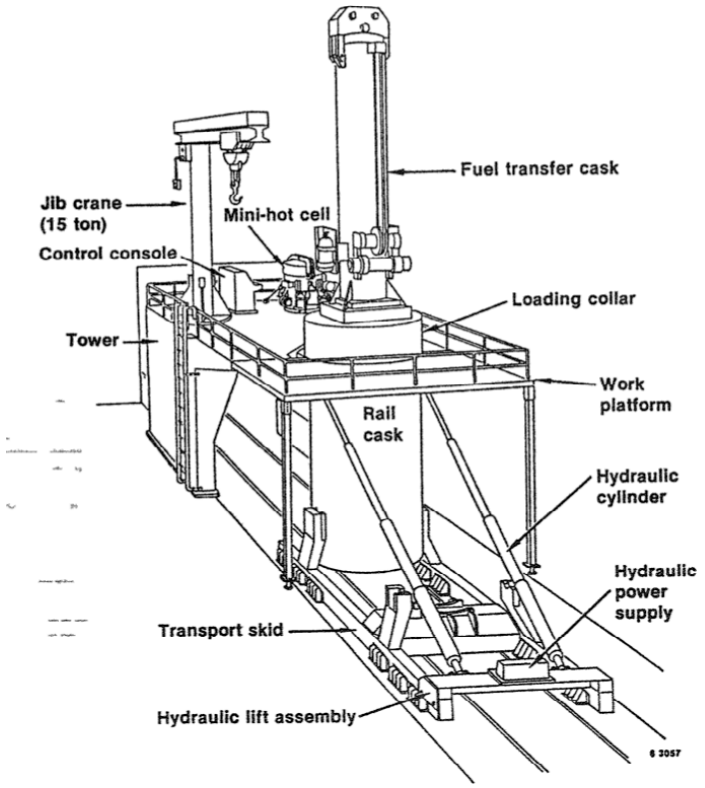

Figure 65. Equipment for dry transfer of debris canisters to rail cask. (Reno, 1986.)

On arrival of the empty cask, the impact limiters were removed before pushing the rail car into the fuel-handling building's truck bay. Then the rail car was pushed into a specific location in the truck bay under the cask-unloading station, where four screw jacks raised the cask and skid from the rail car. The rail car was then removed from the truck bay. The cask-unloading station was then removed from the skid and set aside using an overhead crane. The cask hydraulic-lift assembly was attached to the rail car skid to rotate the empty cask from a horizontal position to a vertical orientation. This unit comprised a pair of hydraulic cylinders that pushed on the upper trunnions to rotate the cask. A work platform was attached around the cask, allowing for removal of the outer and inner cask lids using a jib crane.

Loaded debris canisters were operationally limited to a gross dewatered weight of 1272 kg, with a typical debris load of 750 kg.

Concerns about residual water retention were validated based on differences between empty and loaded, dewatered containers, as shown in Table 6. As may be expected, the filter canister (F-462) has the greatest remaining water.

Table 6. Sample canister water retention.

Canister ID	Canister Weight Empty (kg)	Full (kg)	Dewatered (kg)	Core Debris (kg)	Water Remaining (L)	Total Pay Load	Void Volume (L)
D-180	542	1,393	1,315	743	29	772	72
D-188	542	1,405	1,317	746	29	775	81
D-330	538	1,406	1,327	767	22	789	78
F-462	662	1,218	1,101	310	111	439	120
K-506	458	1,471	1,324	842	23	865	146

As part of the validation process for specifying transport conditions for potential radiolytic hydrogen production, eight of the canisters were sealed and monitored for pressure and periodically sampled for headspace composition. The test canisters remained sealed for between sixteen to 205 days. Pressure values reached as high as 198 kPa in as few as 16 days for the D-188 debris canister. The headspace gas was analyzed at INEL and indicated that, over time, the hydrogen concentration could reach as much as 9 vol% with only 0.2 vol% oxygen in 87% argon after 205 days sealed. The values are tabulated as shown in Table 7 and Table 8.

Table 7. Canister pressure samples sealed test. (Standerfer, 1987)

Canister Number	Rail Shipment	TMI (psi)	First Sample		Second Sample		Third Sample		Fourth Sample	
			psia	Days Closed	psia	Days Closed	psia	Days Closed	psia	Days Closed
D-144	-	29.54	26.33	147	-	-	-	-	-	-
D-148	4	29.52	29.13	26	28.83	48	-	-	-	-
D-145	5	20.54	29.33	27	-	-	-	-	-	-
D-180	6	29.38	18.33[a]	27	19.33	205	-	-	-	-
D-162	7	29.27	29.33	36	28.33	-	-	-	-	-
D-188	7	29.36	29.08	16	28.83	181	28.33	88	27.33	168
D-207	8	29.34	28.83	20	27.33	56	-	-	-	-

Table 8. Sealed Canister Headspace Composition. (Standerfer, 1987)

	Hydrogen (% Volume)				Nitrogen (% Volume)				Oxygen (% Volume)				Argon (% Volume)			
Canister Number	1st	2nd	3rd	4th	1st	2nd	3rd	4th	1st	2nd	3rd	4th	1st	2nd	3rd	4th
D-144	0.77	-	-	-	0.90	-	-	-	0.08	-	-	-	98.20	-	-	-
D-148	1.15	1.47	-	-	0.36	0.70	-	-	0.07	0.13	-	-	98.40	97.70	-	-
D-145	0.74	-	-	-	0.585	-	-	-	0.09	-	-	-	98.6	-	-	-
D-180	1.23	9.05	-	-	1.07	3.75	-	-	0.13	0.02	-	-	97.5	87.19	-	-
D-162	1.005	1.01	-	-	4.36	2.22	-	-	1.02	<0.01	-	-	93.53	96.74	-	-
D-188	1.165	2.43	3.30	5.09	0.50	1.95	2.16	1.81	0.05	0.305	0.26	<0.01	98.26	95.29	94.25	93.1
D-207	0.20	0.46	-	-	0.475	3.82	-	-	0.04	0.72	-	-	93.40	89.66	-	-
D-267	0.12	0.25	-	-	0.90	0.52	-	-	0.17	0.01	-	-	98.80	99.17	-	-

6. Special Nuclear Material Accountancy

Due to the heterogeneous nature of the debris, core removal progressed with mass measurements for each of the canisters and a general understanding that the fuel inventory would be based on a measurable residual amount that would be compared to the masses removed and the original known fuel mass. The mechanisms for transport of fuel outside of the RPV were identified and evaluations were made by visual examination, direct radiological measurements and sampling and destructive analysis of sludge and other surfaces in the system.

Radiological measurements included gamma spectrometry using sodium iodide and high-purity germanium detectors to identify and quantify ^{144}Ce and ^{154}Eu and a fuel value was inferred based on the known average burnup of the core. Gross gamma rate measurements were used to estimate fuel content in piping and water treatment system cubicles. Passive neutron measurements were made using solid-state track recorders (SSTR) that used Highly Enriched Uranium (HEU) foils that fissioned in the presence of fuel, producing fast neutrons that create visible tracks on the acrylic sheets that the foils are sandwiched between. Copper foils placed in the flux were activated to ^{64}Cu, which was read with a sodium iodide coincidence counting system. Despite the low levels of flux in the fuel debris, these methods were used where an exceptionally high gamma background was present. Active neutron measurements were done with an antimony-124/beryllium source to cause fission that was detected as fast neutrons on a helium-4 counter. Alpha detection was used to evaluate the amount of fuel plated out on internal surfaces of the steam generators and cooling-system piping where it was assumed that the fuel had adhered in a thin film that would not absorb the alpha emissions.

Samples of components like the control rod leadscrews were measured to determine the quantity of fuel that could be expected to have adhered to the internal surfaces of piping and reactor-system vessels. Analysis of other samples of core debris have been discussed previously regarding grab and core samples. As mentioned in the discussion of the analysis of grab samples, the solubility of the sample material can be an issue that may limit the precision of the analytical result, especially by methods that depend on having a liquid sample to measure. In general, all discrete samples were analyzed using alpha proportional counting, gamma spectrometry, and mass spectrometry to determine the fuel content present in specific systems. (GPUN, 1990)

Visual examination was performed using video cameras to identify specific locations to derive an estimate of volume of debris in a location and compare sample data to establish a fuel content value. Poor lighting, lack of water clarity and limited access contributed to fuel estimate uncertainty regarding of items identified in the video. Due to the nature of all of these systems, substantial uncertainty exists due to the heterogeneity of the material. It should be remembered that even in a reprocessing facility where fuel is dissolved to the maximum extent practical resulting in an essentially homogeneous product, uncertainty will be present due to the cumulative effect of analytical measurement error, sampling error and mass measurement error. The final accountability inspection to estimate the amount of fuel debris remaining in the vessel was primarily done with the Bore Tech model BT2020 color camera to evaluate the size of residual accumulations. A Rees model R-93 camera was used to inspect the inaccessible areas under the LCSA. The camera was dropped through holes in the LCSA with a right-angle lens mounted to look laterally around the perimeter of the assembly. Thirty hours of video were recorded to provide evidence of the thoroughness of the recovery effort.

When the 33cm-thick LCSA was cut and removed to allow removal of the lower head debris, each piece was measured using a high-purity germanium gamma spectrometer to identify ^{144}Ce as an indicator of fuel adhering to the components. Due to the presence of ^{60}Co from neutron activation of the steel, quantitation was limited, even with count times up to four hours, and estimates were developed based on the minimum detection of ^{144}Ce. In one circumstance the large grid components were counted with a spectrometer surveying the upper surface and another the lower simultaneously.

Some sections of the lower grid were surveyed by alpha particle spectrometry with an Eberline AC-21 probe calibrated with a ^{241}Am source. This scan was of limited value due to uncertainty regarding

the depth of the surface contamination layer and the degree of absorption in that deposit. Quantitation of accountable material by this method was not achieved. (EPRI-NP-7156, 1992)

Some fuel material was displaced from the RPV during the immediate accident process, moving via the primary cooling system to the steam generators, first by the action of the reactor cooling pumps, and then by thermal transients ("burps") that occurred while natural circulation was being employed to cool the core. A minimal amount of fuel was transferred to the Auxiliary and Fuel Handling Buildings, but a majority of that material was removed during decontamination and dose reduction efforts. As much as 125 kg of fuel debris material was deposited on the upper tubesheet of the B side steam generator, which was recovered by mechanical pick up of larger pieces, and flushing decontamination. The fuel in the reactor vessel itself was mechanically removed within the limit of physical access even after cutting out significant amounts of interfering structures. Defueling and recovery work was declared complete on the basis of estimates of inaccessible fuel debris that were used to assure that no reconfiguration or relocation incident could lead to an inadvertent criticality. Criticality analysis projected a Safe Fuel Mass Limit of 140 kg in any specific location would meet the criterion for assuring subcriticality. Based on subtraction from the fuel and material mass removed during RPV defueling, the projected residual fuel mass was estimated at 1125 kg. This mass is distributed throughout the facility on building and piping surfaces and in the form of small particulate. An illustration of pre-retrieval deposits of fuel in the coolant system is shown as Figure 66. (Urland, 1992)

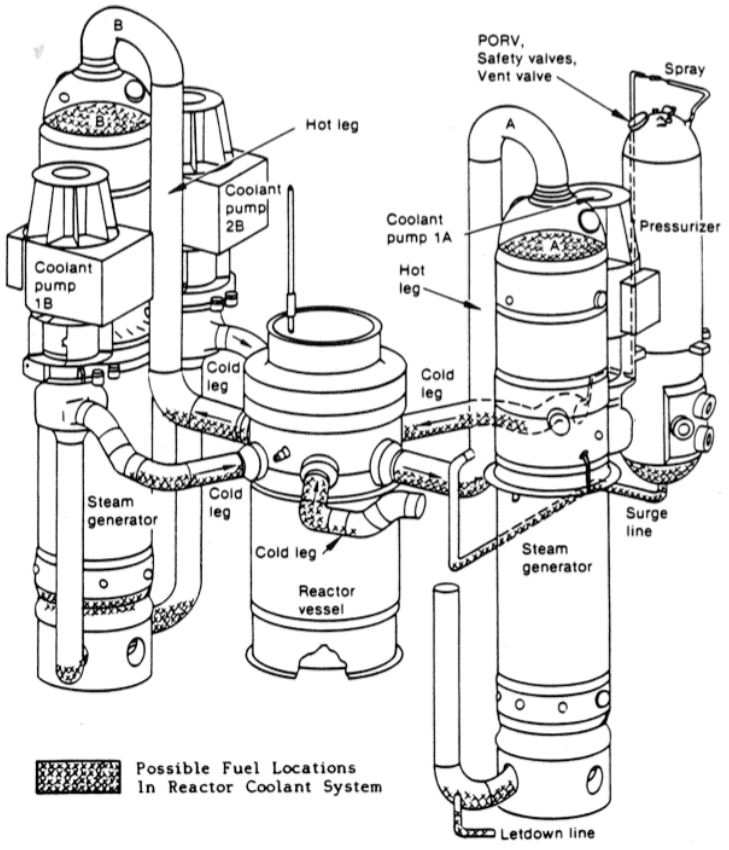

Figure 66. 1983 pre-retrieval proposed displaced fuel locations. (Urland, 1992)

The distribution used for the closure estimate is shown as the listed in Table 9.

Table 9. Unrecovered Fuel Estimate by Location (Standerfer, 1990)

Auxiliary and Fuel Handling Buildings	<17 kg
Reactor building (excluding the RCS)	<75 kg
Reactor Coolant System	<133 kg
Reactor Vessel	<900 kg
Total	<1125 kg

The criticality safety review concluded that the inaccessible material in the reactor vessel posed no problem because there was no credible mechanism that could bring the material into a single location such that, if moderated, it could result in a criticality. This reasoning is based on the concept that the material remained in its location throughout the extensive mechanical defueling processes. (Standerfer, 1990)

A separate estimate of the accountable material in the debris canisters was performed based on the payload mass measured at the time that the canisters were shipped. Using the available information on the lengths of partial assemblies, buckets of core debris and other specifics on the type of material that was loaded into each canister, a fuel value was calculated. Detailed notes regarding the presence of end fittings, control rod spiders and other non-fuel-containing items were subtracted from the reported canister payload mass. The filter and knockout canisters were large contributors to the uncertainty due to the difficulty achieving complete dewatering. Within the USDOE regulatory requirements for accountable material, ^{235}U and $^{239\text{-}241}Pu$ are tracked to a precision of one gram, while ^{238}U is tracked at the kilogram level. This estimate notes that there is an uncertainty of 25% for the nominal value assigned to a given canister as well as the summed system value. (Lasahn, 1993)

Because load cells capable of weighing a 1500 kg canister may commonly be as much as 2 percent of full scale, the ultimate error for accountancy may be limited by the equipment available. Smaller units could be weighed during canister loading to improve precision, but if an entire melted core of several hundred tonnes is to be removed expeditiously it may not be cost- or ALARA-efficient.

7. Transportation Cask

The transportation cask was designed by Nuclear Pacific as a multiple-barrier system. In a normal fuel shipment, intact fuel clad can be credited as a containment barrier. Per transportation regulations, double containment was required because of the plutonium content of the fuel debris. In this design, the canisters were not considered a containment barrier because the debris canisters had removable heads. To provide the necessary barriers, the NuPac 125-B casks were designed with an inner and outer vessel to provide double containment. The inner vessel weighed 15.4 metric tonnes, and the outer vessel weighed 43.5 tonnes.

Seven canisters were fitted inside the cask, each having its own upper shield plug and upper and lower internal-impact-limiter. The internal configuration is shown in Figure 67. The casks were shipped cross country by rail as a dedicated shipment with as many as three rail cars, each cask on its own car. Figure 68 shows the package dimensions and impact-limiter arrangement. A photo of the cask, with impact limiters in place on the rail car, in its skid, is seen in Figure 69.

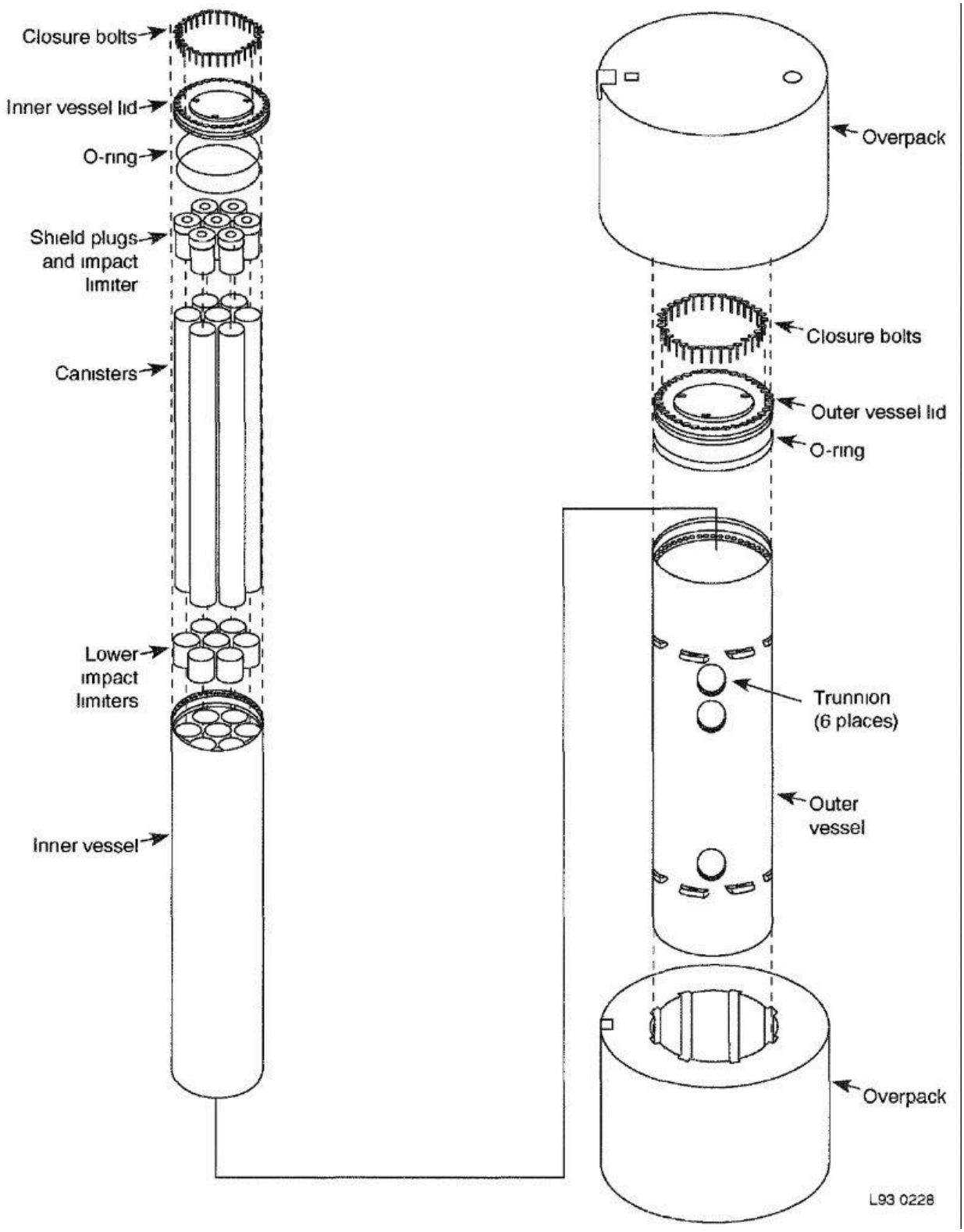

Figure 67. NuPac 125B schematic. (Courtesy NRC/INL tmi2kml.inl.gov)

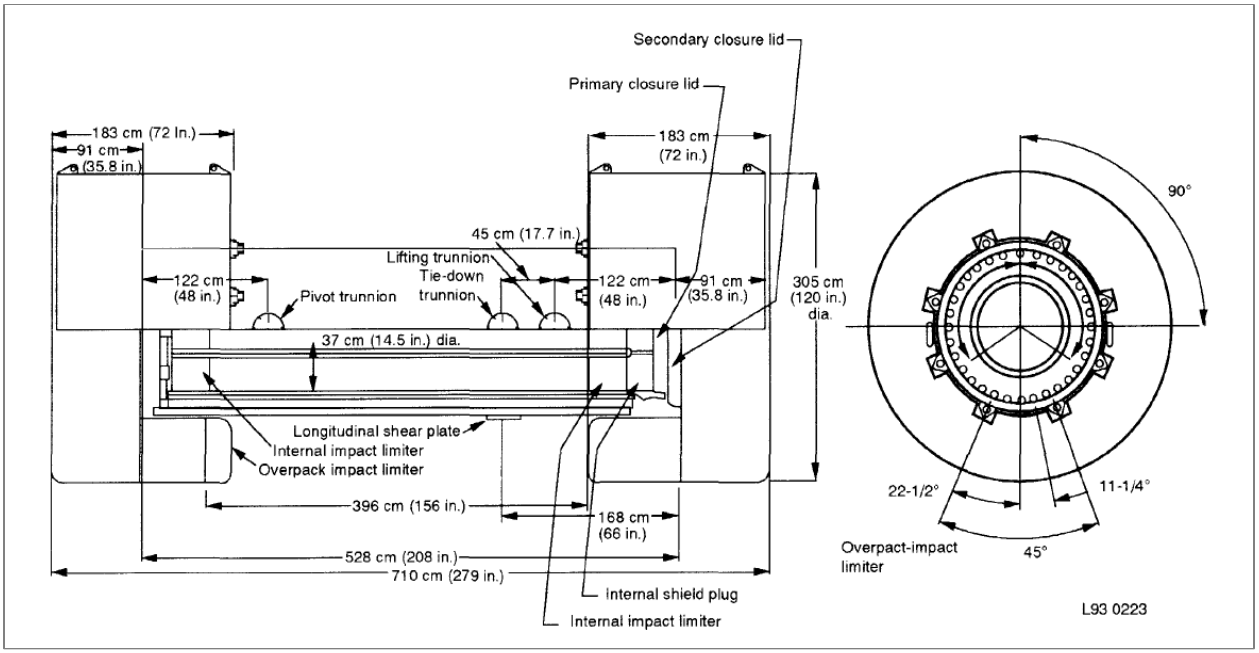

Figure 68. NuPac 125B dimensions and impact-limiter orientation. (Courtesy of INL, 2012)

Figure 69. NuPac 125B cask on rail car. (Courtesy NRC/INL tmi2kml.inl.gov)

The 125B cask was mounted to a skid that was in turn attached to a rail car, as shown in Figure 70.

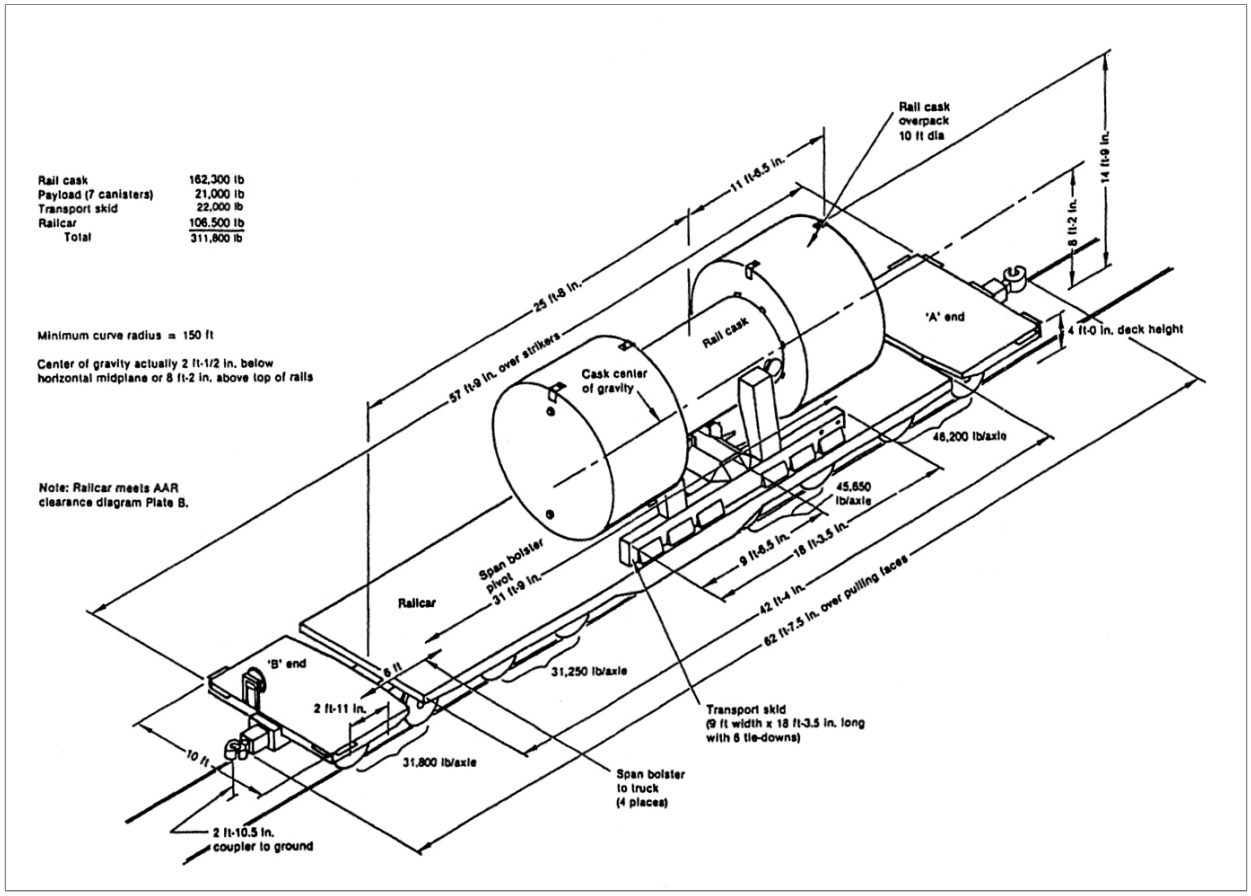

Figure 70. 125B cask rail car configuration. (Courtesy of INL, 2012)

To perform the loading of the transport cask in the fuel-handling building, it was necessary to remove the 125B cask and its transport skid from the rail car. This was performed using the cask-unloading station fixture, as shown in Figure 71.

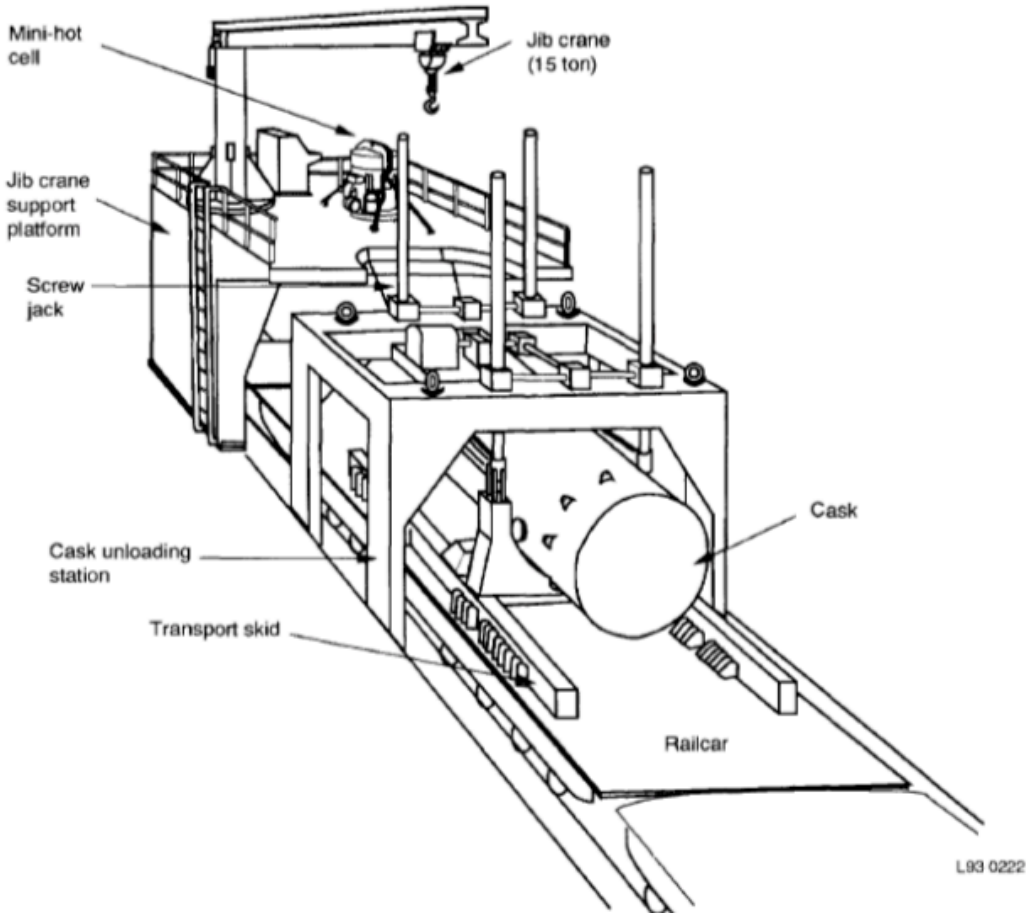

Figure 71. NuPac 125 B cask handling equipment at TMI-2 fuel-handling building (Courtesy of INL, 1986)

7.1 Offloading at INEL

The casks were shipped cross-country via rail, but when the shipment reached INEL, no rail spur was available to complete the journey to the TAN-607 hot shop and pool system. This meant that the casks needed to be unloaded from the rail cars and transported by truck approximately 48 km from the rail terminal at the INEL Central Facilities Area to TAN. The transfer process is depicted in Figure 72. A photo of the cask mounted to the transport skid, suspended from the Central Facilities Area gantry crane is seen in Figure 73. The cask and skid are shown mounted on the truck, being moved to TAN in Figure 74.

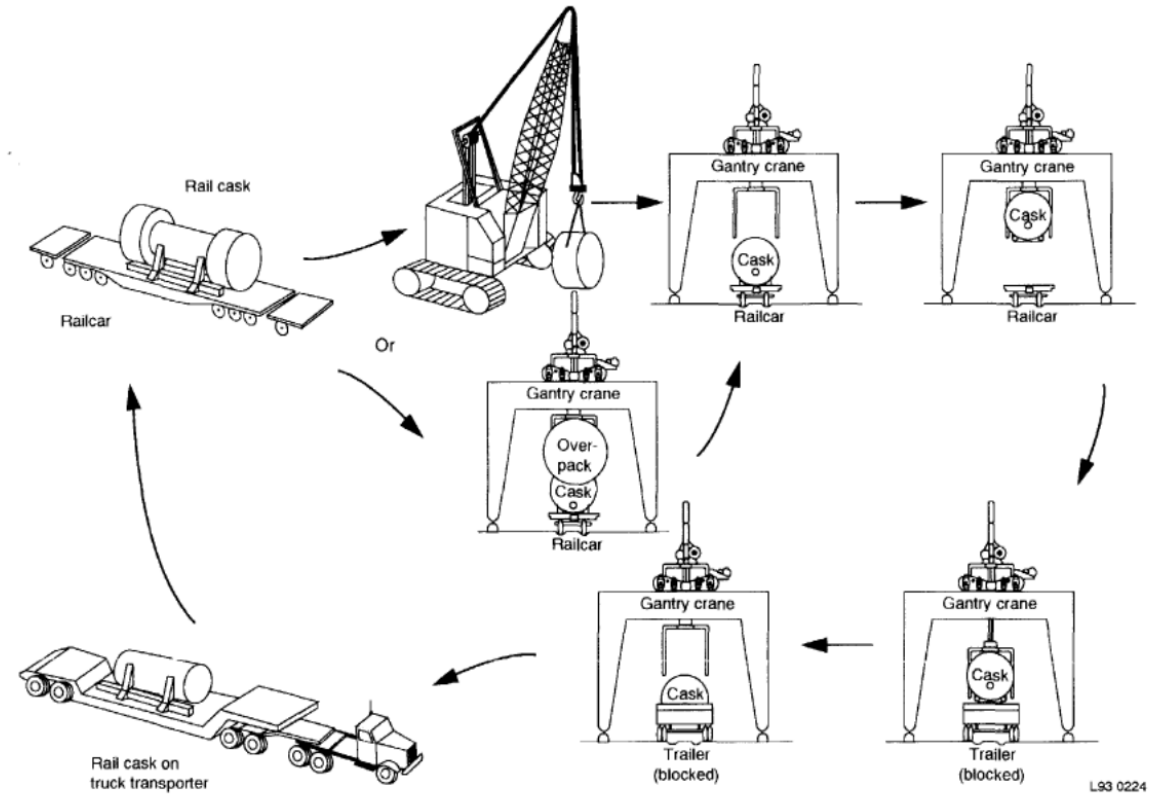

Figure 72. Cask transfer from rail car to truck schematic. (Courtesy of INL, 1986)

Figure 73. Gantry crane removing 125B Cask from rail car. (Courtesy NRC/INL tmi2kml)

Figure 74. 125B cask on transport skid, loaded on trailer. (Courtesy NRC/INL tmi2kml)

7.2 INEL Storage Site TAN-607

The TAN-607 building included a hot shop, which was originally designed for handling test nuclear reactors for a conceptual nuclear airplane. The hot shop was 15.5 m × 50 m × 16.76 m. It was a high-bay cell with a large entry lock sufficient to accommodate a large truck-trailer unit or a rail engine using rail tracks. It featured a 100-tonne bridge crane, nine shielded viewing windows, and one bridge-mounted and three wall-mounted electromechanical manipulators. The main overhead crane was used to lift and position the NuPac 125B casks upright. The manipulators were used to open the casks and retrieve the contents. The truck transport was carefully backed into the hot shop, and the casks were individually removed from the truck skid by rotating the casks upright using the main crane. The casks were placed on a work platform, where the lid bolts were removed, and preparations were made for the remote transfer of the canisters to the storage pool. The rotation and unloading process is shown in Figure 75 and Figure 76.

Figure 75. Cask-unloading in TAN-607 hot shop. (Courtesy NRC/INL tmi2kml)

Figure 76. NuPac 125B cask on the work platform. (Courtesy NRC/INL tmi2kml)

The hot shop had a vestibule that provided access from the dry area to the storage pool. The pool was 14.6 m wide, 21.3 m-long, and 7.3 m deep.

TAN-607 also had a hot cell 3.05 m wide × 35 10.7 m-long × 6.1 m high. It was directly connected to the hot shop, which facilitated receipt of the TMI-2 canisters that contained core bores for inspection. An additional set of four hot cells provided a location for handling of subdivided samples for further analysis. The hot shop plan view with the canister path from the cask to pool rack in the vestibule is shown in Figure 77. A photo of the hot shop during construction is shown in Figure 78. Details of the pool storage systems are shown in Figure 79 through Figure 82.

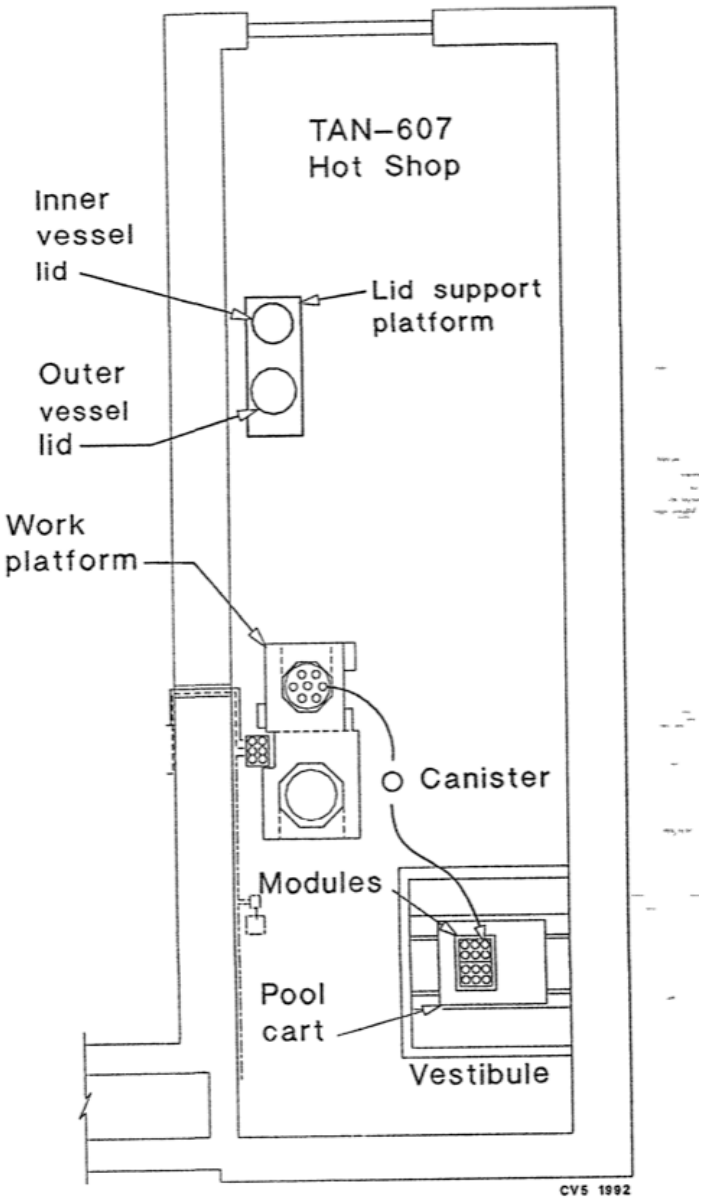

Figure 77.TAN hot shop, hot cell, and pool storage system plan view. (Courtesy of INL, 1986)

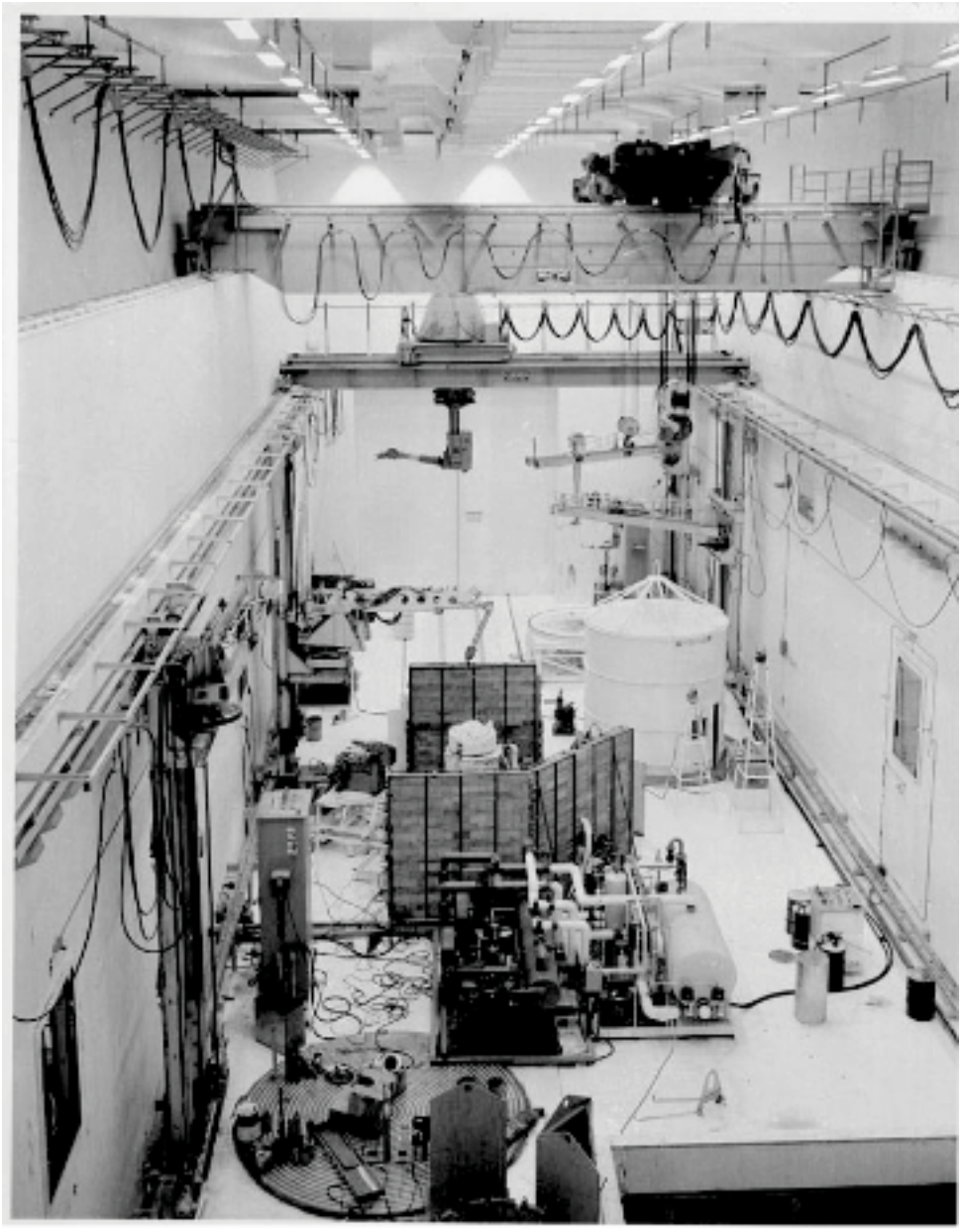

Figure 78.TAN hot shop view, during construction, 1955. (Courtesy of INL)

Figure 79.Canister being removed from 125B cask prior to transfer to TAN-607 pool. (Courtesy of INL)

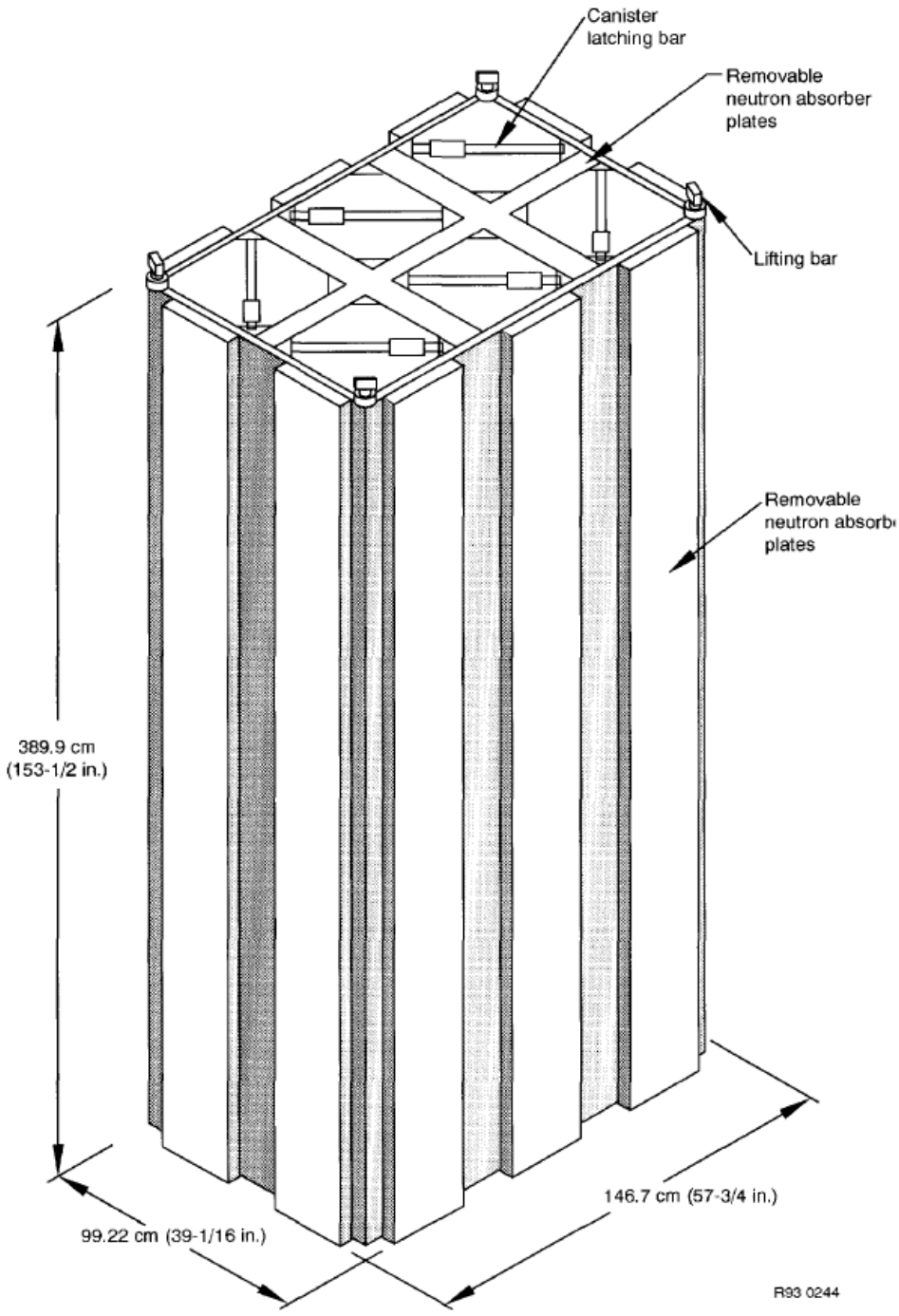

Figure 80. Six-pack canister rack for storage in TAN-607 pool. (Courtesy of INL, 1986)

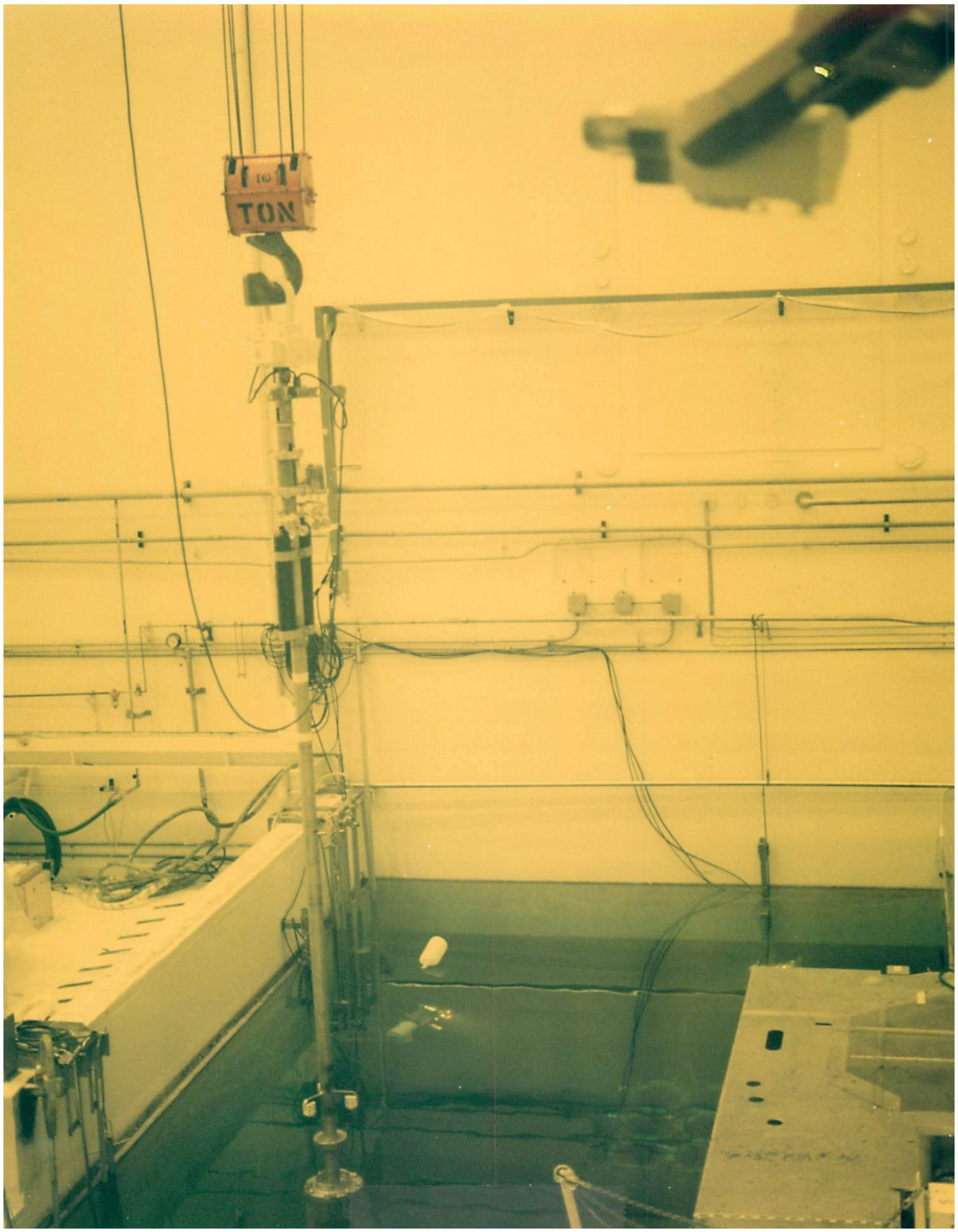

Figure 81. Canister being lowered into six-pack rack in TAN-607 pool. (Courtesy of INL)

Figure 82. TAN-607 pool, showing six-pack racks and individual canister-vent ports (orange caps divert water back into pool). (Courtesy of NRC/INL tmi2kml)

Storage of the canisters in the TAN-607 pool used the six-pack array, with each canister having an individual vent tube extending above the pool surface. The canister internals, including debris, were isolated from the pool water. The canisters were backfilled with deionized water through the vent tube. During the early stages of storage, release of gas from radiolytic hydrogen production caused the water in the canister to be kinetically expelled through the vent tube. Following observation of this phenomenon, the tops of the vent tubes were covered with plastic caps that diverted any expelled water back into the pool.

7.3 Transfer to Dry Storage

At least in part due to legal action by the State of Idaho regarding the U.S. DOE management of nuclear material, a decision was made to transfer the fuel debris from wet-to-dry storage. This decision was made on the basis that dry storage is less expensive to operate and represents a lesser environmental risk; the TAN-607 pool was known to leak. Contaminated water could have eventually reached the Snake River Aquifer.

Design alternatives led to selection of the concrete-shielded Pacific Nuclear Fuel Services NUHOMS design. One primary consideration was the relatively low cost of the concrete shield and dry shielded canister (DSC) design when compared to metal-shielded multipurpose cask designs.

A total of 342 stored canisters were dried and repackaged for dry storage in the hot shop. (A larger number of canisters, 344, were originally shipped from TMI to INEL, but two of the canisters were

handled separately because various epoxy-containing metallographic mounts that were produced during the characterization phase were loaded into these canisters. The two separate canisters contained a minimal amount of fuel debris, and they are stored in one of the 125B transport casks located on the CPP-2707 dry-cask storage pad.) The dry area of the hot shop included access to the wet-storage pool, so the canisters were retrieved from the six-pack storage racks, dewatered, and brought into the dry hot cell for final drying in the heated vacuum drying system (HVDS). Dewatering was performed by removing the vent tube and attaching a gas line to the Hansen connector on the canister and displacing the water with air or nitrogen. The gas released during the dewatering purge process was vented through a high-efficiency particulate air (HEPA) filter and the TAN-607 air-handling system before being released through the TAN-734 stack. Sintered-metal filters were installed on 3/4-in. vent and 1/2-in. purge lines of the filter and knockout canisters in place of Hansen quick-connect fittings. This was a precaution to reduce the chance of fines being released from the canisters during drying. The sintered-metal filters were removed from the canisters prior to placement in the DSC. Installation and removal are shown in Figure 83.

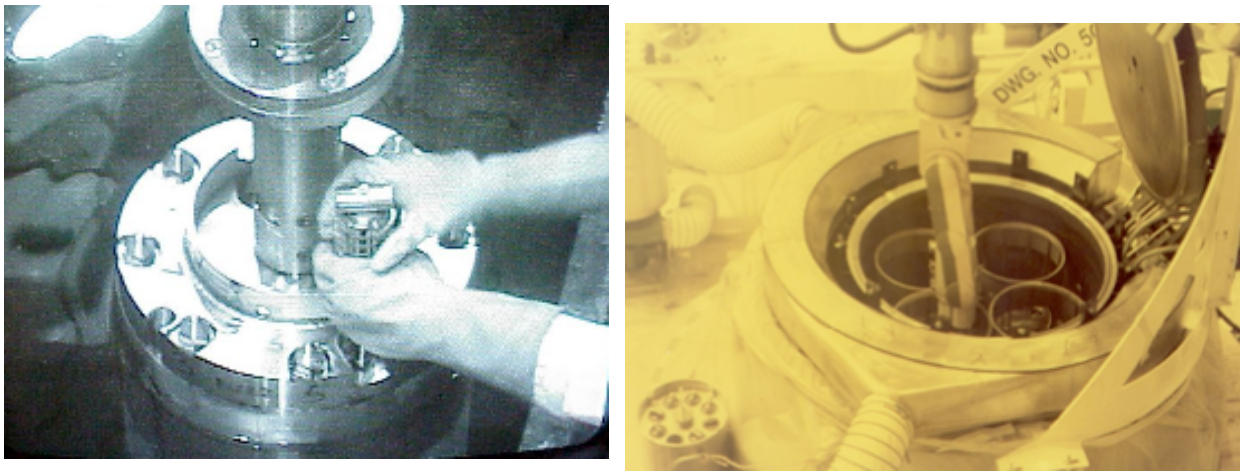

Figure *83* Installation and removal of sintered-metal filters (Both courtesy of INL)

It was calculated that there could be as much as 80 L of water retained in the canister following dewatering. The displaced water was not discharged into the pool to avoid introduction of contamination. The water from selected canisters was sampled and analyzed for dissolved chemical species to determine the degree of leachability of the debris. Canister sample pH was 8.0, except for D-330, with pH of 8.5. Canister data are shown in Table 10. The analysis is shown in Table 11. Table 12 shows tabulated radionuclide concentrations measured in the water. A calculated average radionuclide leach value for all sampled canisters is shown in Table 13.

Table *10.* Leach water from sampled-canisters, description.

Canister	Description	Contained Solid Mass (kg)	Contained Volume (l)	Solid Void Fraction	Volume of TMI Water Shipped (l)	Present Water Volume (l)
D-180	Fuel	742	191	0.404	29.02	77.21
D-188	Fuel	745	191	0.458	29.02	87.53
D-330	Fuel	766	191	0.411	21.77	78.55
F-462	Filter	309	281	0.416	110.66	117.07
K-508	Knockout	841	304	0.482	23.2	146.43

Table 11. Chemical constituents of canister water (Courtesy of INL Letter HLW-100-1074/JDC-8-97).

Species or Elemental Component	D-180 (moles/l)	D-188 (moles/l)	D-330 (moles/l)	F-462 (moles/l)	K-506 (moles/l)
Boron	9.03×10^{-5}	7.24×10^{-2}	6.84×10^{-2}	7.97×10^{-2}	1.02×10^{-1}
Sodium	1.24×10^{-2}	1.07×10^{-2}	1.44×10^{-2}	1.16×10^{-2}	1.67×10^{-2}
Calcium	4.19×10^{-6}	4.07×10^{-6}	3.78×10^{-4}	1.25×10^{-5}	6.94×10^{-6}
Chloride	4.26×10^{-5}	9.00×10^{-5}	2.06×10^{-4}	1.35×10^{-4}	7.87×10^{-5}
Silicon	2.34×10^{-5}	2.16×10^{-5}	7.09×10^{-5}	1.24×10^{-4}	3.20×10^{-5}
pH (pH paper)	8.0	8.0	8.5	8.0	8.0
Hydroxyl	1.0×10^{-6}	1.0×10^{-6}	3.2×10^{-6}	1.0×10^{-6}	1.0×10^{-6}
Barium	1.49×10^{-7}	3.93×10^{-7}	7.03×10^{-7}	6.19×10^{-7}	2.37×10^{-7}
Cadmium	1.87×10^{-7}	1.78×10^{-7}	3.02×10^{-7}	5.16×10^{-7}	1.60×10^{-7}
Lithium	8.65×10^{-6}	1.08×10^{-5}	ND	ND	ND
Bromide	3.30×10^{-6}	ND	ND	2.79×10^{-6}	1.13×10^{-6}
Chromium	1.06×10^{-7}	ND	ND	2.02×10^{-7}	3.37×10^{-7}
Arsenic	ND	ND	ND	ND	ND
Lead	ND	ND	ND	ND	ND
Magnesium	ND	ND	2.22×10^{-4}	ND	ND
Mercury	ND	ND	ND	ND	ND
Selenium	ND	ND	ND	ND	ND
Silver	ND	ND	ND	3.4×10^{-7}	6.0×10^{-6}
Uranium	ND	ND	ND	ND	ND

ND = not detected; below the limits of detection. Detection limits (molar) are Li 7.2×10^{-6}; Br $\times 1.110^{-6}$; Cr $1 \times 10^{-7\pm}$; Mg 4×10^{-6}; As 2.7×10^{-6}; Pb 5×10^{-7}; Hg 5.5×10^{-7}; Se 2.5×10^{-6}; Ag 2×10^{-7}; U 2.5×10^{-8}.

Table 12. Canister Water Radionuclide Content December 1995, (Courtesy of INL, 2012)

	Canister D-180		Canister D-188		Canister D-330		Canister F-462		Canister K-506	
	Max (mg/L)	Min (mg/L)	Max (mg/L)	Min (mg/L)	Max (mg/L)	Min (mg/L)	Max (mg/L)	Min (mg/L)	Max (mg/L)	Min (mg/L)
Pu238	4.92E-06	0.00E+00	< 4.53E-08	0.00E+00	2.75E-06	0.00E+00	4.67E-06	2.71E-06	< 1.74E-07	0.00E+00
Pu239	6.10E-04	0.00E+00	1.18E-03	0.00E+00	3.57E-04	0.00E+00	7.67E-05	0.00E+00	9.41E-04	4.62E-04
Np237	1.02E-01	5.99E-02	1.79E-03	0.00E+00	2.07E-01	1.47E-01	1.90E-03	0.00E+00	1.88E-02	0.00E+00
Am241	3.40E-06	0.00E+00	1.26E-05	0.00E+00	1.22E-05	0.00E+00	9.65E-06	4.16E-06	5.73E-06	0.00E+00
Th228	1.11E-09	0.00E+00	2.53E-08	0.00E+00	2.06E-08	0.00E+00	2.27E-08	0.00E+00	< 5.11E-09	0.00E+00
Th230	3.93E-04	0.00E+00	9.85E-04	0.00E+00	< 1.27E-04	0.00E+00	8.23E-04	0.00E+00	7.46E-04	0.00E+00
Th232	1.14E+02	0.00E+00	< 2.22E+00	0.00E+00	<2.22E+00	0.00E+00	< 2.21E+00	0.00E+00	1.05E+02	0.00E+00
Tc99	6.48E-03	2.86E-03	5.94E-02	5.50E-02	1.93E-02	1.54E-02	3.49E-03	0.00E+00	4.27E-02	3.86E-02

	Canister D-180		Canister D-188		Canister D-330		Canister F-462		Canister K-506	
	Max (mg/L)	Min (mg/L)	Max (mg/L)	Min (mg/L)	Max (mg/L)	Min (mg/L)	Max (mg/L)	Min (mg/L)	Max (mg/L)	Min (mg/L)
Sr90	7.60E-03	7.60E-03	3.79E+03	3.79E+03	9.08E+02	9.08E+02	2.14E+03	2.14E+03	2.00E+03	2.00E+03
H3 (Tritium)	1.09E-06	1.09E-06	1.58E-06	1.58E-06	9.52E-07	9.52E-07	1.26E-06	1.26E-06	1.11E-06	1.11E-06
Cs134	4.22E-06	3.56E-06	5.37E-06	4.57E-06	1.73E-06	1.52E-06	No Data	No Data	3.80E-06	3.31E-06
Cs137	3.60E-02	3.30E-02	4.47E-02	4.11E-02	1.41E-02	1.29E-02	9.90E-04	9.16E-04	2.90E-02	2.66E-02

Table 13. Calculated Maximum Average Radionuclide Leach Rates (Courtesy of INL)

	Average ($g/cm^2/day$)
Pu238	3E-16
Pu239	8E-14
Np237	9E-12
Am241	1E-15
Th228	2E-18
Th230	8E-14
Th232*	< 3E-10
Tc99	3E-12
H3 (Tritium)	2E-16
Cs134	5E-16
Cs137	3E-12

* Excluding canister D-180 and K-506 for Th-232.

The data noted in the reference letter indicate that only a negligible amount of calcium was leached from the light-weight concrete in the debris canisters (i.e., D-180, 188 and 330). This may be related to the limited communication and surface area within the canisters.

In addition, the dewatering skid was fitted with a collimated sodium iodide gamma-ray spectrometer that was calibrated for ^{154}Eu detection. A correlation-to-uranium carryover was used to assure that minimal transfer from the canister to the dewatering system occurred during the water removal process.

Following dewatering, the canisters were raised out of the pool into the main hot shop, where the canisters were placed either into a shielded silo or directly into one of the four positions in the HVDS.

The HVDS was built by Exolon Systems under contract to VECTRA and was designed to receive four canisters at a time. The vacuum furnace vessel had a 388.62 cm internal length and was of 96.52 cm internal diameter. It was equipped with five thermocouples and heated by 54 kW of axial heating elements. The initial vacuum drying vessel was installed in the REA-2023 cask to provide shielding in the cell in the event that personnel entries were required. A second furnace was eventually procured and installed in one of the NuPac 125B casks. The process schematic is shown in Figure 84. The Control Screen and skid configuration are shown in Figure 85.

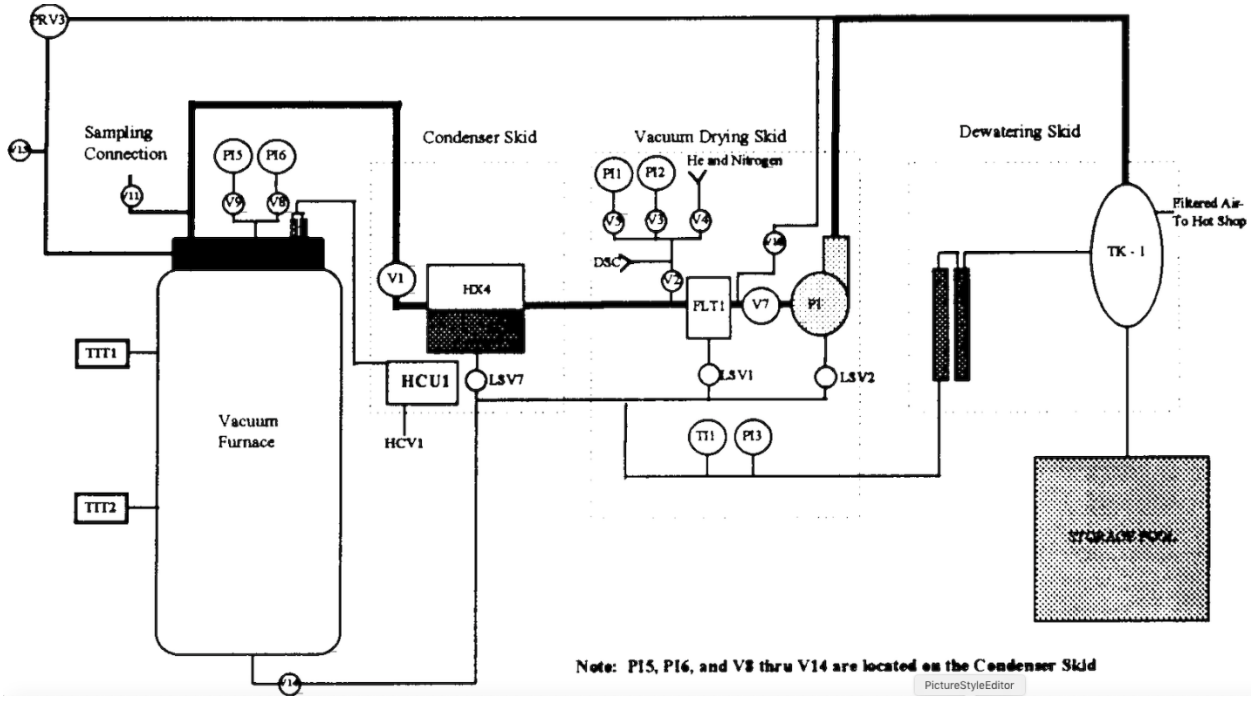

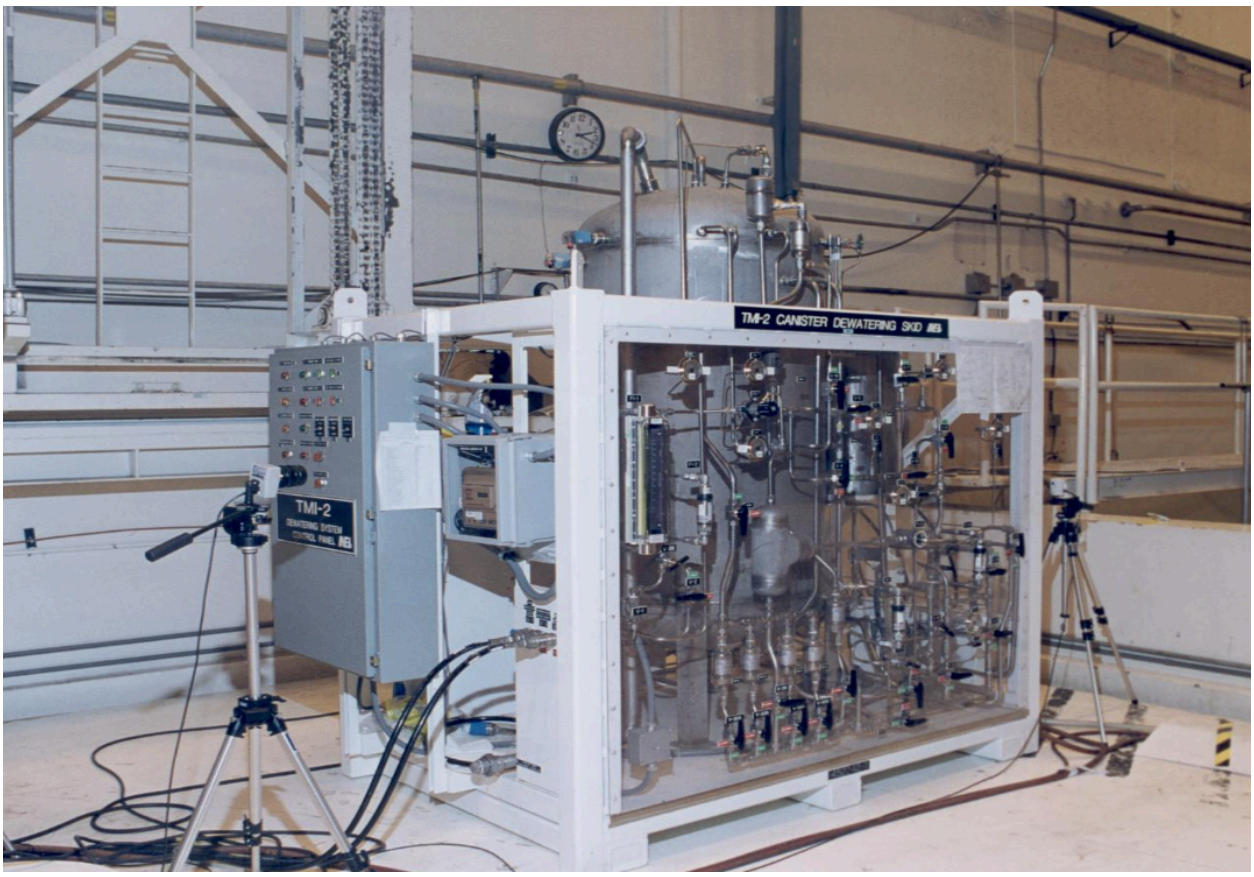

Figure 84. General schematic of dewatering and vacuum drying processes, above (Courtesy of INL); Dewatering skid below. (Courtesy of INL, 2009)

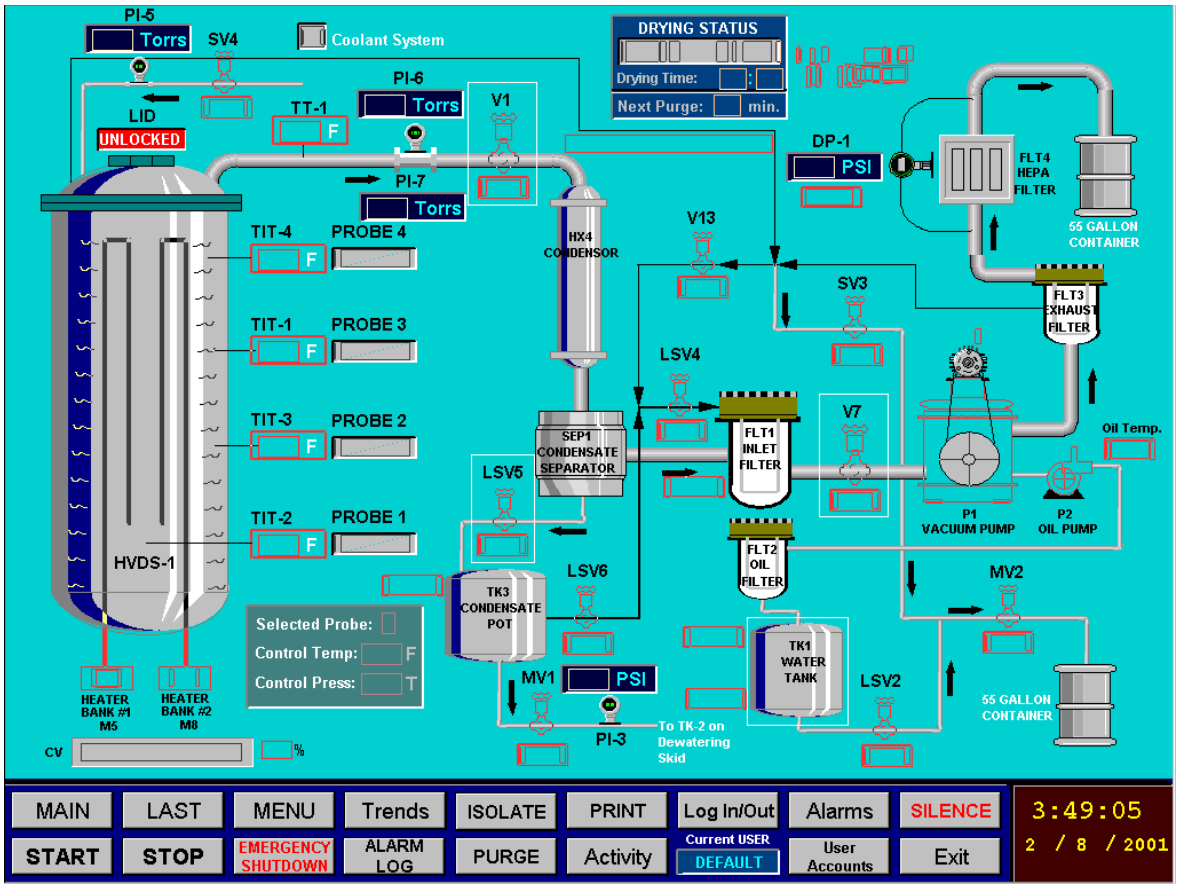

Figure 85. Dewatering-drying process-control operational screen. (Courtesy of INL)

Groups of four canisters were loaded into the HVDS, and the lid was secured. The system heated to 315°C and evacuated. The heater control temperature was a maximum of 482°C, and the debris temperature was estimated to be ~300°C. Because the heater was attached to the vacuum vessel, not to individual canisters, the temperature of the canister was determined by mathematical models. Design temperature was limited to minimize the potential for release of fission products such as ^{137}Cs, which becomes volatile in excess of 500°C. When a vacuum level of 3 torr was reached, the vacuum pump was isolated, and the vessel pressure was monitored. The drying cycles initially were expected to be able to maintain the standard identified in NUREG-1536 of 3 torr for 30 minutes of isolation. During early operation, these values were not achieved, requiring multiple evacuation cycles that took as many as 96 hours to reach the desired vacuum-isolation duration. Because it was impossible to determine whether the inability to maintain vacuum was due to inleakage from incomplete closure of the HVDS vessel head, an alternate approach was used. Due to schedule demand, it was determined that acceptable levels of drying could be achieved by observation of the change in temperature and pressure to identify the change from constant-rate drying to falling-rate drying. The latter is noted by a rise in bulk temperature and a consistent drop in pressure. Falling-rate drying is an indication that the bulk water has been fully evaporated from among the particles of a granular system such as the fuel debris. The HVDS system included a condenser for water removal and a separate pump for removable noncondensible gas. The system design included controls to prevent overtemperature conditions as well as to assure that flammable gas deflagration was not possible. The design allowed for intermittent purge capability, which was used periodically. The canister configuration in the HVDS was also analyzed to assure subcriticality.

The original assumptions used by the INEL Engineering Group (Palmer 1996) were predicated on maintaining the drying temperature below that which would cause the failure of the O-ring on the fuel/debris canister head. When the drying and packaging contract was awarded to VECTRA, the decision was made only to take credit for the dry shielded canister (DSC) as the confinement barrier; no credit was taken for the fuel/debris canister O-ring, meaning that there was no need to run at a temperature (<150°C) that would not damage the O-ring. The four-canister configuration in the HVDS is shown in Figure 86.

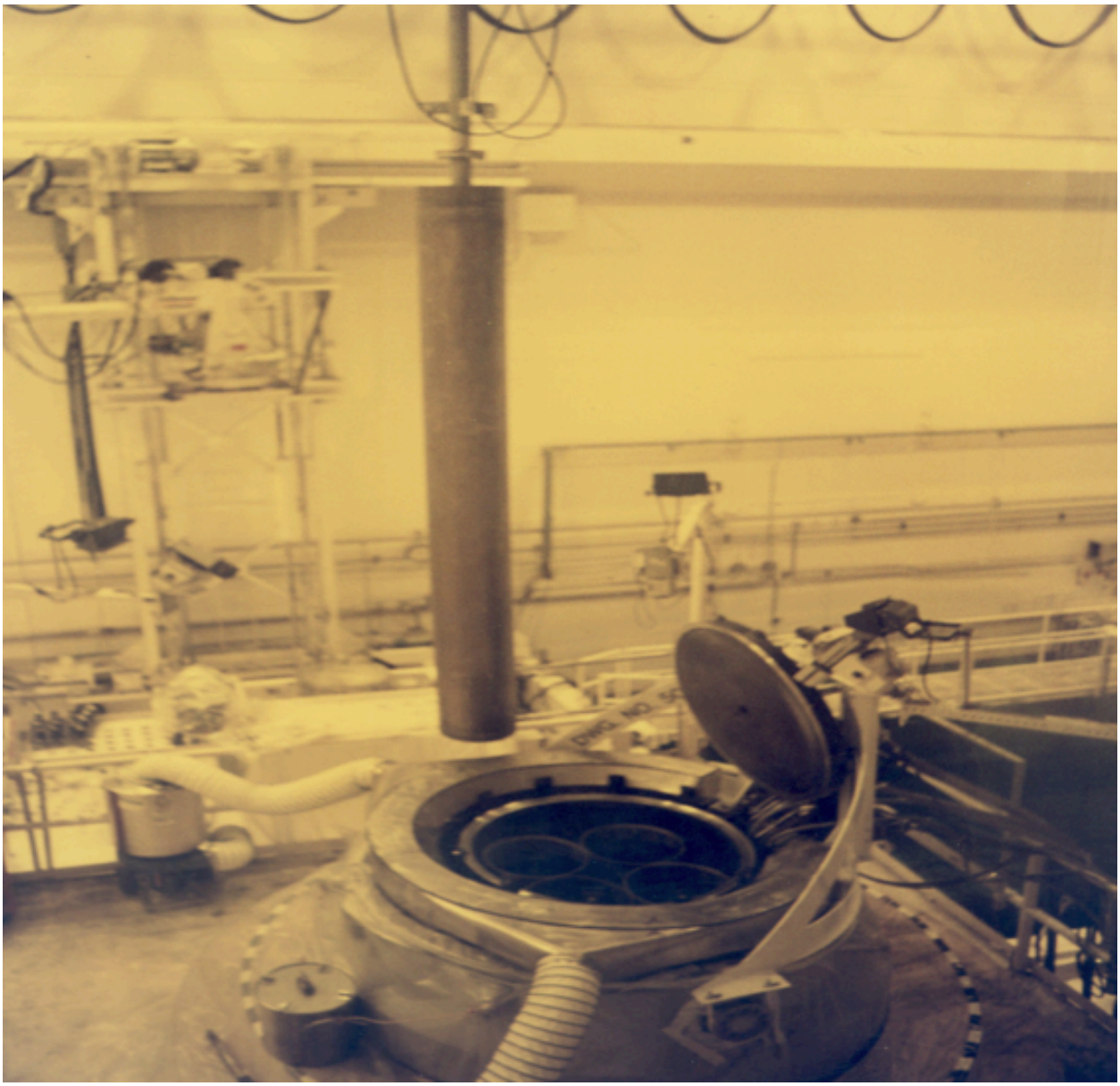

Figure 86. HVDS installed in REA-2023 cask in TAN hot shop. (Courtesy of INL, 2009)

Prior to award of the drying contract, several tests of different materials were performed at INEL, including thermal measurements of bucketed rods, tests on simulated fuel elements in buckets, canned rods, bucketed sand, and TMI-2 debris canisters containing lava rock using heated forced air and heated vacuum drying. Heated vacuum drying was selected as the preferred option.

8. NUHOMS Dry Shielded Canister

The NUHOMS design that was selected for interim dry storage is a modified variant of the standard NUHOMS design that accommodates 24 power assemblies per canister in stainless steel DSCs. The NUHOMS-12T design uses an internal basket configuration that positions twelve of the TMI-2 canisters in a circular array.

The NUHOMS-12T DSCs were fabricated from SA-517, Grade 70 mild steel. The DSC main shell is fabricated of 1.6 cm-thick plate, rolled into a 170-cm-diameter, 426-cm-tall cylinder. The canister configuration is shown in Figure 87.

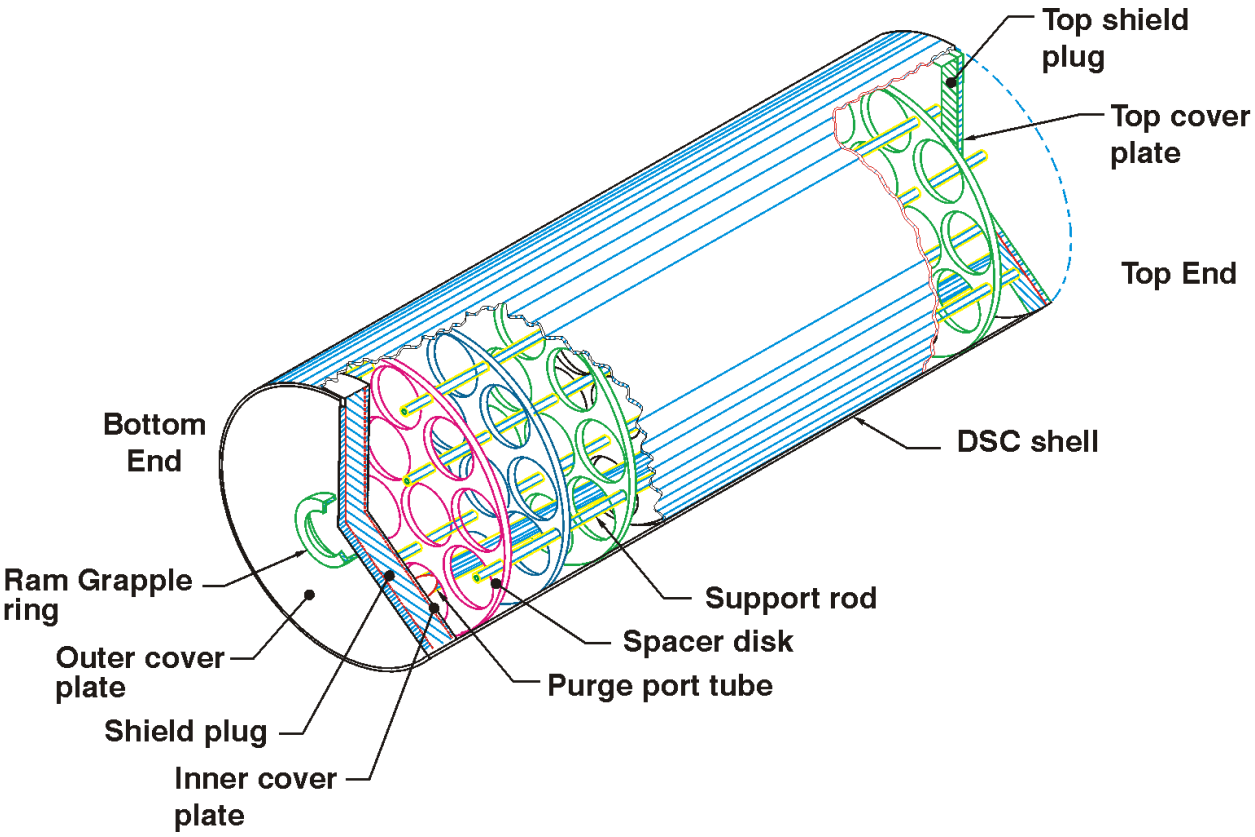

Figure 87. NUHOMS DSC schematic. (Courtesy of INL, 2002)

The DSC has a 2.54 cm-thick welded top plate and a multiple-piece bottom lid that incorporates a 11.5-cm-thick radiological shield plug and two 3.8-cm-thick top cover plate that are welded to the shell to complete the final closure. The bottom end also incorporates a ring on which a hydraulic ram is attached that is used to push the DSC into place in the horizontal storage module as well as retrieve it at the end of interim storage. The ring is visible in the fabrication photo, Figure 88.

Figure 88.Photo of the DSC during fabrication. (Courtesy of INL)

The TMI-2 DSC design required separate certifications from the standard design, at least in part due to its manufacture from carbon steel, which was initially seen as a cost-saving measure. This additional certification included confirmation that certain fabrication welds could be made in a fully compliant manner.

The unique part of the TMI-2 DSC design is the vent that was incorporated to allow any residual water or radiolytic hydrogen to be released from the debris canisters. This vent module is located near the edge of the non-shielded end of the canister and includes four Pall sintered stainless steel filter units as well as an isolation and purge port. If high hydrogen values are observed in a gas sample, the canister can be purged with nitrogen to reduce the concentration to less than the 4 vol% value. If a filter fails to function, the original assumption was that the DSC could be returned to the hot shop, and the filter module, replaced. No filters have failed during testing to date.

Criticality control is primarily a function of moderator exclusion by preventing water ingress. The debris canisters have been extensively dried and the DSC is placed in the horizontal storage modules (HSM) above the design flood elevation. Seventy-five percent credit is taken for the various fixed neutron absorbers present in the canister components. Canister spacing inside the DSC contributes to criticality safety as well. No burnup credit is considered. (SAR-II-8.4, 2018)

Structurally, the entire system was evaluated for specific head load and canister-drop potential. Table 14 shows the design criteria.

Table 14. NUHOMS DSC design criteria. (SAR-II)

Category	Criteria or Parameter (Dimensions Are Nominal)	Value
TMI-2 Canister Criteria:	Maximum Canister Weight	1,327 kg (2,926 lbs.)
	Size (Nominal): Length	3.81 m (150 in)
	Diameter	35.6 cm (15 in)
	Initial Maximum Enrichment (weight % without U-235)	2.98%
	Fuel Burnup (MWd/MTU)	3,175
	Gamma Radiation Source (photons/sec/canister)	6.37×10^{14} (19 yr. cooled)
	Neutron Radiation Source	6.90×10^{5} (19 yr. cooled)
	Thermal Characteristics	
	Max. Decay Heat/Canister	60 W
	Average Decay Heat/Canister	15 W
	Thermal Design Basis	
	Max. Decay Heat per Canister	80 W
	Total Decay Heat for DSC with 12 cans	860 W
Dry Shielded Canister:	Number of TMI-2 Canisters per DSC	Up to 12
	Size (Nominal):	
	Overall Length	4.15 m (163.5 in)
	Outside Diameter	1.71 m (67.2 in)
	Shell Thickness	15.9 mm (5/8 in)
	Heat Rejection	860 W
	Internal Atmosphere	Air
	Design Pressure	15 psig
	Equivalent Cask Drop Deceleration	75g Vertical (end) & Horizontal (side) 25g Oblique (corner)
	Materials of Construction	Carbon Steel
	Service Life	50 years

8.1 DSC Loading and Welding

Dried canisters were then transferred to the NUHOMS-12T DSC in the TAN hot shop. The DSC was staged in the hot shop, positioned in the OS-197 onsite transfer cask with the lid off. The canister loading is shown in Figure 89.

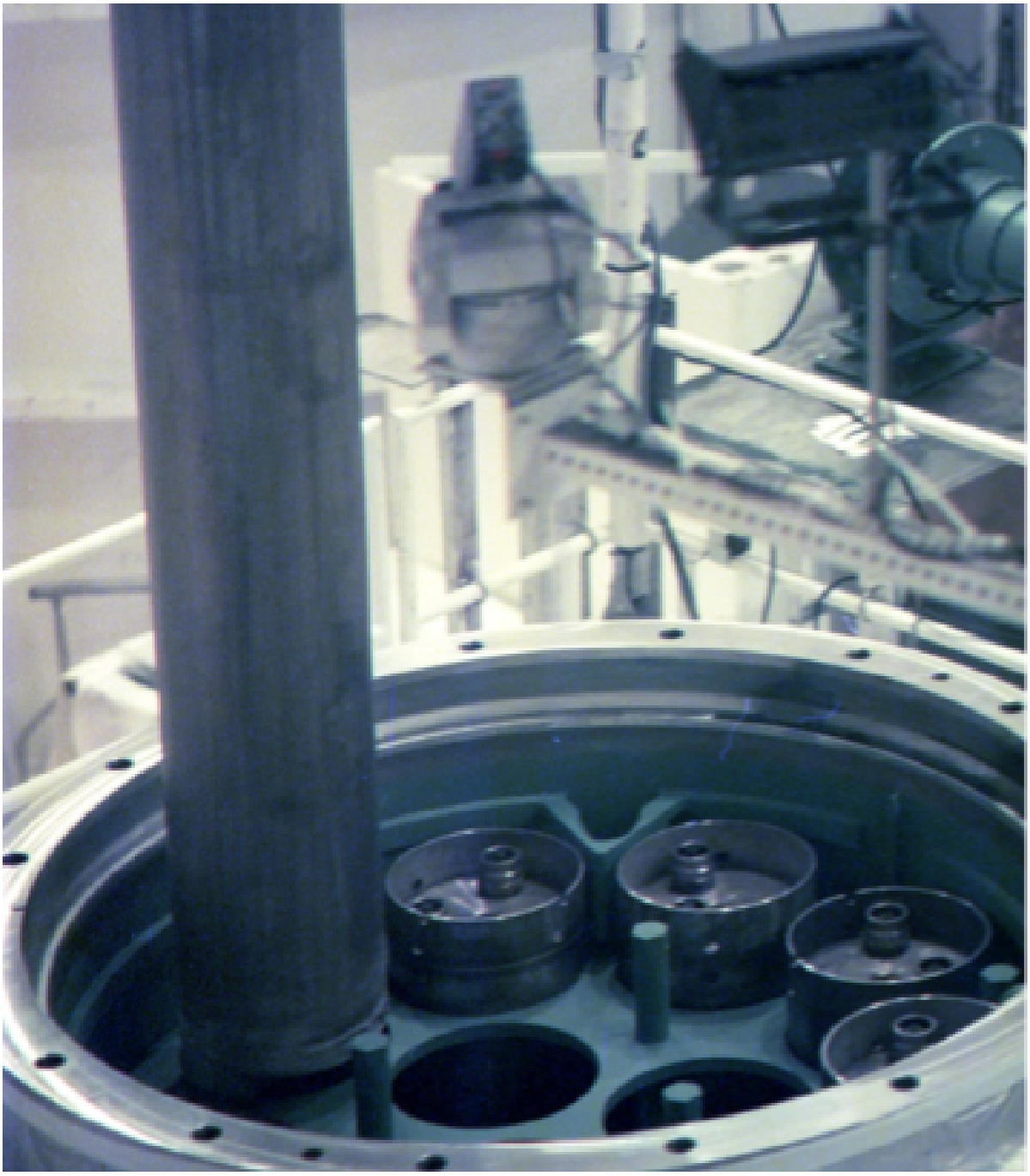

Figure 89. Dried debris canisters being loaded into a DSC. (Courtesy of INL)

Once the twelve-canister payload was inserted into the DSC, the radiological shield plug was inserted, and the final shield plugs were welded into place using the automatic welding machine. Initial welds were performed manually, but in the interest of radiological-dose reduction and improved weld

consistency, an automatic welding machine was used. When the shield plug weld was completed, the weld was visually inspected by remote camera. Both the welding technique and the remote inspection process were validated using mockup canisters prior to implementation. The DSC was then evacuated to 10 torr using the vacuum drying system and backfilled with helium to a 151 kPa pressure, after which a helium leak check was performed. If the DSC failed the helium leak check, the point of leakage would be repaired by grinding and rewelding. The DSC top cover plate was then installed, welded, and visually inspected. The vent and purge ports at the shield-plug end of the DSC were then seal-welded. Lid placement is shown in Figure 90.

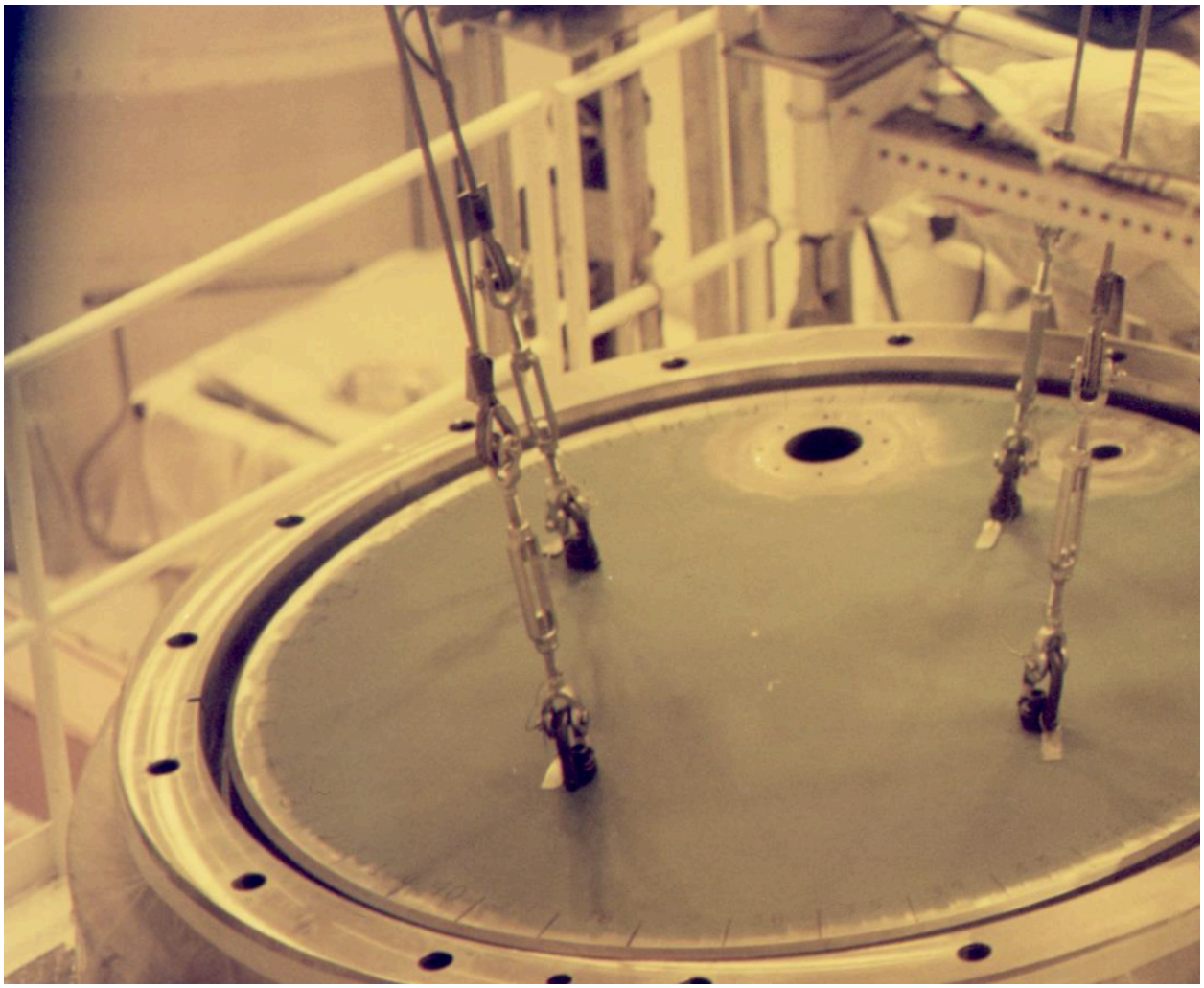

Figure *90* DSC lid placement (Courtesy of INL)

The less-shielded head of the DSC incorporates a replaceable sintered-metal HEPA filter that allows any gas that might be produced from water that was not removed during the drying process to be vented without pressurization of the DSC in storage. Following the top cover weld completion, this filter module was installed on the vent and purge ports. This is shown in Figure 91. A cover was placed over the vent port to seal the canister, and the DSC was then backfilled for transportation.

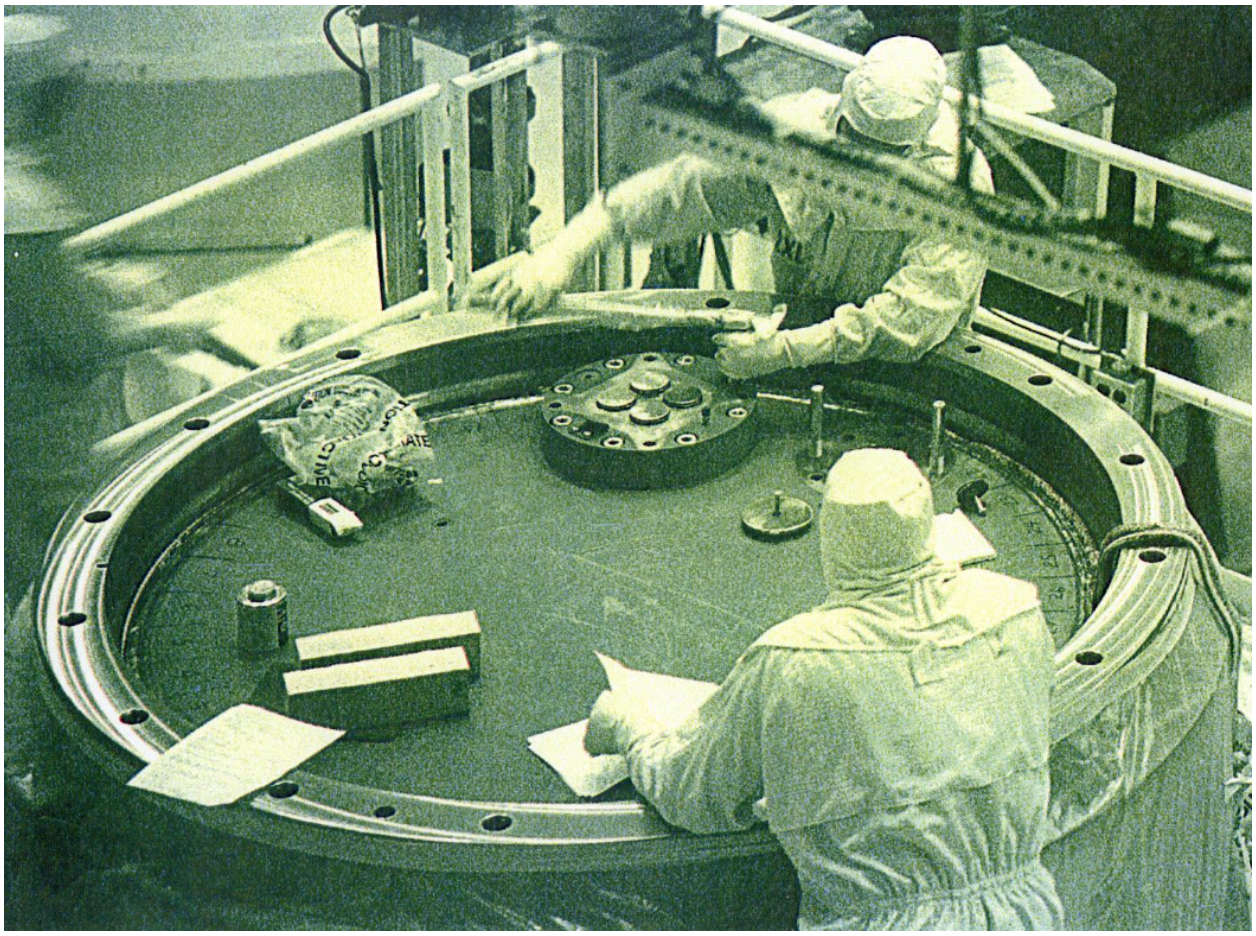

Figure 91 Vent filter installation (Courtesy of INL)

The OS-197 top lid was installed and secured, and helium was leak checked. The cask was lifted, rotated to a horizontal position, and loaded onto the transport trailer. Following survey and decontamination, it was moved out of the TAN-607 hot shop and driven by truck the 30 km to the INTEC.

8.2 DSC Lid-Closure Weld

The final lid-closure weld was performed using gas tungsten arc-welding process using a semiautomatic rotary weld unit. This process uses a non-consumable tungsten electrode operating in an argon fill gas with an automatic wire feed for filler metal. The system used dual gas-cooled torches mounted on a rotary track that were monitored by video cameras. All communication and power-supply cabling was routed outside the cell to allow remote operation. After the first several canisters were assembled, operational issues were resolved, and during the latter stages of the TMI-2 DSC loading campaign, 25 DSC canisters were completed in eight months, amounting to completion of 3500 linear feet of welding with no detected flaws. The multi-section lid arrangement is shown in Figure 92. Manual welding is shown in Figure 93, the automatic welding machine is shown in Figure 94, and closeup photo of the welding apparatus in operation with an observer is shown in Figure 95.

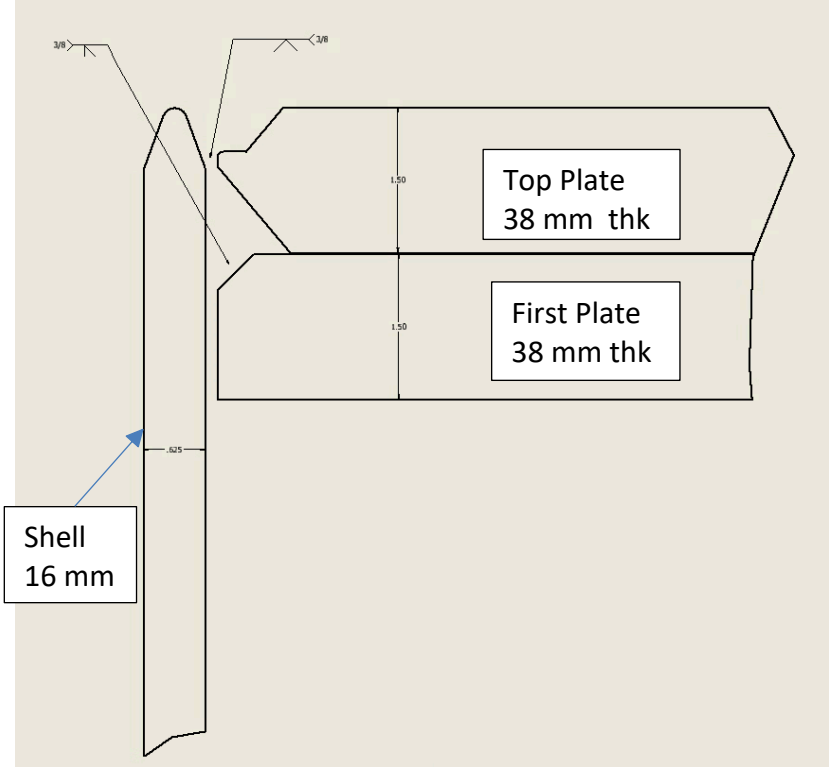

Figure 92. DSC lid-closure weld configuration. (Courtesy of INL)

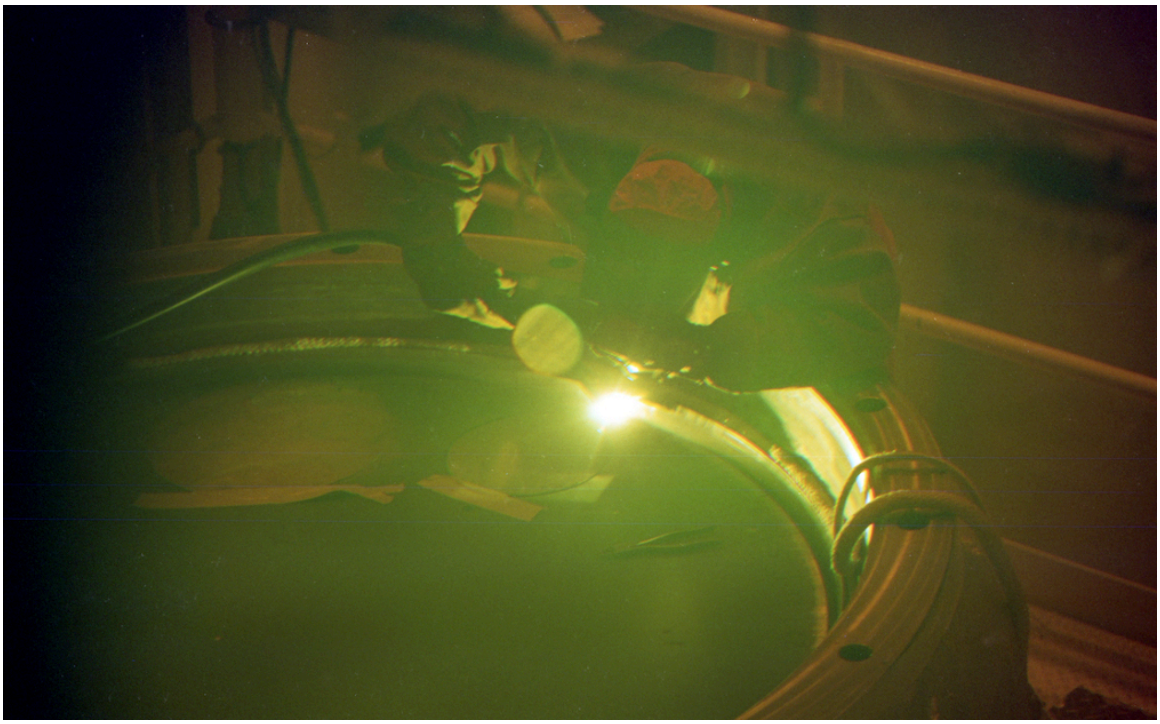

Figure 93 Manual DSC lid welding. (Courtesy of INL)

Figure 9

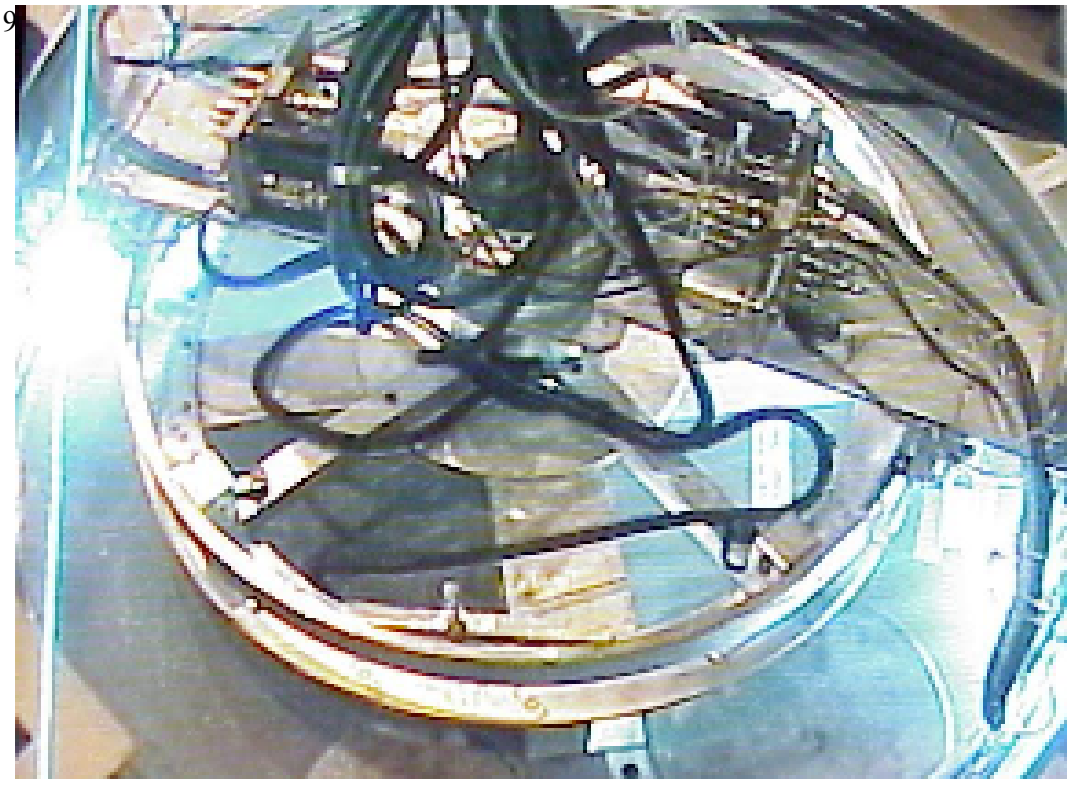

capture). (Courtesy of INL)

Figure 95. Welding of DSC lid. (Courtesy of INL)

8.3 OS-197 Onsite Transport Cask

Because the fuel-loaded DSC is only radiologically shielded on the end that is exposed following loading into the horizontal storage module, shielding is required when it is handled in transport from loading to placement. The shielding around the cylindrical portion of the DSC is provided by the OS-197 cask. The design is intended to be adequate to meet U.S. Department of Transportation radiological-dose-rate values, but is not expected to meet transport-accident criteria at highway speed because it lacks impact limiters. In the case of the TMI-2 canisters, the dose-rate limits were not likely to be challenged because the debris were from a low-burnup core. Onsite transport speed was limited to less than 30 km/h to assure that an impact accident would not result in a radiological release.

One primary function of the OS-197 is to support the DSC during insertion into the HSMs. The lid through which the DSC was loaded is removed, and a smaller plug on the opposite end is removed to allow the hydraulic ram to be attached to the DSC. The transport cask is positioned to precisely align with the HSM cavity, and the hydraulic ram is actuated to push the DSC into the concrete shield. As in several other respects, the TMI-2 installation is unique in that the DSC must be placed in a precise manner to allow the vent port on the DSC to align with the cutout in the concrete vault that allows access to it. Because the debris canisters were not uniformly loaded, it was discovered that certain DSCs tended to rotate out of alignment with the vent port during transport and insertion. Following this discovery, efforts were made to load heavier canisters in positions that would be the bottom when the DSC was rotated to the horizontal position. The specifications of the OS-197 are shown in Table 15. Figure 96 shows a cross-section view of the cask. Figure 97 is a photograph of the cask in transit between TAN and INTEC.

Table 15. OS-197 onsite transport cask design criteria.

OS-197 Cask:	Payload Capacity	37,000 kg (82,000 lbs.)
	Gross Weight	113,000 kg (250,000 lbs.) handling 109,000 kg (240,000 lbs.) transport 123,000 kg (271,200 lbs.) transport with impact limiters
	Equivalent Cask Drop Deceleration	75g Vertical (end) & Horizontal (side) 25g Oblique (corner)

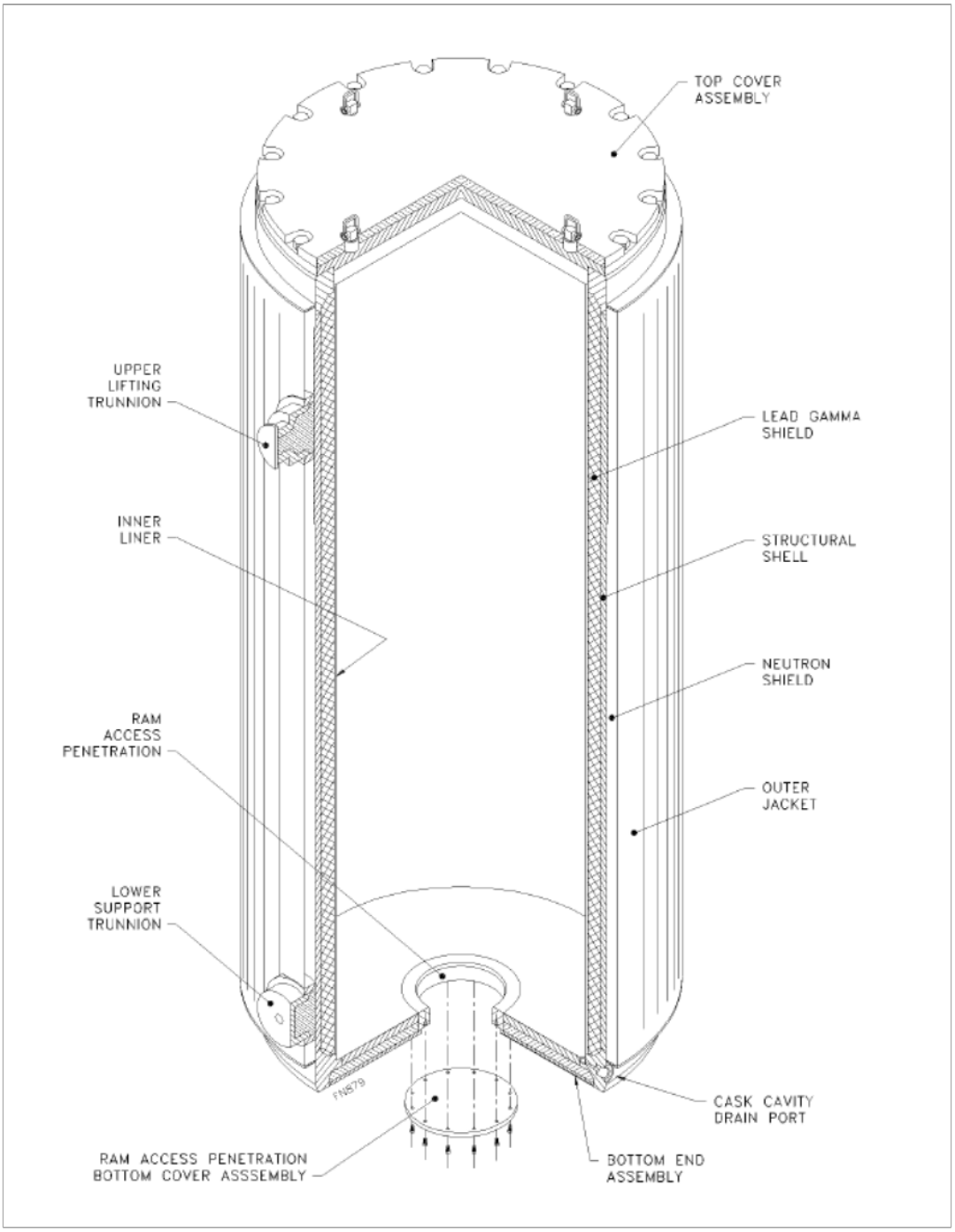

Figure 96. OS-197 onsite transfer cask. (Courtesy of INL, 2012)


Figure 97. OS-197 in transit between TAN and INTEC. (Courtesy of INL)

Once the OS-197 arrived at INTEC, the trailer was unhitched from the truck tractor that pulled it from TAN and was hitched to a rubber-tracked agricultural tractor that had the necessary traction and maneuverability to position the cask trailer accurately between the two rows of HSMs.

The TMI-2 installation (see Figure 98) requires HSMs to be exposed on both ends, one for insertion of the DSC, and the other for access to the canister-vent.

Figure 98. Mating OS-197 to HSM at INTEC CPP-1774 ISFSI for DSC placement. (Courtesy of INL)

8.4 Horizontal Storage Module

As discussed in previous sections, the NUHOMS HSM is constructed of thick concrete sections that provide the primary radiological shielding for the DSC payload. The DSC rests on a steel-rail structure inside the concrete vault. The concrete panels that comprise the vault are bolted together to form the rectangular structure.

The TMI-2/CPP-1774 ISFSI uses a design that departs from the standard in that each module has access at both ends of the DSC and HSM to allow for loading as well as access to the vent port. The TMI-2 design also departs in that no convective-cooling vents are included in the concrete vault due to the low decay heat of the canister contents.

As shown in Figure 99, the vent module access panel includes the connections necessary for testing the filter, isolating the DSC headspace and headspace gas sampling.

The design criteria are shown in Table 16.

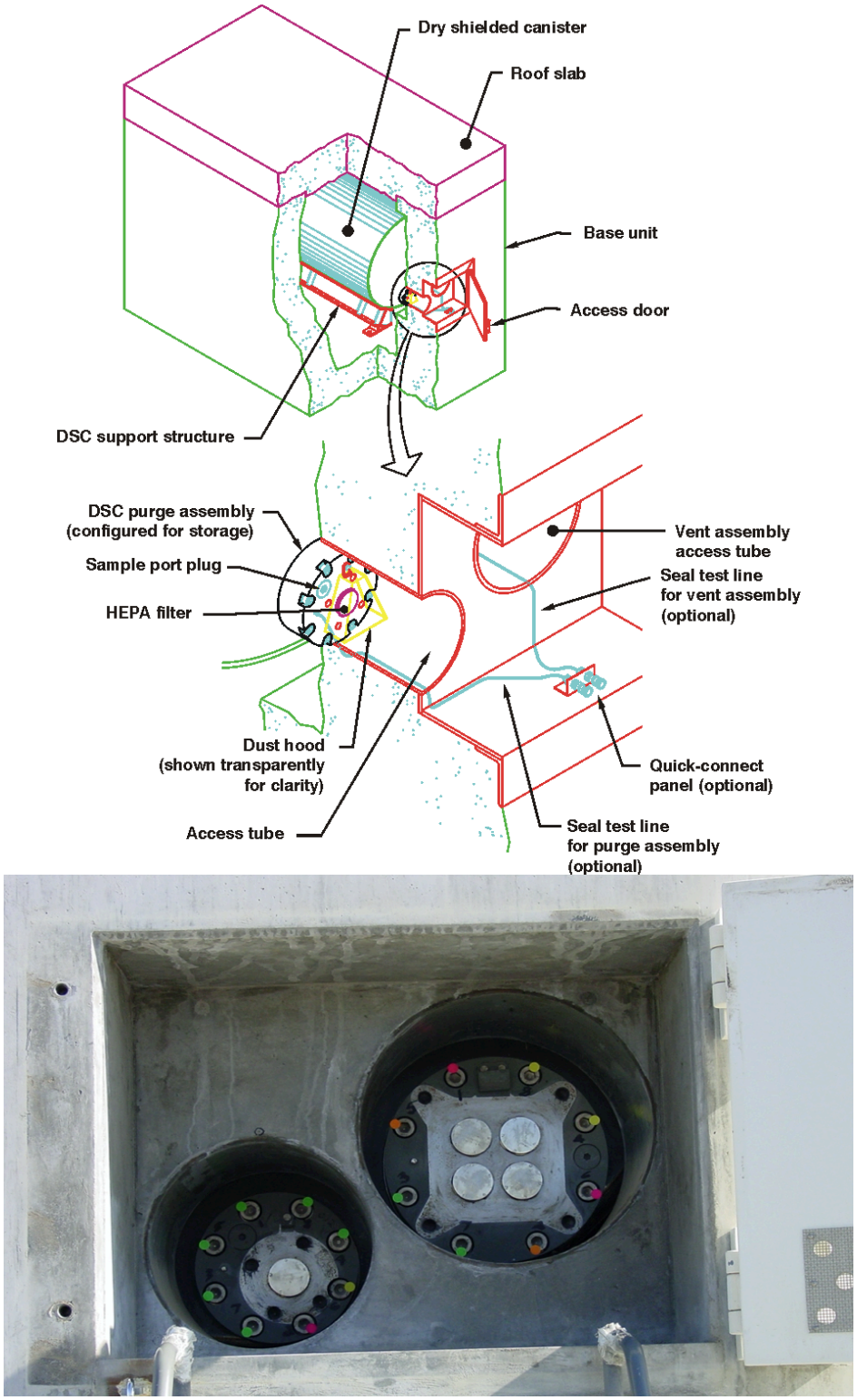

Figure 99. HSM cutaway diagram (top) and photograph showing purge vent and filter port (bottom). (Courtesy of INL 2002).

Table 16. NUHOMS HSM Design Criteria

Capacity	One DSC per HSM
Array Size	Two rows of 15 modules
HSM Size (Nominal)	
Length	5.54 m
Height	4.42 m
Width	3.12 m
Surface Dose Rate	ALARA
Heat Rejection Capacity	860 Watts
Materials of Construction	Reinforced concrete and structural steel
Service Life	50 years

The current (final) ISFSI two-row HSM configuration is shown in Figure 100. There are thirty HSMs, of which 29 contain loaded DSCs. The intent is to provide an additional HSM in the event that one of the DSCs should fail, and an additional position be necessary for any repackaged contents.

Apart from freeze-thaw effects of snowmelt on the bolt pockets that hold the HSM together, no significant degradation has been identified on the structure or systems. The bolt-pocket damage was remedied by use of a polyurethane filler and covered with stainless steel covers.

Figure 100. CPP-1774 ISFSI with HSMs. (Courtesy of INL)

8.5 Ongoing Sampling and Monitoring

In accordance with the safety analysis requirements, a portion of the stored DSCs undergoes headspace-gas sampling annually. Due to uncertainty about the effectiveness of the drying process, the canisters were sampled monthly during the first year following loading. Although the canisters are vented, no radiological contamination and no detected release of airborne radiation has been detected by direct smears or air sampling. Gas sampling during the first year resulted in an indication of as much as 3% hydrogen, but subsequent samples have stabilized in the range of approximately 0.4 vol%. Given the safety analysis report (SAR) assumptions about the potential for radiolysis of residual water in the lightweight concrete (LICON), there is no indication that the hydrogen generation rates approach the predicted values (see Figure 101).

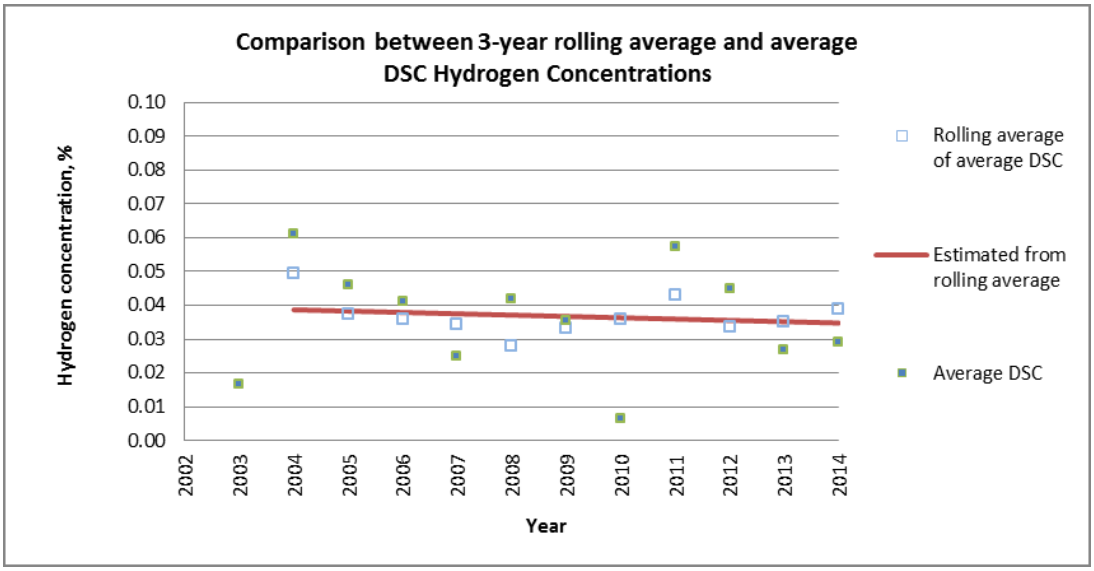

Figure 101. Annual DSC hydrogen concentrations, 2003–2014. (Courtesy of INL, 2016)

SAR values were based on hydrogen transport modeled in stored configuration. The analysis assumed hydrogen generation rates included 7 cm^3/hr due to radiolysis in each canister plus 33 cm^3/hr due to corrosion in DSC, for a total of 40 cm^3/hr. Release of the produced hydrogen was assumed to be driven by diffusion, seasonal and diurnal temperature and pressure fluctuations, and wind fluctuations. The resulting analysis concluded that hydrogen concentrations would reach 1.5 vol% in the DSC, and individual canisters would be as high as 4.5% (SAR Section 2, Radiolysis).

In the interest of time, hydrogen-gas concentrations were determined using a flammable gas detection instrument of the type used in industrial hygiene personnel-access monitoring. During the first few years of operation, monitoring was performed using a Cannonball unit that was not temperature compensated. This type of instrument measures the temperature change in a catalyst bed as an indication of the presence of flammable gas. For precise measurements, calibration needs to be performed at the same temperature as the measured environment. As a means of getting more-consistent results, in recent years, a photo-ionization detector system has been implemented. At the present time, canisters are only monitored annually, rather than monthly.

Part of the 2019 NRC relicensing involved development of a comprehensive aging-management plan. Per the aging-management plan, the HSMs will be monitored for concrete cracking and potential for absorption of water that would lead to cracking in freeze-thaw cycles. This monitoring includes use of water-absorption testing using a Rilem tube. Other proposed inspections involve insertion of miniature borescope cameras into the accessible openings to view the external surface of the DSC and the structural support rail that supports the DSC. Figure 102 shows photographs of example cracking of the HSMs.

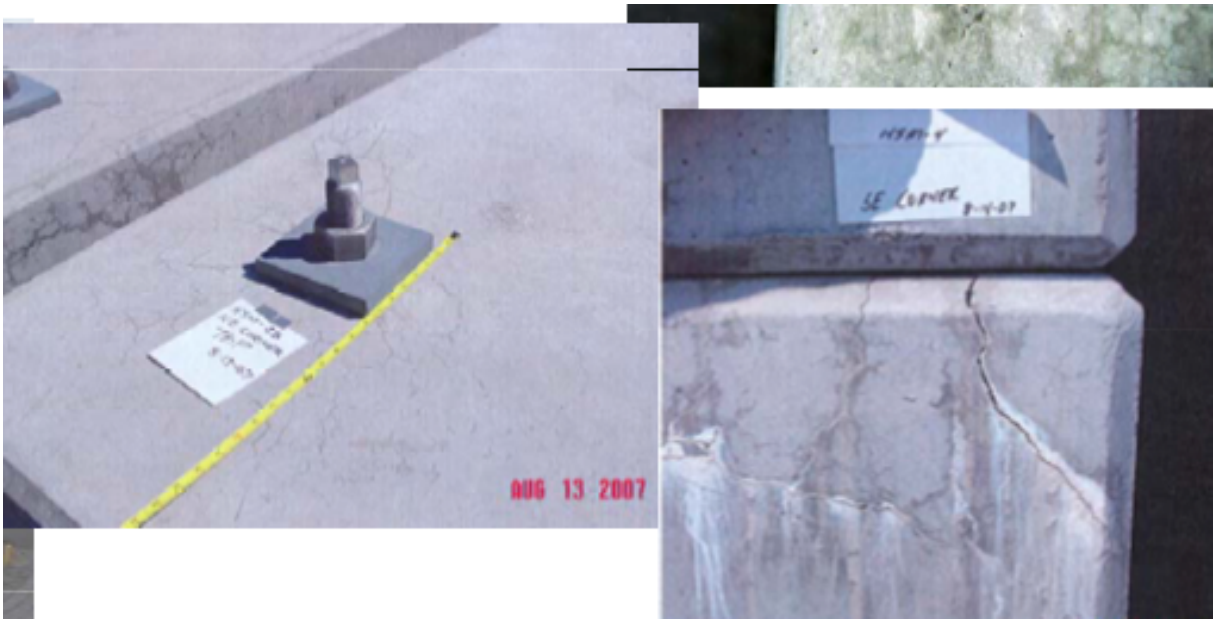

Figure 102. Examples of cracking of HSM concrete. (Beller, 2010)

The storage-facility safety basis includes full analysis of seismic, tornado, flood, and canister-leakage scenarios. Due to its robust construction and the arid remote location, no significant release is expected that would affect offsite population.

8.6 Disposition

In accordance with the terms of the 1995 agreement to settle a lawsuit between the State of Idaho and the U.S. DOE (sometimes known as either the Settlement- or Batt Agreement), the TMI-2 debris are to be removed from Idaho by January 1, 2035. To achieve this goal, it will be necessary to specify a package that will be compatible with proposed disposal approaches. The most developed of the disposal plans was the Yucca Mountain Project design, which was suspended for 8 years starting in 2008 and has not yet been authorized for full construction.

The likely approach for disposal is that the TMI-2 canisters would be removed from the DSC and placed into a unit that has been identified as the DOE standardized canister. This component would function as an overpack and be either selectively placed in a large disposal canister along with high-level waste-glass canisters or loaded as a group into specific disposal canisters.

The DOE standardized canister was developed with the intent of accommodating a variety of fuels and debris in a consistent package that was qualified as a component of the overall final disposal package. It was designed to be constructed of Type 304 stainless steel, available in 457- or 610- mm diameters in either 3.048 or 4.572 m lengths. Packaging of the TMI-2 debris canisters is assumed to use the 610-mm-diameter by 4.572-m-long variant.

One of the proposed disposal combinations includes the placement of a DOE Standard Canister in the center position of a disposal package that would be loaded with vitrified high-level defense process waste glass canisters in five positions around the perimeter of disposal canister.

Once disposal design commitments have been made, it will be necessary to have a facility that is capable of receiving the retrieved DSCs. Once received, the DSCs would be cut open, and the TMI-2 canisters removed and placed into DOE standardized canisters. Independent of the availability of the final repository, the settlement agreement mandates that the fuel be removed from Idaho.

9. Summary

A total of 268 debris (fuel) canisters, containing relatively large fuel debris, 12 knockout canisters containing pieces between 140 microns and 10 millimeters in diameter, and 62 filter canisters containing drilling fines, the diameters of which are greater than 140 microns were ultimately shipped from Pennsylvania to the INEL for research purposes, with ultimate disposition to be dependent on availability of a permanent repository. Upon receipt at the TAN-607 hot shop, the canisters were fitted with a standpipe to isolate canister water from pool water, filled with deionized water and transferred to the TAN-607 pool where they were stored in steel racks containing six canisters. The canisters remained in wet storage until 1999 when they were dried at up to 600°C and a target pressure of 2 torr using an HVDS. The elevated temperature drying was presumed to be necessary to adequately dry the LICON in the fuel canisters. Drying was necessary to eliminate moderator that would affect criticality potential, promote corrosion, and provide a medium that would produce free hydrogen resulting from radiolysis that could pressurize a sealed canister.

Drying was certified complete by the falling-rate method, in which the temperature underwent a rapid increase due to evaporation of the bulk pore water in the debris, and the remaining surface water evaporated with little change in the vacuum reading.

The dried canisters were placed in VECTRA NUHOMS DSC, 12 debris canisters per DSC, which were then welded shut and transferred to INTEC using the OS-197 onsite transfer package. The DSC was placed in the concrete HSM that provides shielding against the canister gamma-ray and neutron dose. Due to uncertainty in the effectiveness of drying, the DSC/HSM design was modified to incorporate a stainless steel sintered-metal filter into the vent path on the lid. This filter provides a vent path and sample and purge connection to the headspace of the DSC, preventing accumulation of potential radiolytic hydrogen in the canister.

Following the first year of monthly sampling which saw gas sample data indicating up to 3 vol% hydrogen, the measured hydrogen concentration was 0.03 vol%, suggesting that the debris was fully dry. The hydrogen values detected show a gradually declining trend and do not depart significantly from that expected from radiolysis of moisture in ambient air.

10. References

Adam, J. A Slow Comeback: IEEE Spectrum Vol. 21, Issue 4, Institute of Electrical and Electronics Engineers, 1984

Akers, D.W., E.R. Carlson, B.A. Cook, S.A. Ploger, and J.O. Carlson, TMI-2 Core Debris Grab Samples-Examination and Analysis, Part 1, GEND-INF-075, September 1986.

Akers, D.W., E.R. Carlson, B.A. Cook, S.A. Ploger, and J.O. Carlson, TMI-2 Core Debris Grab Samples-Examination and Analysis, Part 2, GEND-INF-075, September 1986.

Akers, D.W., McCardell, R.K., Russell, M.L., and Worku, G., "TMI-2 Core Materials and Fission Product Inventory", *Nucl. Eng. Design* 118 (1990) 451-461

Akers, D.W., G. Bart, P. Bottomley, A. Brown, D.S. Cox, P. Hofman, S.M. Jensen, H. Kleykamp, A. J. Manley, L.A. Neimark, and M. Trotabas, TMI-2 Examination Results from the OECD/CSNI Program, Vol. 1, EGG-OECD-9168, April 1992.

Argyle, M.D., Aging Management Review of the TMI-2 ISFSI Dry Shielded Canister, Overpack, and TMI-2 Canisters Stored Within, Engineering Design File EDF-10807, March 30, 2016.

Beller, Barbara, U.S. DOE, Presentation to Technology Innovation and International Partnership Workshop, Idaho Spent Nuclear Fuel Stabilization and Disposition, September 14, 2010.

Beller, Barbara, U.S. DOE, Presentation to NWTRB, Management of Aging Storage Facilities and Spent Nuclear Fuel, August 6, 2014.

Beller, Larry S. and Harry L. Brown, Design and Operation of the Core Topography Data Acquisition System for TMI-2, GEND-INF-012, May 1984.

Bottomley, P.D, and Michel Coquerelle, Metallurgical Examples of Core Samples from the Three-Mile Island Unit 2 Reactor Core, Nuclear Technology, V87, 1989.

Calhoun, Gregory., Fuel Removal Equipment for Three Mile Island Unit 2, Nuclear Technology Vol 87, Nov. 1989.

Christensen, A.B., K. Custer, R. Gardner, J. Kaylor, J. Stalnaker, Receipt and Storage Issues at the TMI-2 Irradiated Fuel Storage Installation, ICONE-10-22649, April 2002.

Christian, J. D., Analysis of TMI-2 Canister Water, JDC-08-97/ WM-100-1074, December 5, 1997.

Croft, K M, Helbert, H J, and Laney, W M. TMI-2 core boring machine, EG & G Idaho, Inc., Idaho Falls (USA) EGG-M-08986; 1986.

EG&G Idaho, Mechanical Engineering Technical Bulletin Index No. 6, TMI Air Lift System, 1987.

Electric Power Research Institute, The Cleanup of Three Mile Island Unit 2, A Technical History 1979 to 1990, EPRI-NP-6931, October 1990.

Electric Power Research Institute, NSAC-80-1, Analysis of Three Mile Island-Unit 2 Accident, March 1980.

Evans, Danny L., TMI-2 Fuel Recovery Plant Feasibility Report, EGG-TMI-6130, EG&G Idaho, December 1982.

Falk, Diane E. and Clark E. Swenson, TMI-2 Defueling System Design Description, GEND-INF-065, General Public Utilities, et. al., March 1985.

Gardner, Rick, TMI-ISFSI Overview, CH2M-WG Idaho, January 27, 2009.

General Public Utility (GPU) 1993-08-05 Accident-Generated Water Disposal Completion Report.

Gold, R., Neutron Dosimetry with Solid State Track Recorders in the Three-Mile Island Unit-2 Reactor Cavity, Nuclear Tracks and Radiation Measurements, Vol 10, Issue 3, 1985.

Green, Russell, Mark Ford, and Ed Bradley, TMI Unit 2 Post-Accident Defueling, Global 2011, Makuhari Japan Dec-11-16, 2011.

Green, Russell, Presentation, Defueling TMI-2, 2011.

Henrie, J., et al., "Hydrogen Control in the Handling, Shipping, and Storage of Wet Radioactive Waste", GEND-052, 1986.

Hess, C.J, (editor) TMI-2 Technical Information and Examination Program 1984 Annual Report, GEND-049, April 1985.

Hobbins, R.R., M.L. Russell, C.S. Olsen, and R.K. McCardell, Molten Material Behavior in the Three Mile Island Unit 2 Accident, Nuclear Technology, V. 87, 1989.

Hofmann, Peter, et al. "Reactor Core Materials Interactions at Very High Temperatures," Nuclear Technology, Vol 87, Aug 1989, p: 146-–186.

Jensen, S.M., D.W. Akers, R. W. Garner, and G.S. Roybal, GEND-INF-082 Examination of the TMI-2 Core Distinct Components, September 1987.

Kirkland, H.W., M.A. Nemser, and W.M. Laney, Drilling Operations to Remove the Lower Core Support Assembly at Three Mile Island Unit 2, Nuclear Technology Vol. 887, No. 4, July 1989.

Lassahn, G.D., Uranium and Plutonium Content of TMI-2 Defueling Canisters, EG&G Technical Report RCS-27-93, September, 1993.

Lobner, P, C. Donahoe, and C. Cavallin, Overview and Comparison of U.S. Commercial Nuclear Power Plants, NUREG/CR-5640, U.S. Nuclear Regulatory Commission, 1989.

McConnell, J. W. Jr., D. A. Johnson, and R. D. Sanders, Sr. Radiation degradation in EPICOR-2 ion exchange resins. INEL, Idaho Falls, ID, NUREG CR-5594

McGough, M.S., W.E. Austin and G.J. Knetl, Underwater Plasma Arc Cutting in Three Mile Island's Reactor, Welding Journal Vol. 68, Issue 7, American Welding Society, 1989.

McCardell, R.K., M.L. Russell, D.W. Akers, and C.S. Olsen, Summary of Core Sample Examinations, Nuclear Engineering and Design 118, 1990.

Miller, C.J., Review of Destructive Assay Methods for Nuclear Materials Characterization from the Three Mile Island Fuel Debris, INL/EXT-13-30078, Idaho National Laboratory, September 2013.

Holton, W.C., C.A Nagin, S.L Owrutsky, The Cleanup of Three Mile Island Unit 2: Technical History 1979 to 1990. EPRI NP-6931 September 1990.

Osetek, D.J., J. M. Broughton, and R. R. Hobbins, TMI-2 Accident Evaluation Program, EGG-M-89109, CONF-89-0546, May 1989.

Palmer, A. Joseph, et al., "Drying Tests Conducted on Three Mile Island Fuel Canisters Containing Simulated Debris", CONF-9606116-18, 1996.

Pincock, L.F., Three-Mile Island Core Debris Packaging, Transportation, and Storage Summary LTD-11-22779. Idaho National Laboratory Limited Release Report, February 2012.

Pincock, Layne and Wendell Hintze, Stability of Molten Core Materials, INL/EXT-12-27136, January 2013.

PLN-3660, "Three Mile Island Unit 2 Independent Spent fuel Storage Installation License Renewal Project Plan," PLN-3660, Idaho Cleanup Project, May 3, 2011.

Reno, H.W., Fuel Removal, Transport and Storage, EGG-M-09386, EG&G Idaho, 1986.

Rosztoczy, Z.R., Root Causes of the Three Mile Island Accident, Nuclear News p 29-32, March 2019.

Russell, Malcolm L., Richard K. McCardell, James M. Broughton, and Douglas W. Akers, TMI-2 Accident Evaluation Program Sample Acquisition and Examination Plan for FY-1988 and Beyond, EGG-TMI-7992, February 1988.

Ryan, R.F. and R. Blumberg, Lower Core Support Assembly Defueling Plans and Tools, GEND-INF-093, October 1988.

Settlement Agreement: Public Service Co. of Colorado v. Batt, No. CV 91-0035-S-EJL (D. Id.) and United States v. Batt, No. CV-91-0065-S-EJL (D. Id.), October 17, 1995.

Standerfer, F.R., (GPU Director, TMI-2) Letter to US Nuclear Regulatory Commission Defueling "Canister Gas Sampling", October 21, 1987.

Standerfer, F.R., (GPU Director, TMI-2), General Public Utility Nuclear (GPUN), TMI-2 Defueling Completion Report, 1990.

Stickler, L.A., J.L. Rempe, S.A. Chavez, G.L Thinnes, S.D. Snow, R.J. Witt, M.L. Corradini, and J.A. Kos, NUREG/CR-6196/EGG-2733, Calculations to Estimate the Margin to Failure in the TMI-2 Vessel, February 1994.

Strosnider, J., K. Wichman, B. Elliot, C. Fairbanks, E. Hackett, S. Sheng, J. Tsao, L. Lois, M. Mayfield, and M. Mitchell, NUREG-1511, Reactor Pressure Vessel Status Report, Nuclear Regulatory Commission, December 1994.

Three Mile Island Accident of 1979 Knowledge Management Digest – Recovery and Cleanup (NUREG/KM-0001, Supplement 1).

TMI-2 SAR-II-8.4, "Three-Mile Island Unit 2 Debris Independent Spent Fuel Storage Installation (ISFSI) Safety Analysis Report," Rev. 6, September 27, 2018. TMI-2 SAR-II-8.4 Section 2.

TMI-2 SAR-II-8.4, "Three-Mile Island Unit 2 Debris Independent Spent Fuel Storage Installation (ISFSI) Safety Analysis Report," Rev. 6, September 27, 2018. TMI-2 SAR-II-8.4 Section 3.

Tolman, E. L., R. P. Smith, M. R. Martin, R. K. McCardell, and J. M. Broughton, TMI-2 Core Bore Acquisition Summary Report, EGG-TMI-7385, February 1987.

Trotabas, M., et al,. TMI-2 Core Materials Examination at (CEA), December 1989. SEMCI-89-DT-667.

Urland, C.S, TMI-2 Postaccident Data Acquisition and Analysis Experience, EPRI, April 1992.

Vinjamuri, K. D.W. Akers, and R.R. Hobbins, "Preliminary Report: Examination of the H8 and B8 Leadscrews from Three Mile Island Unit 2, EGG-TMI-6685, EG&G Idaho, April 1985.

Wolf, J.R., J.L. Rempe, L.A. Stickler, G.E. Korth, D.R. Diercks, L.A. Niemark, D.W. Akers, B.K. Shuetz, T.L. Shearer, S.A. Chaves, G.L. Thinnes, R.J. Witt, M.L. Corradini, and J.A. Kos, TMI-2 Vessel Investigation Project Integration Report, NUREG/CR-6197/EGG-2734, March 1994.

Zirker, L. R., R. A. Rankin, and L. J. Ferrell, "Processes, Techniques, and Successes in Welding the Dry Shielded Canisters of the TMI-2 Reactor Core Debris." WM'02 Conference, February 24-–28, 2002, Tucson, AZ.